

Reviewer 1#

The work by Liu et al present field measurements of HONO, a key source of radicals in the boundary layer, along with supplementary gas and particle-phase measurements in over a 5-month period in Beijing. The authors used this dataset to probe the sources and their contributions to ambient HONO, with a focus on pollution events. Using a steady state approach, the authors calculated the contributions of different sources to the HONO budget and concluded that traffic emission (via direct emission and conversion of NO by homogenous reactions) was the key source of HONO during winter pollution events. Liu et al present a comprehensive and interesting long-term dataset that enables the authors to perform a budget analysis to investigate the main sources of HONO. The main sources of HONO in Beijing and urban area in general is an open research topic, and consequently this work would be of interest to the community, particularly their HONO budget analysis of the haze events.

Response: Thank you so much for your positive comments.

There are, however, a few issues that in my opinion should be addressed prior to publication. While the manuscript is mostly well written, it is long. For example, Section 3.1 and 3.2 could be much shorter. In my opinion much of the text in these sections is unnecessary and could be reduced, without losing the key points.

Response: Thank you so much for your instructive suggestions. We have revised the redundant descriptions in Section 3.1 and 3.2.

In Section 3.1, the paragraph “In particular, the frequency of severe polluted episodes in March was obviously higher than that in the rest months (Fig. 1 and S3), resulting in the highest monthly mean concentration of PM_{2.5} ($88.5 \pm 60.0 \mu\text{g m}^{-3}$) and NR-PM_{2.5} ($67.0 \pm 56.8 \mu\text{g m}^{-3}$). This can be explained by both intensive emission during the heating season, which is supported by the high concentration of primary pollutants including CO, SO₂ and BC (Table S1), and the stagnant meteorological conditions that physically and chemically promote the accumulation of pollutants. For example, the low wind speed ($< 2 \text{ m s}^{-1}$) mainly from south-based directions accompanied with the low planetary boundary layer (PBL) height frequently occurred in March compared with other months (Fig. S4A).” has been shortened as “**Both the frequency of severe**

polluted episodes and the mean mass concentration of PM_{2.5} and NR-PM_{2.5} were obviously higher in March than that in the rest months (Fig. 1 and S3). This can be explained by both the intensive emission during the heating season as evidenced by the high concentration of primary pollutants including CO, SO₂ and BC (Table S1) and the stagnant meteorological conditions supported by the low wind speed (<2 m s⁻¹) and the low planetary boundary layer (PBL) height in March (Fig. S4A)” from lines 249 to 255 in the revised manuscript. In addition, we also deleted the sentences “It should be noted that the median mass concentrations of nitrate and OA also were higher in March than that in other months (Fig. S4C). The median mass concentrations of nitrate were 1.42, 8.76, 6.30, 3.15, and 3.23 μg m⁻³ from February to June, respectively. And the corresponding OA concentrations were 4.78, 14.04, 11.64, 13.89, and 14.08 μg m⁻³. Secondary formation is the major source of OA and nitrate in the atmosphere” from line 232 to 237 in the original version of the manuscript.

In Section 3.2, we deleted the following sentences “The hourly averaged $P_{\text{OH-HONO}}/P_{\text{OH-O}_3}$ ratio varied in the range of 1-25.4 during the daytime, while it varied from 0.3 to 2.8 from April to June” (lines 284-288, in the original manuscript), “Although the high loading of fine particles in polluted days could reduce the surface solar radiation (Li et al., 2017), subsequently, the OH concentration, the noon-time OH radical concentrations observed in polluted wintertime of Beijing were $2.4 \times 10^6 \text{ cm}^{-3}$ compared with $3.6 \times 10^6 \text{ cm}^{-3}$ in clean days (Tan et al., 2018). It was around 2 times compared to places such as Tokyo (Kanaya et al., 2007) and New York City (Ren et al., 2006)” (lines 295-300, in the original manuscript), and “ This implies that oxidation of atmospheric trace gases by OH may still be highly effective even in wintertime, thereby facilitating the vigorous formation of secondary pollutants in Beijing” (lines 301-304, in the original manuscript).

The most interesting work is presented in Section 3.3, where a detailed and comprehensive budget analysis is presented. However, throughout section 3.3 some of the calculations and equations need more explanation, as it was not always clear from section 2.2 how they were performed. Some examples are given below in the minor comments. It would also help the reader if the equation used to calculate the rates of emission for each source (I.e. the eqn

numbers) were referenced throughout section 3.3.

Response: Thank you for your good suggestions. We have referenced all the equation numbers throughout the revised manuscript. For example, in [line 389](#) in the revised manuscript, “The E_{vehicle} was calculated according to Eq. (2) using the relative emission rate of HONO to NO_x and the emission inventory of NO_x from vehicles”; In [lines 446-448](#) in the revised manuscript, “The lower limit, the middle value and the upper limit of the E_{soil} are $0.0032\pm 0.0027-0.013\pm 0.014$, $0.0046\pm 0.0039-0.020\pm 0.20$ and $0.0057\pm 0.0047-0.025\pm 0.024$ ppbv h^{-1} , respectively, calculated according to Eq. (2)”; In [lines 473-475](#) in the revised manuscript, “Thus, the lower limit, the middle value and the upper limit of $P_{\text{NO-OH}}$ were $0.007\pm 0.019-0.43\pm 0.26$, $0.026\pm 0.053-0.99\pm 0.79$ and $0.028\pm 0.053-2.14\pm 1.71$ ppbv h^{-1} , respectively, calculated according to Eqs. (3) and (4)”; In [lines 495-498](#) in the revised manuscript, “Therefore, the corresponding daytime lower limit, the middle value and the upper limit of HONO from photolysis of nitrate were $0.0011\pm 0.0021-0.096\pm 0.092$, $0.0072\pm 0.0021-0.66\pm 0.092$ and $0.042\pm 0.082-3.86\pm 0.008$ ppbv h^{-1} , respectively, calculated in the light of Eqs. (3) and (8)”; And in [lines 499-501](#) in the revised manuscript, “The production of HONO from heterogeneous reactions of NO_2 on aerosol surface was calculated according to Eqs. (3) and (5)”.

We also added the more details about budget calculations. For example, we added the following paragraphs “Oswald et al. (2013) measured the emission flux of HONO from 17 soil samples, including eucalyptus forest, tropical rain forest, coniferous forest, pasture, woody savannah, grassland, stone desert, maize field, wheat field, jujube field and cotton field etc. Tropical rain forest, coniferous forest and grassland are the typical plants in downtown Beijing (Huang et al., 2017a). At the same time, their emission fluxes of HONO are comparable (Oswald et al., 2013). Thus, we used the emission flux from grassland to calculate the emission rate of HONO from soil in Beijing because the temperature and water holding content dependent emission flux of HONO was available for grassland soil” [lines 433-441](#); “The method for the photolysis rates calculation were shown in the SI and the time series of the photolysis rates were shown in Fig. S7” in [lines 458-460](#); “The time series of the measured nitrate concentration and the middle value of J_{nitrate} were shown in Fig. 1 and Fig. S7, respectively” in [lines 493-495](#); “The A_s of aerosols varied from 1×10^{-4} to $4.8\times 10^{-3} \text{ m}^{-1}$ with a mean value of $1.4\pm 0.5\times 10^{-3} \text{ m}^{-1}$ during pollution events. This value is comparable with that

used in modeling studies (Zhang et al., 2016;Aumont et al., 2003). The A_s of ground surface which was calculated according to Eq. (6) and (7) varied from 1.5×10^{-3} to $3.85 \times 10^{-2} \text{ m}^{-1}$ with a mean value of $1.3 \pm 0.9 \times 10^{-2} \text{ m}^{-1}$ during pollution events. The surface roughness was 3.85 calculated according to Eq. (7). The Y_{HONO} was set to 0.5 because of the hydrolysis reaction of NO_2 (Liu et al., 2015), while it was 0.8 for light enhanced reaction (Liu et al., 2019;Ndour et al., 2008) and on BC (Han et al., 2013)” in lines 523-530 in the revised manuscript.

My major comment is from Section 3.3, the way the OH concentration was estimated is problematic in my opinion. As the authors rightly point out, to measure OH is difficult and requires highly specialized kit and therefore as they did not have access to these instruments, OH concentration needs to be estimated for this study. I am not sure about the way the OH concentration was calculated, as the equations they use (e.g. 13), use the levels of ozone and NO_2 . The problem is that during winter, the main source of OH in Beijing is HONO photolysis, as the authors themselves state earlier in the manuscript (Section 3.2, line 288, with references), and is in fact one of their conclusions from Fig 2. Therefore, without considering OH produced from HONO photolysis, how can they be sure that their estimated OH concentration is reasonable, especially in winter? I think that for an atmosphere as chemically complex as Beijing, to estimate the OH concentration requires a box-model approach. It is important as the estimated OH concentration will affect the budget analysis, both sources and loss terms, and therefore the conclusions drawn from it. If this is not possible, then the uncertainties with their approach to estimating OH concentrations should at least be discussed/quantified.

Response: Thank you for your instructive suggestion. We agree with you that OH concentration is an important parameter when calculating the HONO source from homogenous reaction between NO and OH. Some uncertainties of OH concentration should be resulted from the estimation approaches used in this work. In strictly speaking, it is better to directly measure OH concentration using a LIF or a CIMS. However, these instruments are unavailable at the present time. A box-model simulation is an other choice as you suggested because both the source and sink terms can be considered. A comprehensive sheet of VOCs including different isomers is required when doing box-model simulation because the reactivity varies greatly among different isomers even with the same mass to charge ratio (m/z). Unfortunately, the

VOCs concentration was measured using a SPI-MS in this work. Similar to a PTR-MS, this instrument cannot separate the isomers with the same m/z . Therefore, we did not simulate OH concentration using a box-model. If we had the measured or modeled OH concentration, we could parameterize the J_{HONO} and C_{HONO} into the Eq. (15).

We indirectly verified the estimated OH concentration by comparison with diurnal curves of OH concentration in this work and that reported in literatures (Tan et al., 2019). Overall, the estimated OH concentration was comparable with that measured in the literature (Fig. S10). In addition, we further compared it with the OH concentration derived from the measured H_2SO_4 concentration using a nitrate-CIMS from December 2019 to February 2020. In a box model, we considered the daytime source of H_2SO_4 from oxidation of SO_2 by OH and the sinks of H_2SO_4 using the measured concentration of the monomer and the dimer of H_2SO_4 , the condensation sink (CS, from 1 nm to 10 μm of aerosol) and the meteorological parameters. Then, OH concentration was calculated using a steady state method. As shown in Fig. R1, the predicted OH concentrations was generally comparable between these two different methods. This means the estimated OH concentration in this work is overall credible.

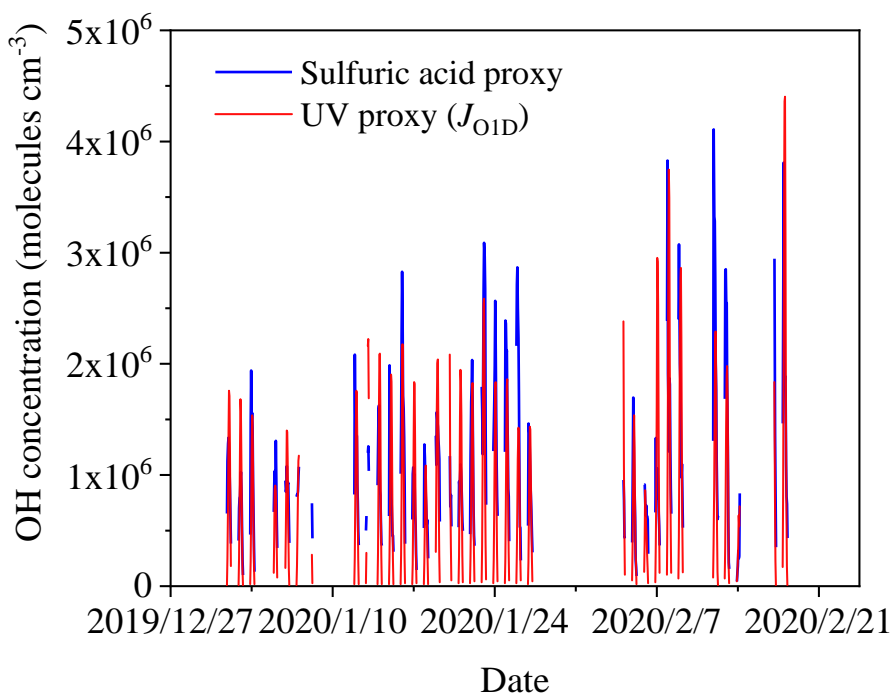


Fig. R1. Comparison of OH concentration between UV proxy method and H_2SO_4 proxy method.

In the revised manuscript (lines 482-488), we added the discussion about the uncertainties

from OH concentration estimation as you suggested. “It should be noted that OH concentration was estimated based on $J_{\text{O}1\text{D}}$ (Tan et al., 2019; Tan et al., 2018) or $J_{\text{O}1\text{D}}$ and $J_{\text{NO}2}$ (Li et al., 2018). As discussed in Section 3.2, HONO was an important primary OH source in the daytime. Unfortunately, it could not be parameterized for calculating OH concentration because the measured or modelled OH concentration was unavailable in this work. This might underestimate the early daytime OH concentration, subsequently, the contribution of homogeneous reaction of NO with OH to HONO source. This need to be further investigated in the future”.

Minor comments Line 82: I assume you mean nitrous acid not nitric acid?

Response: Thank you. It is nitrous acid. We have corrected this error in [line 81](#) in the revised manuscript..

Line 112: it would be good to specify that your ACSM was configured for $\text{PM}_{2.5}$, as many of these instruments measure PM_{10}

Response: Thank you. It has been pointed out in the revised manuscript in [lines 136-137](#) as “Then a Time-of-Flight Aerosol Chemical Speciation Monitor equipped a $\text{PM}_{2.5}$ aerodynamic lens (ToF-ACSM, Aerodyne)”.

Line 207: Why does it matter if $\text{PM}_{2.5}$ is above $75 \mu\text{g m}^{-3}$? I assume you are referring to the regulatory limits, but it is good to be clear on this.

Response: Thank you. Yes, it the regulatory limits. The air quality is in pollution level if the $\text{PM}_{2.5}$ concentration is above $75 \mu\text{g m}^{-3}$ according to the national air quality standards. In the revised manuscript ([lines 247-249](#)), we revised the sentences “During the observation period, 20-60% of hourly $\text{PM}_{2.5}$ concentration was higher than $75 \mu\text{g m}^{-3}$ (the criterion for pollution according to the national air quality standards) in each month (Fig. S3A)”

Line 211: I am a bit confused by your explanation for there being more pollution episodes and higher concentrations of BC, CO and $\text{PM}_{2.5}$ in March, as it was the heating season. But isn't February just as cold? So why would there more heating in March?

Response: Thank you for your comments. In Beijing, the air quality is always determined by both the emission and meteorological conditions. In both February and March are in heating season. However, in March the meteorological condition is more favorable for haze formation due to low wind speed and low PBL height. This is a long sentence in the original manuscript. We revised it as “**This can be explained by both the intensive emission during the heating season as evidenced by the high concentration of primary pollutants including CO, SO₂ and BC (Table S1) and the stagnant meteorological conditions supported by the low wind speed (<2 m s⁻¹) and the low planetary boundary layer (PBL) height, in particular, in March (Fig. S4A)**” in [lines 251-255](#) in the revised manuscript.

Line 222: Are the percentages listed for nitrate, chloride and ammonium also monthly means?

Response: Yes, they are monthly means. It has been pointed out in the revised manuscript. “At the same time, **the monthly mean fraction of** nitrate and chloride decreased from 26.7±8.8 % to 16.7±12.8 % and from 7.7±6.1 % to 0.3±0.2 %, respectively” in [lines 260-262](#) in the revised manuscript.

Line 226: I am bit surprised that fireworks is regionally transported from Tangshan, are there no fireworks in Beijing?

Response: Thanks. According to the regulation on fireworks of Beijing government, firework burning is totally forbidden within the fifth ring road of Beijing. Based on back trajectory analysis of air masses, we found that firework burning in Tangshan should also contribute to the high mass concentration of chloride in Beijing during Chinese New Year.

Line 232-240: As example to one of my main comments above, I found that this paragraph was repeating much of the information presented in the preceding one. Perhaps these two paragraphs could be edited and combined.

Response: Thank you for your suggestion. We deleted the paragraph “It should be noted that the median mass concentrations of nitrate and OA also were higher in March than that in other months (Fig. S4C). The median mass concentrations of nitrate were 1.42, 8.76, 6.30, 3.15, and 3.23 $\mu\text{g m}^{-3}$ from February to June, respectively. And the corresponding OA concentrations

were 4.78, 14.04, 11.64, 13.89, and 14.08 $\mu\text{g m}^{-3}$. Secondary formation is the major source of OA and nitrate in the atmosphere” in [lines 232-237](#) in the original manuscript.

Line 272: why have you chosen to subset the data based on ‘when the $\text{PM}_{2.5}$ concentration was larger than $50 \mu\text{g m}^{-3}$ and the RH was less than 90 %’. Furthermore, as you state ‘Under these conditions, local chemistry should be more important as 75 % of the wind speed was less than 1.0 m s^{-1} . Why not then subset the data based solely on wind speed if local sources are of interest?’

Response: Thank you for your comment. Because the aim of this paper is to understand the influence of HONO on secondary aerosol formation and the possible HONO source during pollution events. The dataset based solely on wind speed less than 1.0 m s^{-1} could be also meaningful to discuss local chemistry. However, there are around one third data with low wind speed ($<1.0 \text{ m s}^{-1}$) and low $\text{PM}_{2.5}$ concentration ($< 50 \mu\text{g m}^{-3}$). Therefore, the concentration of $\text{PM}_{2.5}$ was considered as one of the standards in this work. In the revised manuscript ([lines 307-311](#)), we revised it as “We simply compared the OH production via photolysis of HONO ($P_{\text{OH-HONO}}=J_{\text{HONO}}\times\text{CHONO}$) and O_3 ($P_{\text{OH-O}_3}=J_{\text{O}_3}\times\text{CO}_3$) in Fig. 2 when the $\text{PM}_{2.5}$ concentration was larger than $50 \mu\text{g m}^{-3}$ and the RH was less than 90 % **to understand the chemistry in pollution events**”.

Line 275: How where these maximal $P_{\text{OH-HONO}}$ and $P_{\text{OH-O}_3}$ values calculated? I could not find the equation in the methods or reference.

Response: Thank you for your comment. They were calculated according to $P_{\text{OH-HONO}}=J_{\text{HONO}}*\text{CHONO}$ and $P_{\text{OH-O}_3}=J_{\text{O}_3}*\text{CO}_3$. In [lines 307-311](#) in the revised manuscript, we defined them. “We simply compared the OH production via photolysis of HONO ($P_{\text{OH-HONO}}=J_{\text{HONO}}\times\text{CHONO}$) and O_3 ($P_{\text{OH-O}_3}=J_{\text{O}_3}\times\text{CO}_3$) in Fig. 2 when the $\text{PM}_{2.5}$ concentration was larger than $50 \mu\text{g m}^{-3}$ and the RH was less than 90 % **to understand the chemistry in pollution events**”. In addition, the J values were also added in Fig. S7 and Fig. R2.

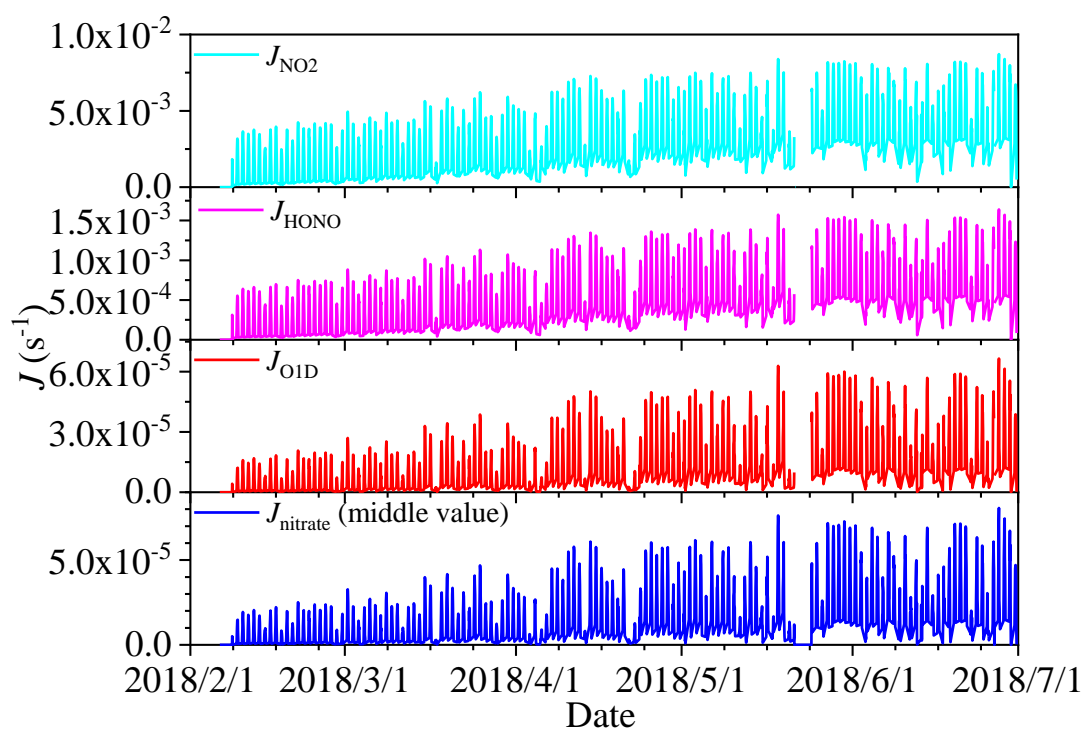


Fig. R2. The photolysis rate of NO₂, HONO, O₃ (O1D) and nitrate (middle value) from 8:00 am to 6:00 pm.

Line 304: Is it not the production of the OH that changes in winter relative to summer, rather than the rate of oxidation of VOC by OH? Please clarify

Response: Thank you. We mean OH production from photolysis of HONO will compensate the relative weak sunlight in winter. As you suggested above, we removed this redundant sentences (This implies that oxidation of atmospheric trace gases by OH may still be highly effective even in winter, thereby facilitating the vigorous formation of secondary pollutants in Beijing) in [lines 301-304](#) in the original manuscript.

Line 318-20 and Fig 2: I am not so sure that is 'reasonable to mainly ascribe the increase of OA concentration to local secondary formation initiated by OH radical from HONO photolysis'. This is because if only OH from HONO photolysis was driving secondary formation, then shouldn't the OA/CO peak earlier, as the ambient HONO is essentially run out by 10am?

Response: Thank you for your instructive comment. During pollution events in winter in Beijing, the absolute HONO concentration was still above 0.6 ppb at noon (Fig. R3). The

instrument automatically carried out zero point calibration twice per day during our observation. The measured HONO concentration at noon was much higher than the detection limit (10 ppt). Therefore, it reflected the real HONO concentration. Thus, it means that a photochemical steady state should be achieved between the daytime HONO sources and sinks and OH from photolysis of HONO should play an important role in initiation the HO_x and RO_x chemistry even after 10:00 am. In lines 350-353 in the revised manuscript, we revised this sentence to “...it was reasonable to ascribe the increase of OA concentration to local secondary formation initiated by OH radical and photolysis of HONO should play an important role in initiation the HO_x and RO_x chemistry”.

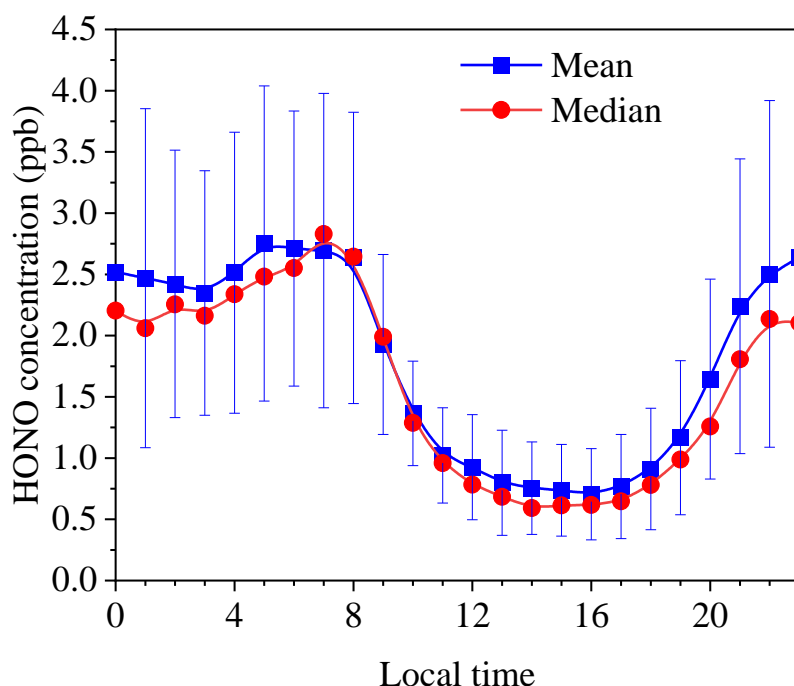


Fig. R3. The diurnal curve of HONO concentration during pollution events in winter.

Line 324: But can't there also be anthropogenic sources of alkenes? For example, isoprene can also be from vehicle emissions (See e.g. Zou et al 2019).

Response: Thank you. We agree with you that vehicles can also emit isoprene. In August, 2019, we measured the isoprene using a GC-FID, the mean isoprene concentration was 0.35 ppb. And the mean concentration was 0.5 ± 0.3 ppb at noon and 0.11 ± 0.11 ppb in night, respectively. The nighttime isoprene concentration was comparable with that in winter (0.13 ppb) in Guangzhou (Zou et al., 2019). If we assume the isoprene concentration in winter being

equivalent to the nighttime concentration in August, the SOA formation potential of isoprene is $0.015 \pm 0.015 \mu\text{g m}^{-3}$. This contributes less than 0.5 % to the typical increase of OA concentration observed in this work. Therefore, we think the contribution of isoprene to the observed increase of OA concentration should be unimportant. In lines 358-360 in the revised manuscript, we added a sentence as “Although vehicles can emit isoprene (Zou et al., 2019), the contribution of isoprene to the observed increase of OA concentration should be unimportant due to the low concentration of isoprene in winter (Zou et al., 2019)”.

Line 379: at the start of the sentence, you state that hourly NO_x EI were available, yet than go to give a yearly emission factor? Why wasn't hourly EI used, and did you consider your measured NO_x concentrations, as the diurnal variation in NO_x would be important? Please clarify in more detail how the Vehicle was calculated Especially as emission inventories can have significant bias (See for example very recent work for Beijing by Squires et al, 2020).

Response: Thank you for your good suggestion. In this work, we used the hourly emission inventory of NO_x (Fig. R4A) (Yang et al., 2019) to calculate the emission rate of HONO from vehicles. When calculating the emission rate of HONO, we converted the the hourly emission inventory (*EI*) to hourly emission flux ($F=EI/A$, where *A* is the area of Beijing). Then, the emission flux was normalized to the hourly mean PBL height according to Eq. (2). This resulted into the diurnal variation of NO_x. If the annual emission inventory was used to calculate the emission rate of HONO, the daily emission inventory was required to normalize to the measured NO_x concentration to catch the diurnal variation. As shown in Fig. R4B, the emission rate of HONO using these two methods are overall comparable, but the daytime emission rate of HONO based on the hourly emission inventory is higher than that calculated using the annual emission inventory. We used the hourly emission inventory because it contained the traffic details on road such as emission factor of NO_x for vehicle category, speed, traffic volume and congestion map and so on (Yang et al., 2019).

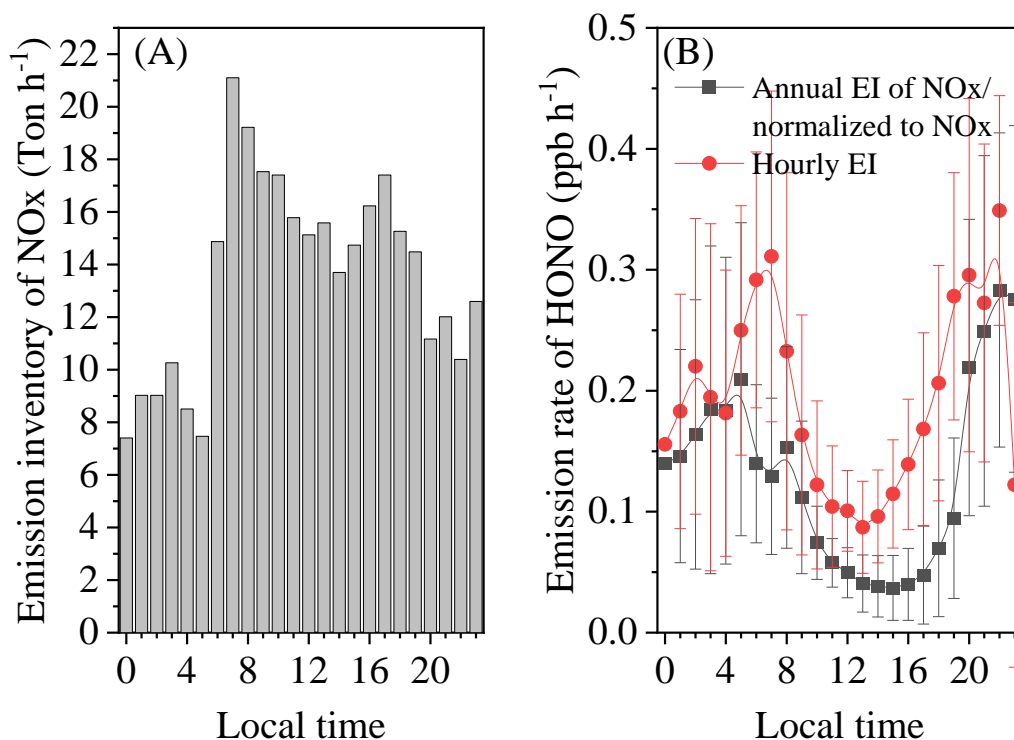


Fig. R4. (A) Hourly emission inventory of NO_x from vehicles in Beijing (Yang et al., 2019) and calculated emission rate of HONO from vehicles using different methods.

To make it clearer, in lines 180-185 the revised manuscript, we added more details as “The emission rate (E_{HONO} , ppbv h⁻¹) was calculated based on the emission flux ($F_{HONO}=EI_{HONO}/A$, g m⁻² s⁻¹) and PBL height (H , m) according to the following equation,

$$E_{HONO} = \frac{\alpha \cdot F_{HONO}}{H} \quad (2)$$

where, EI_{HONO} , is the emission inventory of HONO (g s⁻¹), A is the urban area of Beijing (m²),

α is the conversion factor ($\alpha = \frac{1 \times 10^9 \cdot 3600 \cdot R \cdot T}{M \cdot P} = \frac{2.99 \times 10^{13} \cdot T}{M \cdot P}$), M is the molecular weight (g mol⁻¹), T is the temperature (K) and P is the atmospheric pressure (Pa)”.

In lines 421- 423 in the revised manuscript, we revised the sentence “The $E_{vehicle}$ was calculated using the hourly NO_x emission inventory from vehicles in Beijing (Yang et al., 2019) after converted to emission flux of HONO ($F_{HONO}=F_{NO_x} \times HONO/NO_x$) and the PBL height as described in Section 2.2”

We agree with you that a bias should exist for the emission inventory. According to the most recent work, the MEIC 2013 emissions inventory might significantly overestimate the

emission of NO_x in Beijing (Squires et al., 2020). In this work, we used the newest emission inventory (Yang et al., 2019) but not the MEIC 2013. We compared the wintertime emission flux of NO_x calculated using the emission inventory from Yang et al. (2019) with the emission flux reported by Squires et al. (2020) (Fig. R5). The former emission flux is as 2.4±0.5 times as the later one. This will introduce an additional uncertainty to our estimation. In lines 712-716 in the revised manuscript, we added a paragraph “The source of HONO from vehicles was calculated based on the emission inventories, which should have a significant bias (Squires et al., 2020). For example, the emission flux of NO_x calculated using the emission inventory from Yang et al. (2019) is as 2.4±0.5 times as the reported emission flux reported by Squires et al. (2020).”.

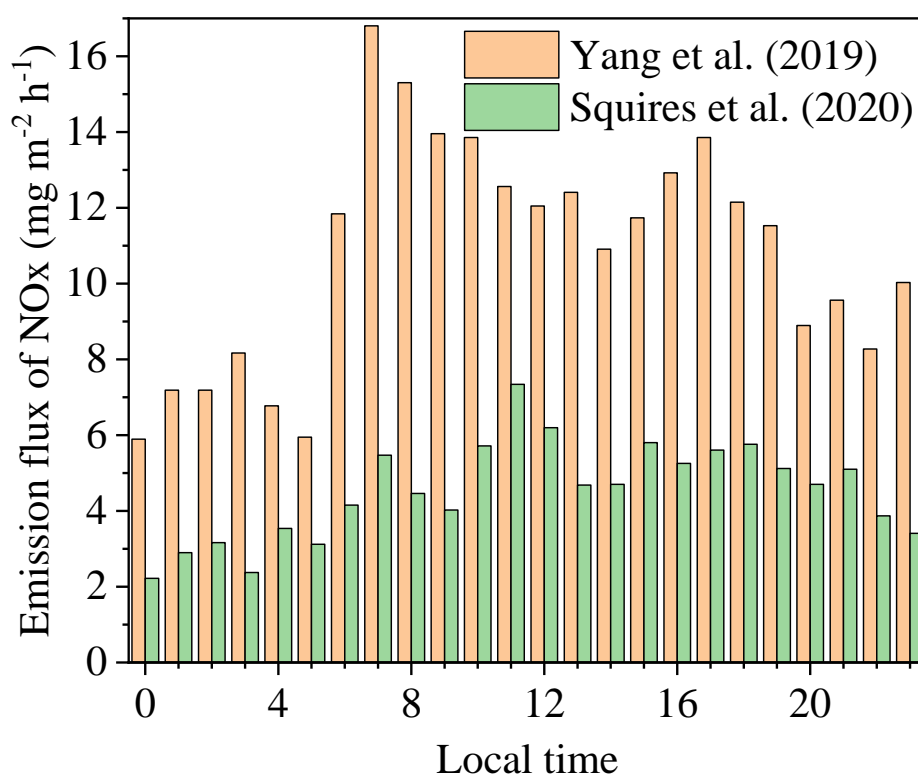


Fig. R5. Comparison of the wintertime emission flux of NO_x based on different emission inventory.

Line 381: This may be related to the above comment, but how did you report a range for calculated middle value of vehicle, when the NO_x EI rate is constant and the HONO/NO_x is constant? Furthermore, what does the middle value refer to? Daily avg? hourly avg? please

specify. This applies throughout this section

Response: Thank you. As discussed above, the hourly emission of NO_x reflected the diurnal variation vehicle emission. In addition, the variation of PBL height was considered when we calculating the emission rate. Although the HONO/NO_x was constant, the emission rate should show a diurnal variation. Three different emission rates of HONO were calculated because we chose three levels of HONO/NO_x, i.e., the lower limit is 0.18% measured using a Chassis dynamometer test (Liu et al., 2017), 1.17% calculated using the low limit correlation of field data and 1.8 % using the empirical analysis of field data in this work. We called “middle value” for the emission rate calculated using HONO/NO_x=1.17%. In lines 423-425 in the revised manuscript, we added a sentence “Thus the calculated emission rate reflected the diurnal variation of both the emission inventory and the PBL height”. In lines 425-427 in the revised manuscript, the sentence was revised “The calculated hourly middle value of E_{vehicle} using the HONO/NO_x of 1.17% was from 0.085 ± 0.038 to 0.34 ± 0.15 ppbv h⁻¹, which was slightly higher than the daytime emission rate of HONO in Xi’an (Huang et al., 2017b)”.

Line 386: the reported range for the upper limit is the same as reported for the lower limit, I’m guessing a typo?

Response: Thank you. From line 428 to 431 in the revised manuscript, “The lower limit of E_{vehicle} was $0.013 \pm 0.006 - 0.053 \pm 0.023$ ppbv h⁻¹, which was close to the estimated emission rate of HONO in Jinan (Li et al., 2018). The upper limit was in the range of $0.13 \pm 0.06 - 0.53 \pm 0.23$ ppbv h⁻¹”. The upper limit is one order of magnitude higher than the lower limit because the corresponding HONO/NO_x is 0.18 % and 1.8%.

Line 389: Please give the reference for the emission flux you used, the value and also why grassland was the most appropriate.

Response: Thank you. Oswald et al. measured the emission flux of HONO from 17 soil samples, including eucalyptus forest, tropical rain forest, coniferous forest, pasture, woody savannah, grassland, stone desert, maize field, wheat field, jujube field an cotton field etc. (Oswald et al., 2013). Tropical rain forest, coniferous forest and grassland are the typical plants in downtown Beijing (Huang et al., 2017a). At the same time, their emission fluxes of HONO

are comparable (Oswald et al., 2013). Thus, we used the emission flux from grassland to calculate the emission rate of HONO from soil in Beijing because the temperature and water holding content dependent emission flux of grassland was available (Fig. R6). We added this paragraph “Oswald et al. (2013) measured the emission flux of HONO from 17 soil samples, including eucalyptus forest, tropical rain forest, coniferous forest, pasture, woody savannah, grassland, stone desert, maize field, wheat field, jujube field an cotton field etc. Tropical rain forest, coniferous forest and grassland are the typical plants in downtown Beijing (Huang et al., 2017a). At the same time, their emission fluxes of HONO are comparable (Oswald et al., 2013). Thus, we used the emission flux from grassland to calculate the emission rate of HONO from soil in Beijing because the temperature and water holding content dependent emission flux of HONO from grassland soil was available” in lines 433-441 in the revised manuscript.

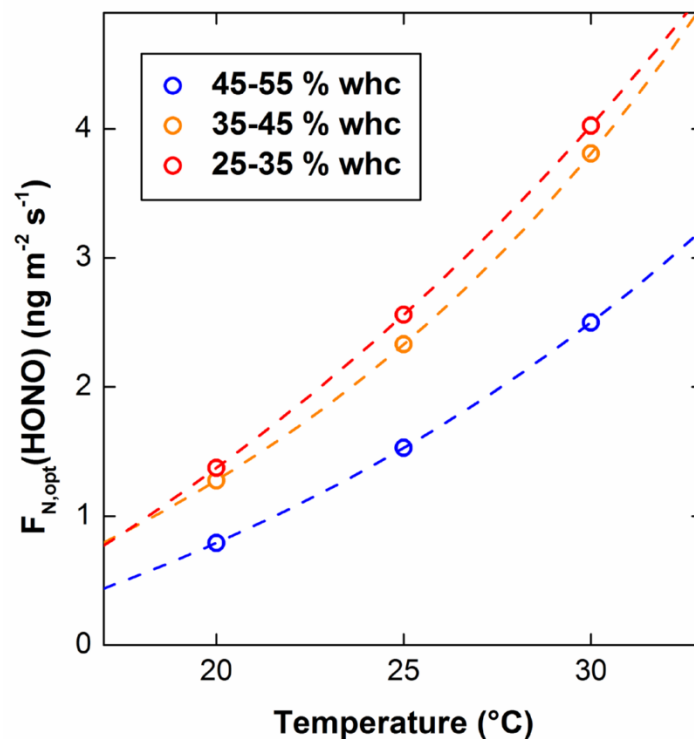


Fig. R6. The emission flux of HONO from grassland at different temperature and water holding capacity (Oswald et al., 2013).

Line 397: why does only the middle values for E_{soil} have uncertainty calculated? Also how did you estimate the uncertainty for E_{soil} ? And why did you use a range of soil water content for lower, middle and upper, why not just use a single value?

Response: Thank you. We added the uncertainties of other values in [lines 446-448](#) in the revised manuscript. “The lower limit, the middle value and the upper limit of the E_{soil} are $0.0032\pm 0.0027-0.013\pm 0.014$, $0.0046\pm 0.0039-0.020\pm 0.20$ and $0.0057\pm 0.0047-0.025\pm 0.024$ ppbv h⁻¹, respectively, **calculated according to Eq. (2)**”. The uncertainty is the standard deviation when calculating the diurnal curve. We didn’t measure the water content of the soil, while it should vary with seasons. Thus, we used a range of soil water content rather than a single value. For other sources, we also added all the uncertainties in the revised manuscript.

Line 416: Please provide more information on the night time temperature dependence of OH concentration, and the equations used in this calculation.

Response: Thank you. In the night, OH concentration usually varied from 1.0×10^5 molecules cm⁻³ (Li et al., 2012; Tan et al., 2018) in winter to 5×10^5 molecules cm⁻³ in summer (Tan et al., 2017). In the original manuscript, we linearly calculated the nighttime OH from 1×10^5 to 4×10^5 molecules m⁻³ according to

$$c_{OH,night} = 1 \times 10^5 + 4 \times 10^5 \times \frac{T - T_{min,night}}{T_{max,night} - T_{min,night}} \quad (\text{R1}).$$

In the revised manuscript, we updated the calculation method as suggested by another reviewer. Because the nighttime OH is mainly generated from reaction of O₃ with alkenes measured with the SPIMS, we changed the estimation method using

$$c_{OH,night} = 1 \times 10^5 + 4 \times 10^5 \times \frac{(c_{O_3} \times c_{alkenes})_{night} - (c_{O_3} \times c_{alkenes})_{night,min}}{(c_{O_3} \times c_{alkenes})_{night,max} - (c_{O_3} \times c_{alkenes})_{night,min}} \quad (\text{R2}).$$

In [lines 468-471](#) in the revised manuscript, we changed it as “**The nighttime OH concentration was estimated linearly correlated with the product of nighttime O₃ concentration and alkenes concentration, namely,**

$$c_{OH,night} = 1 \times 10^5 + 4 \times 10^5 \times \frac{(c_{O_3} \times c_{alkenes})_{night} - (c_{O_3} \times c_{alkenes})_{night,min}}{(c_{O_3} \times c_{alkenes})_{night,max} - (c_{O_3} \times c_{alkenes})_{night,min}} \quad (16)”$$

Line 419: Please give the reported OH concentrations by Li et al (2018) and Huang et al (2017) and if they were calculated or measured OH levels.

Response: Thank you. Here we compared the production rate of HONO from homogenous reaction between NO and OH among different researches but not OH concentration. In [lines 475-478](#) in the revised manuscript, we added the corresponding $P_{\text{NO-OH}}$ as “The calculated

middle value of $P_{\text{NO-OH}}$ (with mean daytime value of $0.49 \pm 0.35 \text{ ppb h}^{-1}$) was comparable with these estimated values by Li et al. (2018) (0.4 ppb h^{-1}) and Huang et al. (2017b) (0.28 ppb h^{-1})”.

Line 433: How was the HONO from nitrate photolysis calculated? Which equation (give number)? What do these ranges represent?

Response: Thank you. HONO formation from nitrate photolysis was calculated according to Eqs (3) and (8). Bao et al. reported the J_{nitrate} at zenith angle of 0° . We normalized the J_{nitrate} with the zenith angle at our observation station. The time series of the middle value was shown in Fig. R2 and was also added in Fig. S7. In lines 489-495 in the revised manuscript, we revised it. “A recent work reported the photolysis rate of nitrate (J_{nitrate}) in ambient $\text{PM}_{2.5}$ at a solar zenith angle of 0° (Bao et al., 2018). The J_{nitrate} varied from 1.22×10^{-5} to $4.84 \times 10^{-4} \text{ s}^{-1}$ with the mean value of $8.24 \times 10^{-5} \text{ s}^{-1}$. These values were further normalized according to the zenith angle and UV light at our observation station to calculate the low limit, the upper limit and the middle J_{nitrate} . The time series of the measured nitrate concentration and the middle value of J_{nitrate} were shown in Fig. 1 and Fig. S7, respectively”. In addition, the equation numbers was pointed out in line 498 in the revised manuscript. “The corresponding daytime lower limit, the middle value and the upper limit of HONO from photolysis of nitrate were 0.0011 ± 0.0021 - 0.096 ± 0.092 , 0.0072 ± 0.0021 - 0.66 ± 0.092 and 0.042 ± 0.082 - $3.86 \pm 0.008 \text{ ppbv h}^{-1}$, respectively, calculated in the light of Eqs. (3) and (8)”.

Line 447: by the end of this paragraph, it was not at all clear to me which uptake co-efficient you actually used. Please clarify.

Response: Thank you. In the dark, the low limit, middle value and upper limit of P_{aerosol} were calculated using the RH dependent γ_{NO_2} on kaolin ($4.47 \times 10^{39} / (1.75 \times 10^{46} + 1.93 \times 10^{45} \text{RH})$) (Liu et al., 2015), the fixed γ_{NO_2} (1.2×10^{-8}) recommended by Crowley et al. (Crowley et al., 2010) and the RH dependent γ_{NO_2} on kaolin on hematite ($\gamma_{\text{NO}_2} = 4.46 \times 10^{39} / (6.73 \times 10^{44} + 3.48 \times 10^{44} \text{RH})$) (Liu et al., 2015), respectively, along with the γ_{NO_2} on black carbon (1.17×10^{-5}). In the daytime, the light enhanced uptake γ of NO_2 (1.9×10^{-6}) on mineral dust was parameterized (Ndour et al., 2008) after normalized to the solar radiation intensity in Beijing.

For P_{ground} , the low limit, middle value and upper limit of P_{ground} were calculated using the same γ_{NO_2} as P_{aerosol} in night, while γ_{NO_2} of NO_2 on urban regime ($\gamma_{\text{NO}_2}=7.4 \times 10^{-7}+5.5 \times 10^{-8}$ RH) (Liu et al., 2019) was used after normalized to the light intensity at BUCT in the daytime. In the revised manuscript, we pointed out these equations as “($\gamma_{\text{NO}_2}=4.47 \times 10^{39}/(1.75 \times 10^{46} + 1.93 \times 10^{45}\text{RH}$)”, “($\gamma_{\text{NO}_2}=4.46 \times 10^{39}/(6.73 \times 10^{44} + 3.48 \times 10^{44}$ RH)” and “($\gamma_{\text{NO}_2}=7.4 \times 10^{-7}+5.5 \times 10^{-8}$ RH)” in lines 507-508, 509 and 521, respectively.

Line 477-9: the authors state that ‘Heterogeneous reactions of NO_2 on aerosol surface and ground surfaces were unimportant compared with other sources because of the very low uptake coefficient’. What do you mean by the very low uptake coefficient, low compared to what? Is the issue more that you used the wrong co-efficient?

Response: Thank you. For heterogeneous reaction of NO_2 on aerosol surface, the production rate is determined by the uptake coefficient according to Eqs. (3)-(5). Modelling studies have found that a given chemical process should be important in the tropospheric chemistry if the uptake coefficient of a trace gas on particles is greater than 10^{-5} (Zhang and Carmichael, 1999;Zheng et al., 2015). As discussed in this work, the typical uptake coefficient of NO_2 on aerosol is on the order of 10^{-7} - 10^{-8} . It was it was recommended to be 1.2×10^{-8} (Crowley et al., 2010). Furthermore, we also performed laboratory studies about uptake of NO_2 on kaolin, hematite and soot particles. The uptake coefficient on mineral dust is on the order of 10^{-7} - 10^{-8} (Liu et al., 2015). In addition, we found that the $\gamma_{\text{NO}_2, \text{BET}}$ at steady state (or after aged in air) was one order of magnitude lower than that of fresh sample. Therefore, we chose the $\gamma_{\text{NO}_2, \text{BET}}$ 10^{-7} - 10^{-8} in this work. It was lower than that (10^{-6}) used in modeling studies (Zhang et al., 2016;Aumont et al., 2003).

We double checked the parameters for budget calculation. We found a bug when calculating the heterogeneous reaction of NO_2 on black carbon. A conversion factor of time from second to hour was missed. So, the contribution of heterogeneous reaction to HONO source was underestimated. Now, the P_{aerosol} was 0.038 ± 0.030 - 0.088 ± 0.072 . It was on the same orders as soil emission. In the revised manuscript, we updated Figures 3-5 and the corresponding numbers in section 3.3.

In lines 544-554 the revised manuscript, we added a paragraph “It should be pointed out

that HONO production from heterogeneous reaction of NO₂ on both aerosol and ground surface greatly depend on the $\gamma_{\text{NO}_2, \text{BET}}$ and A_s . The A_s of aerosols was comparable with the modeling input. However, the small nighttime $\gamma_{\text{NO}_2, \text{BET}}$ (10^{-8} - 10^{-7}) on dust were used in this work rather than the $\gamma_{\text{NO}_2, \text{BET}}$ (1×10^{-6}) used in modelling studies (Zhang et al., 2016; Aumont et al., 2003; Gall et al., 2016). This leads to a lower production rate of HONO from heterogeneous reaction of NO₂ on aerosols. As for heterogeneous reaction of NO₂ on ground surface, besides the small $\gamma_{\text{NO}_2, \text{BET}}$ used in this work, the A_s of ground surface (0.0015 to 0.0385 m⁻¹) calculated using the surface roughness and PBL height was also significantly lower than the fixed value of 0.3 m⁻¹ in modeling studies that might overestimate the contribution of HONO production from heterogeneous reaction of NO₂ on ground surface”. In lines 558-561 in the revised manuscript, we revised the sentences as “These results mean that heterogeneous reaction might not be a major HONO source. This is consistent with a recent work that heterogeneous reaction should be unimportant when compared with traffic emission during haze events in winter in Beijing (Zhang et al., 2019)”. And in lines 605-607 in the revised manuscript, we also revised the sentence “Heterogeneous reactions of NO₂ on aerosol surface and ground surfaces were not the major HONO source during night unlike the modelled results (Zhang et al., 2016; Aumont et al., 2003).”.

Fig 2D: if you take the bottom and top points in Feb/Mar (blue), I am not sure there this a correlation. It would be good to check if you get a similar slope and r² without these 2 points.

Response: Thank you. If we remove these two points as you suggested, the correlation coefficient will decrease from 0.74 to 0.31. A positive correlation can be still observable when the uncertainty is taken into consideration (Fig. R7). We think it is unreasonable to remove them because these data points are valid. We agree with you that it should be better if more data points are available. This will be further investigated in the future.

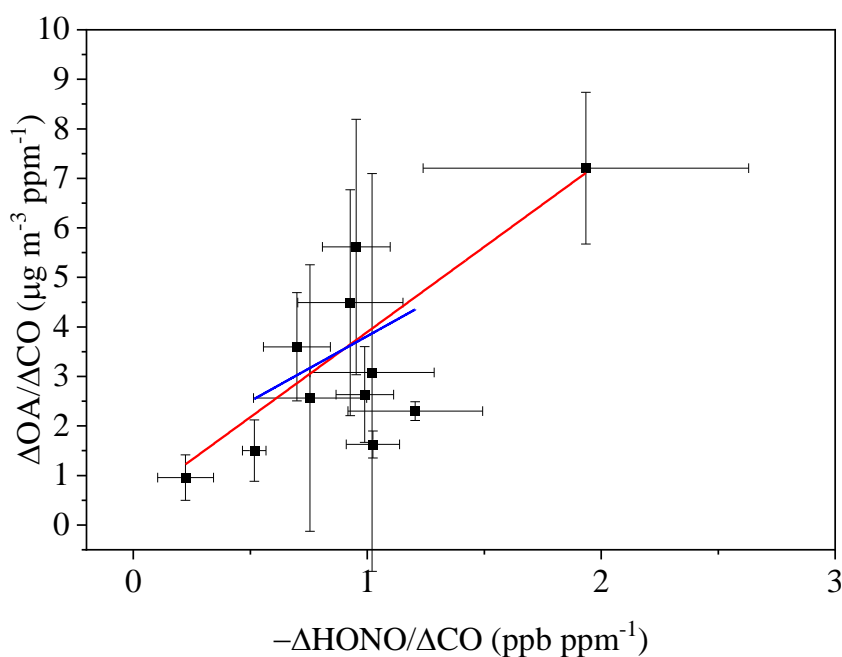


Fig. R7 Correlation of the daytime OA/CO increased and consumed HONO/CO in March.

References

- Aumont, B., Chervier, F., and Laval, S.: Contribution of HONO sources to the NO_x/HO_x/O₃ chemistry in the polluted boundary layer, *Atmos. Environ.*, 37, 487-498, [https://doi.org/10.1016/S1352-2310\(02\)00920-2](https://doi.org/10.1016/S1352-2310(02)00920-2), 2003.
- Bao, F., Li, M., Zhang, Y., Chen, C., and Zhao, J.: Photochemical Aging of Beijing Urban PM_{2.5}: HONO Production, *Environ. Sci. Technol.*, 52, 6309-6316, [10.1021/acs.est.8b00538](https://doi.org/10.1021/acs.est.8b00538), 2018.
- Crowley, J. N., Ammann, M., Cox, R. A., Hynes, R. G., Jenkin, M. E., Mellouki, A., Rossi, M. J., Troe, J., and Wallington, T. J.: Evaluated kinetic and photochemical data for atmospheric chemistry: Volume V – heterogeneous reactions on solid substrates, *Atmos. Chem. Phys.*, 10, 9059-9223, doi: 10.5194/acp-10-9059-2010, 2010.
- Gall, E. T., Griffin, R. J., Steiner, A. L., Dibb, J., Scheuer, E., Gong, L., Rutter, A. P., Cevik, B. K., Kim, S., Lefer, B., and Flynn, J.: Evaluation of nitrous acid sources and sinks in urban outflow, *Atmos. Environ.*, 127, 272-282, <https://doi.org/10.1016/j.atmosenv.2015.12.044>, 2016.
- Han, C., Liu, Y., and He, H.: Role of Organic Carbon in Heterogeneous Reaction of NO₂ with Soot, *Environ. Sci. Technol.*, 47, 3174-3181, [10.1021/es304468n](https://doi.org/10.1021/es304468n), 2013.
- Huang, H., Chen, Y., Clinton, N., Wang, J., Wang, X., Liu, C., Gong, P., Yang, J., Bai, Y., Zheng, Y., and Zhu, Z.: Mapping major land cover dynamics in Beijing using all Landsat images in Google Earth Engine, *Remote Sensing of Environment*, 202, 166-176, <https://doi.org/10.1016/j.rse.2017.02.021>, 2017a.
- Huang, R.-J., Yang, L., Cao, J., Wang, Q., Tie, X., Ho, K.-F., Shen, Z., Zhang, R., Li, G., Zhu, C., Zhang, N., Dai, W., Zhou, J., Liu, S., Chen, Y., Chen, J., and O'Dowd, C. D.: Concentration and sources of atmospheric nitrous acid (HONO) at an urban site in Western China, *Sci. Total Environ.*, 593, 165-172, [10.1016/j.scitotenv.2017.02.166](https://doi.org/10.1016/j.scitotenv.2017.02.166), 2017b.
- Kanaya, Y., Cao, R., Akimoto, H., Fukuda, M., Komazaki, Y., Yokouchi, Y., Koike, M., Tanimoto, H., Takegawa, N., and Kondo, a. Y.: Urban photochemistry in central Tokyo: 1. Observed and modeled OH and HO₂ radical concentrations during the winter and summer of 2004, *J. Geophys. Res.- Atmos.*, 112, [10.1029/2007JD008670](https://doi.org/10.1029/2007JD008670),

2007.

Li, D., Xue, L., Wen, L., Wang, X., Chen, T., Mellouki, A., Chen, J., and Wang, W.: Characteristics and sources of nitrous acid in an urban atmosphere of northern China: Results from 1-yr continuous observations, *Atmos. Environ.*, 182, 296-306, <https://doi.org/10.1016/j.atmosenv.2018.03.033>, 2018.

Li, X., Brauers, T., H^äseler, R., Bohn, B., Fuchs, H., Hofzumahaus, A., Holland, F., Lou, S., Lu, K. D., Rohrer, F., Hu, M., Zeng, L. M., Zhang, Y. H., Garland, R. M., Su, H., Nowak, A., Wiedensohler, A., Takegawa, N., Shao, M., and Wahner, A.: Exploring the atmospheric chemistry of nitrous acid (HONO) at a rural site in Southern China, *Atmos. Chem. Phys.*, 12, 1497-1513, 2012.

Li, Z. Q., Guo, J. P., Ding, A. J., Liao, H., Liu, J. J., Sun, Y. L., Wang, T. J., Xue, H. W., Zhang, H. S., and Zhu, B.: Aerosol and boundary-layer interactions and impact on air quality, *Natl. Sci. Rev.*, 4, 810-833, [10.1093/nsr/nwx117](https://doi.org/10.1093/nsr/nwx117), 2017.

Liu, J., Li, S., Mekic, M., Jiang, H., Zhou, W., Loisel, G., Song, W., Wang, X., and Gligorovski, S.: Photoenhanced Uptake of NO₂ and HONO Formation on Real Urban Grime, *Environmental Science & Technology Letters*, 6, 413-417, [10.1021/acs.estlett.9b00308](https://doi.org/10.1021/acs.estlett.9b00308), 2019.

Liu, Y., Han, C., Ma, J., Bao, X., and He, H.: Influence of relative humidity on heterogeneous kinetics of NO₂ on kaolin and hematite, *Phys. Chem. Chem. Phys.*, 17, 19424-19431, doi: 10.1039/C5CP02223A, 2015.

Liu, Y., Lu, K., Ma, Y., Yang, X., Zhang, W., Wu, Y., Peng, J., Shuai, S., Hu, M., and Zhang, Y.: Direct emission of nitrous acid (HONO) from gasoline cars in China determined by vehicle chassis dynamometer experiments, *Atmos. Environ.*, 169, 89-96, [10.1016/j.atmosenv.2017.07.019](https://doi.org/10.1016/j.atmosenv.2017.07.019), 2017.

Ndour, M., D'Anna, B., George, C., Ka, O., Balkanski, Y., K., J., S., and K., A., M.: Photoenhanced uptake of NO₂ on mineral dust: Laboratory experiments and model simulations, *Geophys. Res. Lett.*, 35, L05812, doi:05810.01029/02007GL032006, 2008.

Oswald, R., Behrendt, T., Ermel, M., Wu, D., Su, H., Cheng, Y., Breuninger, C., Moravek, A., Mougins, E., Delon, C., Loubet, B., Pommerening-Röser, A., Sörgel, M., Pöschl, U., Hoffmann, T., Andreae, M. O., Meixner, F. X., and Trebs, I.: HONO Emissions from Soil Bacteria as a Major Source of Atmospheric Reactive Nitrogen, *Science*, 341, 1233-1235, [10.1126/science.1242266](https://doi.org/10.1126/science.1242266), 2013.

Ren, X., Brune, W. H., Mao, J., Mitchell, M. J., Leshner, R. L., Simpas, J. B., Metcalf, A. R., Schwab, J. J., Cai, C., Li, Y., Demerjian, K. L., Felton, H. D., Boynton, G., Adams, A., Perry, J., He, Y., Zhou, X., and Hou, J.: Behavior of OH and HO₂ in the winter atmosphere in New York City, *Atmos. Environ.*, 40, 252-263, <https://doi.org/10.1016/j.atmosenv.2005.11.073>, 2006.

Squires, F. A., Nemitz, E., Langford, B., Wild, O., Drysdale, W. S., Acton, W. J. F., Fu, P., Grimmond, C. S. B., Hamilton, J. F., Hewitt, C. N., Hollaway, M., Kotthaus, S., Lee, J., Metzger, S., Pinguha-Durden, N., Shaw, M., Vaughan, A. R., Wang, X., Wu, R., Zhang, Q., and Zhang, Y.: Measurements of traffic dominated pollutant emissions in a Chinese megacity, *Atmos. Chem. Phys. Discuss.*, 2020, 1-33, [10.5194/acp-2019-1105](https://doi.org/10.5194/acp-2019-1105), 2020.

Tan, Z., Fuchs, H., Lu, K., Hofzumahaus, A., Bohn, B., Broch, S., Dong, H., Gomm, S., H^äseler, R., He, L., Holland, F., Li, X., Liu, Y., Lu, S., Rohrer, F., Shao, M., Wang, B., Wang, M., Wu, Y., Zeng, L., Zhang, Y., Wahner, A., and Zhang, Y.: Radical chemistry at a rural site (Wangdu) in the North China Plain: observation and model calculations of OH, HO₂ and RO₂ radicals, *Atmos. Chem. Phys.*, 17, 663-690, [10.5194/acp-17-663-2017](https://doi.org/10.5194/acp-17-663-2017), 2017.

Tan, Z., Rohrer, F., Lu, K., Ma, X., Bohn, B., Broch, S., Dong, H., Fuchs, H., Gkatzelis, G. I., Hofzumahaus, A., Holland, F., Li, X., Liu, Y., Liu, Y., Novelli, A., Shao, M., Wang, H., Wu, Y., Zeng, L., Hu, M., Kiendler-Scharr, A., Wahner, A., and Zhang, Y.: Wintertime photochemistry in Beijing: observations of RO_x radical concentrations in the North China Plain during the BEST-ONE campaign, *Atmos. Chem. Phys.*, 18, 12391-12411, [10.5194/acp-18-12391-2018](https://doi.org/10.5194/acp-18-12391-2018), 2018.

Tan, Z. F., Lu, K. D., Jiang, M. Q., Su, R., Wang, H. L., Lou, S. R., Fu, Q. Y., Zhai, C. Z., Tan, Q. W., Yue, D. L.,

- Chen, D. H., Wang, Z. S., Xie, S. D., Zeng, L. M., and Zhang, Y. H.: Daytime atmospheric oxidation capacity in four Chinese megacities during the photochemically polluted season: a case study based on box model simulation, *Atmos. Chem. Phys.*, 19, 3493-3513, 10.5194/acp-19-3493-2019, 2019.
- Yang, D., Zhang, S., Niu, T., Wang, Y., Xu, H., Zhang, K. M., and Wu, Y.: High-resolution mapping of vehicle emissions of atmospheric pollutants based on large-scale, real-world traffic datasets, *Atmos. Chem. Phys.*, 2019, 8831–8843, 10.5194/acp-2019-32, 2019.
- Zhang, L., Wang, T., Zhang, Q., Zheng, J., Xu, Z., and Lv, M.: Potential sources of nitrous acid (HONO) and their impacts on ozone: A WRF-Chem study in a polluted subtropical region, *Journal of Geophysical Research-Atmospheres*, 121, 3645-3662, 10.1002/2015jd024468, 2016.
- Zhang, W., Tong, S., Ge, M., An, J., Shi, Z., Hou, S., Xia, K., Qu, Y., Zhang, H., Chu, B., Sun, Y., and He, H.: Variations and sources of nitrous acid (HONO) during a severe pollution episode in Beijing in winter 2016, *The Science of the total environment*, 648, 253-262, 10.1016/j.scitotenv.2018.08.133, 2019.
- Zhang, Y., and Carmichael, G.: Interactions of mineral aerosol with tropospheric chemistry, *J Appli. Meteor.*, 38, 353-366, 1999.
- Zheng, B., Zhang, Q., Zhang, Y., He, K. B., Wang, K., Zheng, G. J., Duan, F. K., Ma, Y. L., and Kimoto, T.: Heterogeneous chemistry: a mechanism missing in current models to explain secondary inorganic aerosol formation during the January 2013 haze episode in North China, *Atmos. Chem. Phys.*, 15, 2031-2049, doi: 10.5194/acp-15-2031-2015, 2015.
- Zou, Y., Deng, X. J., Deng, T., Yin, C. Q., and Li, F.: One-Year Characterization and Reactivity of Isoprene and Its Impact on Surface Ozone Formation at A Suburban Site in Guangzhou, China, *Atmosphere*, 10, 10.3390/atmos10040201, 2019.

1 **The promotion effect of nitrous acid on aerosol formation in**
2 **wintertime Beijing: possible contribution of traffic-related**
3 **emission**

4

5 Yongchun Liu^{1*}, Yusheng Zhang¹, Chaofan Lian^{2,6}, Chao Yan³, Zeming Feng¹, Feixue
6 Zheng¹, Xiaolong Fan¹, Yan Chen^{2,6}, Weigang Wang^{2,6*}, Biwu Chu^{3,4}, Yonghong Wang³,
7 Jing Cai³, Wei Du³, Kaspar R. Daellenbach³, Juha Kangasluoma^{1,3}, Federico Bianchi^{1,3},
8 Joni Kujansuu^{1,3}, Tuukka Petäjä³, Xuefei Wang⁶, Bo Hu⁵, Yuesi Wang⁵, Maofa Ge²,
9 Hong He⁴ and Markku Kulmala^{1,3*}

10

11 1. Aerosol and Haze Laboratory, Advanced Innovation Center for Soft Matter Science and
12 Engineering, Beijing University of Chemical Technology, Beijing, 100029, China

13 2. State Key Laboratory for Structural Chemistry of Unstable and Stable Species, Beijing
14 National Laboratory for Molecular Sciences, Institute of Chemistry, Chinese Academy of
15 Sciences, Beijing 100190, China

16 3. Institute for Atmospheric and Earth System Research/Physics, Faculty of Science, University
17 of Helsinki, P.O. Box 64, FI-00014, Finland

18 4. State Key Joint Laboratory of Environment Simulation and Pollution Control, Research
19 Center for Eco-Environmental Sciences, Chinese Academy of Sciences, Beijing, 100085, China

20 5. State Key Laboratory of Atmospheric Boundary Layer Physics and Atmospheric Chemistry,
21 Institute of Atmospheric Physics, Chinese Academy of Sciences, Beijing, 100029, China

22 6. University of Chinese Academy of Sciences, Beijing 100049, PR China

23 *Correspondence to:* liuyc@buct.edu.cn, wangwg@iccas.ac.cn or markku.kulmala@helsinki.fi

24

25 **Abstract**

26 Secondary aerosol is a major component of PM_{2.5}, yet its formation mechanism in the
27 ambient atmosphere is still an open question. Based on field measurements in
28 downtown Beijing, we show that the photolysis of nitrous acid (HONO) could promote
29 the formation of organic and nitrate aerosol in wintertime Beijing as evidenced by the
30 growth of the mass concentration of organic and nitrate aerosols linearly increasing as
31 a function of consumed HONO from early morning to noon. The increased nitrate also
32 lead to the formation of particulate matter ammonium by enhancing the neutralization
33 of nitric acid by ammonia. We further illustrate that over 50 % of the ambient HONO
34 during pollution events in wintertime Beijing might be related to traffic-related
35 emission including direct emission and formation via the reaction between OH and
36 vehicle-emitted NO. Overall, our results highlight that the traffic-related HONO plays
37 an important role in the oxidative capacity and in turn, contribute to the haze formation
38 in winter Beijing. Mitigation of HONO and NO_x emission from the vehicles might be
39 an effective way to reduce secondary aerosol mass formation and severe haze events in
40 wintertime Beijing.

41

42 **1. Introduction**

43 China is one of the most suffering countries from the pollution of fine particulate matter
44 with diameter less than or equal to 2.5 μm ($\text{PM}_{2.5}$) (Lelieveld et al., 2015). Although
45 the regional air quality has been continuously improving since the central government
46 of China issued the Clean Air Act in 2013 (Vu et al., 2019), $\text{PM}_{2.5}$ concentration is still
47 significantly higher than that in developed countries (Fu et al., 2014;An et al., 2019).
48 Nowadays, a consensus has been reached that haze events are driven by local emissions
49 (An et al., 2019), regional transport (Zheng et al., 2015b) and secondary formation
50 (Huang et al., 2014;He et al., 2018) of pollutants under unfavorable meteorological
51 conditions (stagnant atmosphere and high relative humidity) (Zhu et al., 2018;Liu et al.,
52 2017c). A feedback loop between meteorological parameters and haze formation has
53 also been found playing an important role in the evolution of haze events (Zhang et al.,
54 2018).

55 Secondary aerosol can contribute up to ~70 % to the aerosol mass concentration on
56 polluted days (Huang et al., 2014). Several reaction pathways have been proposed in
57 the atmospheric chemistry community, such as sulfate formation via heterogeneous
58 oxidation of SO_2 promoted by H_2O_2 and/or NO_2 on mineral dust (Huang et al., 2015;He
59 et al., 2014), aqueous oxidation of SO_2 promoted by NO_2 in the presence or absence of
60 NH_3 in particle-bound water film (He et al., 2014;Wang et al., 2016), catalytic
61 conversion of SO_2 to sulfate by black carbon (Zhang et al., 2020), nitrate formation via
62 efficient hydrolysis of N_2O_5 on aerosol surfaces (Wang et al., 2017c;Wang et al.,
63 2019;Kulmala, 2018;Li et al., 2017), and the haze formation initiated by new particle

64 formation and growth (Guo et al., 2014;Guo et al., 2020). During the past years, strict
65 control of coal combustion has successfully reduced the SO₂ concentration, resulting in
66 a reduction of sulfate (SO₄²⁻) component in PM_{2.5}; in stark contrast, the contributions
67 from organic and nitrate become increasingly more significant in China (Lang et al.,
68 2017).

69 The formation of secondary organic aerosol (SOA) starts from the gas-phase
70 oxidation of volatile organic compounds (VOCs) leading to various oxidized low-
71 volatility and semi-volatile products (Bianchi et al., 2019), followed by their
72 partitioning into the particle phase (Hallquist et al., 2009). Similarly, the formation of
73 nitrate aerosol in the daytime is largely due to the partitioning of gaseous nitric acid,
74 which is formed via the oxidation of NO₂ by OH (Seinfeld and Pandis, 2006;Wang et
75 al., 2019). It is traditionally believed that the wintertime atmospheric oxidation capacity
76 is weak due to the weak solar radiation, which limits the formation of SOA and nitrate
77 (Sun et al., 2013). However, it is very recently shown that the peak OH concentration
78 on polluted days in winter Beijing varies from 2×10⁶ to 6×10⁶ molecules cm⁻³, which
79 is 6-10 times higher than what is predicted by the global model (Tan et al., 2018). This
80 discrepancy can be largely reduced after accounting for other OH production processes
81 in model simulations, which shows that the photolysis of nitrous acid (HONO)
82 dominates the initiation of HO_x (OH and HO₂) and RO_x (RO and RO₂) radical chain in
83 wintertime Beijing (Tan et al., 2018), and some other cities (Ren et al., 2006;Stutz et
84 al., 2013).

85 The HONO concentration has been measured with a wide rang from 0.18 to 9.71

86 ppbv at different locations, such as Beijing (Zhang et al., 2019d;Hu et al.,
87 2002;Hendrick et al., 2014;Wang et al., 2017b), Shanghai (Wang et al., 2013;Zhang et
88 al., 2019b), Guangdong (Hu et al., 2002;Su et al., 2008a), Hongkong (Xu et al., 2015),
89 Shandong (Li et al., 2018), Xi'an (Huang et al., 2017b) and so on in China since 2000.
90 More recently, modelling studies have suggested that nitrous acid (HONO) could
91 enhance secondary aerosols formation in Beijing-Tianjin-Hebei (BTH) region (Zhang
92 et al., 2019c), Pearl-River-Delta (PRD) region of China (Zhang et al., 2019a;Xing et al.,
93 2019) and Houston (Czader et al., 2015). These results imply that the role of HONO in
94 haze chemistry might be crucial in wintertime Beijing, while the direct evidence from
95 observation has not been reported, yet. On the other hand, the HONO budget has been
96 investigated via modelling studies (Liu et al., 2019c;Zhang et al., 2019c) and
97 photostationary state calculations (Wang et al., 2017b;Li et al., 2018;Huang et al.,
98 2017b;Lee et al., 2016;Oswald et al., 2015;Zhang et al., 2019d) at different locations.
99 At the present time, the study of the HONO budget is still far from closed, which would
100 require a significant effort on both the accurate measurement of HONO and the
101 determination of related kinetic parameters for its production pathways (Liu et al.,
102 2019c). For example, photo-enhanced conversion of NO₂ (Su et al., 2008b) and
103 photolysis of particulate nitrate were found to be the two major mechanisms with large
104 potential of HONO formation during noontime, but the associated uncertainty may
105 reduce their importance (Liu et al., 2019c). The heterogeneous reactions of NO₂ on
106 ground/aerosol surfaces were proposed to be an important HONO source during
107 nighttime (Wang et al., 2017b;Zhang et al., 2019c) and daytime in Beijing-Tianjin-

108 Hebei (BTH) (Zhang et al., 2019c), but it was unimportant compared with the unknown
109 sources and the homogeneous reaction between NO and OH in Ji'an (Li et al., 2018) or
110 compared with the traffic emission on haze days in Beijing (Zhang et al., 2019d). The
111 traffic emission was found to be an important HONO source during nighttime and a
112 minor daytime HONO source in BTH (Zhang et al., 2019c). However, it was proposed
113 that direct emission of HONO from vehicles should contribute about 51.1 % (Meng et
114 al., 2019) and 52 % of HONO source on haze days in Beijing (Zhang et al., 2019d).
115 These results mean that more studies are still required on the HONO budget. In
116 particular, it is meaningful to analyze the HONO budget in polluted events for
117 understanding the possible influence of HONO sources on secondary pollutants
118 formation.

119 In this work, we carried out comprehensive measurements at a newly constructed
120 observation station (Aerosol and Haze Laboratory, Beijing University of Chemical
121 Technology, AHL/BUCT Station) located in the western campus of Beijing University
122 of Chemical Technology in downtown Beijing. We show observational evidence that
123 HONO has a prominent promotion effect on the secondary aerosol mass formation in
124 winter. Traffic-related emission seems to be a vital contributor to ambient HONO
125 during the pollution events in winter in Beijing.

126 **2. Materials and methods**

127 **2.1 Field measurements.** Field measurements were performed at AHL/BUCT Station
128 (Lat. 39°56'31" and Lon. 116°17'52") from February 1 to June 30, 2018. The
129 observation station is on a rooftop of the main building, which is 550 m from the 3rd

130 ring road in the East, 130 m from the Zizhuyuan road in the North and 565 m from the
131 Nandianchang road in the West (Figure S1). The station is surrounded by both traffic
132 and residential emissions, thus, is a typical urban observation site.

133 Ambient air was sampled from the roof of the main building with five floors (~18
134 m above the surface). A PM_{2.5} inlet (URG) was used to cut off the particles with
135 diameter larger than 2.5 μm before going to a Nafion dryer (MD-700-24, Perma Pure).
136 Then a Time-of-Flight Aerosol Chemical Speciation Monitor equipped a PM_{2.5}
137 aerodynamic lens (ToF-ACSM, Aerodyne) and an Aethalometer (AE33, Magee
138 Scientific) were connected to the manifold of aerosol sampling tube. The Reynolds
139 number in the aerosol sampling tube was 800 with the total flow rate of 16.7 lpm and
140 the residence time of 6.5 s. The details about ToF-ACSM measurement was described
141 in the Supplement information. Ambient air was drawn from the roof using a Teflon
142 sampling tube (BMET-S, Beijing Saak-Mar Environmental Instrument Ltd.) with the
143 residence time <10 s for gas phase pollutants measurements. Trace gases including NO_x,
144 SO₂, CO and O₃ were measured with the corresponding analyzer (Thermo Scientific,
145 42i, 43i, 48i and 49i). Volatile organic compounds (VOCs) was measured using an
146 online Single Photon Ionization Time-of-flight Mass Spectrometer (SPI-ToF-MS
147 3000R, Hexin Mass Spectrometry) with unit mass resolution (UMR). The principle and
148 the configuration of the instrument has been described in detail elsewhere (Gao et al.,
149 2013) and the Supplement information. HONO concentration was measured using a
150 home-made Long Path Absorption Photometer (LOPAP) (Tong et al., 2016). The details
151 are described in the Supplement information. Particle size and number concentration

152 from 1 nm to 10 μm were measured with Scanning Mobility Particle Sizer (SMPS 3936,
153 TSI), particle size magnifier (PSM, Airmodus) and Neutral Cluster and Air Ion
154 Spectrometer (NIAS, Airedt Ltd.). Meteorological parameters including temperature,
155 pressure, relative humidity (RH), wind speed and direction were measured using a
156 weather station (AWS310, Vaisala). Visibility and planetary boundary layer (PBL)
157 height were measured using a visibility sensor (PWD22, Vaisala) and a ceilometer
158 (CL51, Vaisala), respectively

159 **2.2 HONO budget calculation.** Multiple sources of ambient HONO have been
160 identified, such as emission from soil (E_{soil}) (Oswald et al., 2015; Meusel et al., 2018)
161 and vehicle exhaust (E_{vehicle}) (Trinh et al., 2017), production through homogeneous
162 reaction between NO and OH ($P_{\text{NO-OH}}$) in the atmosphere, photolysis of nitrate (P_{nitrate})
163 (Bao et al., 2018), nitrous acid (P_{HNO_3}) and nitrophenol ($P_{\text{nitrophenol}}$) (Sangwan and
164 Zhu, 2018), heterogeneous reaction of NO_2 on aerosol surface (P_{aerosol}) (Liu et al., 2015)
165 and ground surface (P_{ground}) (Liu et al., 2019c; Li et al., 2018; Wang et al., 2017b).
166 However, the photolysis of HNO_3 and nitrophenol were excluded in this work because
167 they were believed as minor sources (Lee et al., 2016) and their concentrations were
168 unavailable during our observation. The removal pathways of HONO including
169 photolysis ($L_{\text{photolysis}}$), the homogeneous reaction with OH radical ($L_{\text{HONO-OH}}$) and dry
170 deposition ($L_{\text{deposition}}$) (Liu et al., 2019c) were considered.

171 The **HONO budget** could be calculated by,

$$172 \frac{dc_{\text{HONO}}}{dt} = E_{\text{HONO}} + P_{\text{HONO}} - L_{\text{HONO}} + T_{\text{vertical}} + T_{\text{horizontal}} \quad (1)$$

173 where $\frac{dc_{\text{HONO}}}{dt}$ is the observed change rate of HONO mixing ratios (ppbv h^{-1}); E_{HONO}

174 represents the emission rate of HONO from different sources (ppbv h⁻¹); P_{HONO} is the
 175 in-situ production rate of HONO in the troposphere (ppbv h⁻¹); L_{HONO} is the loss rate of
 176 HONO (ppbv h⁻¹) (Li et al., 2018); $T_{vertical}$ and $T_{horizontal}$ are the vertical and horizontal
 177 transport (Soergel et al., 2011), which can mimic source or sink terms depending on the
 178 HONO mixing ratios of the advected air relative to that of the measurement site and
 179 height (Soergel et al., 2011).

180 The emission rate (E_{HONO} , ppbv h⁻¹) was calculated based on the emission flux
 181 ($F_{HONO}=EI_{HONO}/A$, g m⁻² s⁻¹) and PBL height (H , m) according to the following equation,

$$182 \quad E_{HONO} = \frac{\alpha \cdot F_{HONO}}{H} \quad (2)$$

183 where, EI_{HONO} , is the emission inventory of HONO (g s⁻¹), A is the urban area of Beijing
 184 (m²), α is the conversion factor ($\alpha = \frac{1 \times 10^9 \cdot 3600 \cdot R \cdot T}{M \cdot P} = \frac{2.99 \times 10^{13} \cdot T}{M \cdot P}$), M is the molecular
 185 weight (g mol⁻¹), T is the temperature (K) and P is the atmospheric pressure (Pa).

186 The production rates of HONO (P_{HONO} , ppbv h⁻¹) in the troposphere was calculated
 187 by,

$$188 \quad P_{HONO} = 3600 \cdot k_1 \cdot c_{precursor} \quad (3)$$

189 where, k_1 is the quasi first-order reaction rate constant (s⁻¹), $c_{precursor}$ is the concentration
 190 of precursor (ppbv). For homogeneous reaction between NO and OH,

$$191 \quad k_1 = k_2 \cdot c_{OH} \quad (4)$$

192 where, k_2 is the second-order reaction rate constant (7.2×10^{-12} cm³ molecule⁻¹ s⁻¹) (Li et
 193 al., 2012), c_{OH} is the OH concentration (molecules cm⁻³). For heterogeneous reaction,

$$194 \quad k_1 = \frac{\gamma \cdot A_s \cdot \omega}{4} \cdot Y_{HONO} \quad (5)$$

195 where, A_s is the surface area concentration of the reactive surface (m² m⁻³), ω is the

196 molecular mean speed (m s^{-1}), γ is the uptake coefficient of the precursor, Y_{HONO} is the
197 yield of HONO. For ground surface, the surface area concentration is

$$198 \quad A_s = \frac{\delta}{H} \quad (6)$$

199 where δ is the surface roughness, which is calculated according to the mean project area,
200 perimeter and height of the buildings in Beijing.

$$201 \quad \delta = \frac{f_{\text{building}} \cdot (A_{\text{projected}} + h \cdot P_{\text{building}})}{A_{\text{projected}}} + f_{\text{blank}} \quad (7)$$

202 where f_{building} (0.31) and f_{blank} (0.69) are the fraction of the projected area ($A_{\text{projected}}$) of
203 buildings and blank space, respectively; P_{building} and h are the perimeter and the height
204 of the building, respectively. The f_{building} and P_{building} are measured from ~1000 buildings
205 randomly selected on the Google Map using ImageJ software. The mean height (44.5
206 m) of the building in Beijing is linearly extrapolated from the literature data based on
207 remote measurement using Light Detection and Ranging (LiDAR) sensor from 2004 to
208 2008 (Cheng et al., 2011). The δ in Beijing is calculated to be 3.85, which is slightly
209 higher than the value (2.2) used by Li et al. (2018).

210 As for photolysis reaction, the first-order reaction rate was

$$211 \quad k_1 = J \quad (8)$$

212 where, J is the photolysis rate to produce HONO (s^{-1}).

213 The loss rates of HONO by photolysis ($L_{\text{photolysis}}$), homogeneous reaction with
214 OH radicals ($L_{\text{HONO-OH}}$) and dry deposition ($L_{\text{deposition}}$) (Liu et al., 2019c) were calculated
215 according to the following equations.

$$216 \quad L_{\text{photolysis}} = 3600 \cdot J_{\text{HONO}} \cdot c_{\text{HONO}} \quad (9)$$

$$217 \quad L_{\text{HONO-OH}} = 3600 \cdot k_{\text{HONO-OH}} \cdot c_{\text{OH}} \cdot c_{\text{HONO}} \quad (10)$$

218 $L_{deposition} = \frac{3600 \cdot v_d \cdot c_{HONO}}{H}$ (11)

219 where, J_{HONO} is the photolysis rate of HONO (s^{-1}), $k_{HONO-OH}$ is the second-order reaction
 220 rate constant between HONO and OH ($6 \times 10^{-12} \text{ cm}^3 \text{ molecule}^{-1} \text{ s}^{-1}$) (Atkinson et al.,
 221 2004), and v_d is the dry deposition rate of HONO (0.001 m s^{-1}) (Han et al., 2017).

222 Vertical transport by advection ($T_{vertical}$), which is an important sink of HONO in
 223 the night (Gall et al., 2016; Meng et al., 2019), can be calculated according to equation
 224 (12).

225 $T_{vertical} = -K_h(z, t) \frac{\partial c(z, t)}{\partial z} \frac{1}{h}$ (12)

226 where $K_h(z, t)$ is the eddy diffusivity of heat ($\text{m}^2 \text{ s}^{-1}$) at height z (m) and time t , h is the
 227 height of the second layer (18 m in this study) (Gall et al., 2016). On the other hand,
 228 both the vertical and horizontal transport can be estimate according to Eq. (13),

229 $T_{vertical} = k_{dilution}(c_{HONO} - c_{HONO, background})$ (13)

230 where $k_{dilution}$ is a dilution rate (0.23 h^{-1} , including both vertical and horizontal transport)
 231 (Dillon et al., 2002), c_{HONO} and $c_{HONO, background}$ is the HONO concentration at the
 232 observation site and background site, respectively (Dillon et al., 2002).

233 In addition, even though all the current known sources had been considered in
 234 models, the modelled daytime HONO concentrations were still lower than the observed
 235 concentration (Tang et al., 2015; Michoud et al., 2014). Therefore, the HONO
 236 concentration could be described in equation (14).

237 $\frac{dc_{HONO}}{dt} = E_{soil} + E_{vehicle} + P_{NO-OH} + P_{nitrate} + P_{aerosol} + P_{ground} + P_{unknown} -$
 238 $L_{photolysis} - L_{HONO-OH} - L_{deposition} + T_{vertical} + L_{horizontal}$ (14)

239 **3. Results and discussion**

240 **3.1 Overview of the air pollution.** The mass concentration of non-refractory PM_{2.5}
241 (NR-PM_{2.5}) and HONO along with metrological parameters are shown in Fig. 1. The
242 time series of other pollutants (SO₂, CO, O₃, benzene, toluene and black carbon) are
243 shown in Fig. S2 in the Supplement information.

244 Similar to previous measurements (Guo et al., 2014; Wang et al., 2016), the air
245 pollution events showed a periodic cycle of 3-5 days during the observation, as
246 indicated by the concentration of NR-PM_{2.5} (Fig. 1A), gaseous pollutants and the
247 visibility. During the observation period, 20-60% of hourly PM_{2.5} concentration was
248 higher than 75 µg m⁻³ (the criterion for pollution according to the national air quality
249 standards) in each month (Fig. S3A). Both the frequency of severe polluted episodes
250 and the mean mass concentration of PM_{2.5} and NR-PM_{2.5} were obviously higher in
251 March than that in the rest months (Fig. 1 and S3). This can be explained by both the
252 intensive emission during the heating season as evidenced by the high concentration of
253 primary pollutants including CO, SO₂ and BC (Table S1) and the stagnant
254 meteorological conditions supported by the low wind speed (<2 m s⁻¹) and the low
255 planetary boundary layer (PBL) height, in particular, in March (Fig. S4A).

256 OA and nitrate dominated the NR-PM_{2.5}, while their relative contribution varied
257 significantly during the observation (Fig. 1B and Table S1). This is similar to the
258 previously reported NR-PM_{1.0} composition (Sun et al., 2015). The monthly mean
259 fraction of OA varied from 45.9±10.2 % to 52.6±18.7 %, which was accompanied by a
260 slight increase of sulfate from 16.0±9.1 % to 18.2±8.0 % (Fig. S4D). At the same time,
261 the monthly mean fraction of nitrate and chloride decreased from 26.7±8.8 % to

262 16.7±12.8 % and from 7.7±6.1 % to 0.3±0.2 %, respectively. Ammonium showed a
263 peak value (14.2±2.8 %) in March, then slightly decreased to 12.2±5.2 %. The intensive
264 emission of chloride from coal combustion during heating season (Cho et al., 2008) and
265 firework burning (Zhang et al., 2017), which was transported from Tangshan during
266 Chinese New Year (Fig. S5A and B), led to high fraction of chloride in February and
267 March. The decrease in nitrate and ammonium fractions from February to June should
268 be related to **the increase in temperature** (Fig. S2) which was in favor of NH₄NO₃
269 decomposition (Wang et al., 2015). Besides the reduction of the contribution from other
270 components, secondary formation due to increased UV light (Fig. S4C) might also
271 favor the increased OA fraction (Huang et al., 2014). This means that chemical
272 transformation in March should still be vigorous although the UV light intensity in
273 March is lower than in summer (Fig. S4C). It also implies other factors may compensate
274 the weak UV light intensity in March.

275 HONO, which has been recognized as the important precursor of **primary** OH
276 radical (Ren et al., 2006; Alicke et al., 2003), ranged from 0.05 to 10.32 ppbv from
277 February 1 to June 30, 2018 (Fig. 1C) with the mean value of 1.26±1.06 ppbv. In winter
278 (February and March), HONO concentration was 1.15±1.10 ppbv and comparable to
279 the previous results (1.05±0.89 ppbv) measured in the winter of Beijing (Wang et al.,
280 2017b; Hou et al., 2016), while it was slightly lower than that from April to June
281 (1.35±1.11 ppbv) in this work and those measured in the summer of Shanghai (2.31
282 ppbv, in May) (Cui et al., 2018) and Guangzhou (2.8 ppbv, in July) (Qin et al., 2009).
283 The mean HONO concentration in March (1.53±1.25 ppbv) was higher than that in

284 February and April (Fig. S3D), while was slightly higher or close to that in May and
285 June. Chamber studies have found that HONO is responsible for the initiation of
286 photosmog reactions (Rohrer et al., 2005). It is reasonable to postulate that HONO
287 probably play an important **role** in the secondary chemistry of particle formation in
288 March.

289 **3.2 Promotion effect of HONO photolysis on aerosol formation in winter.** Oxidation
290 of precursors by OH radicals is the main mechanism regarding to secondary aerosol
291 formation in the troposphere. After partially ruling out the possible influence of PBL
292 variation by normalizing the concentrations of all pollutants to CO (Cheng et al., 2016)
293 **or BC (Liggio et al., 2016)**, we found all secondary species including sulfate, nitrate
294 and ammonium show obvious daytime peaks from 7:00 am to 6:00 pm (Figure S5C)
295 (Cheng et al., 2016). The similar trends were observed after the concentrations of
296 pollutants were normalized to BC (not shown). This suggests they might connect with
297 photochemistry.

298 Photolysis of H₂O₂, HCHO, O₃ and HONO, and **the reaction between NO and HO₂**
299 are known as sources of OH radical in the atmosphere (Alicke et al., 2003; Volkamer et
300 al., 2010; Tan et al., 2018; Tang et al., 2015). In this work, the concentration of H₂O₂,
301 HCHO and **HO₂** are unavailable. Thus, their contributions to OH production were not
302 discussed here. However, it has been well recognized that the photolysis of HONO is
303 the **dominant** source of OH in the dawn and dusk period (Holland et al., 2003), even
304 contributes up to 60% of daytime OH source in winter (Spataro et al., 2013; Rohrer et
305 al., 2005). **In addition, it has been confirmed that HONO dominates the primary OH**

306 source at various locations (Tan et al., 2018; Liu et al., 2019c; Tan et al., 2017; Aumont
307 et al., 2003). Therefore, it is meaningful to discuss the contribution of HONO to
308 secondary aerosol formation through OH production. We simply compared the OH
309 production via photolysis of HONO ($P_{\text{OH-HONO}}=J_{\text{HONO}}\times C_{\text{HONO}}$) and O₃ ($P_{\text{OH-}}$
310 $\text{O}_3=J_{\text{O}_3}\times C_{\text{O}_3}$) in Fig. 2 when the PM_{2.5} concentration was larger than 50 μg m⁻³ and the
311 RH was less than 90 % to understand the chemistry in pollution events. Under these
312 conditions, local chemistry should be more important as 75 % of the wind speed was
313 less than 1.0 m s⁻¹ (Fig. S6). The details about the J_{HONO} and J_{O_3} calculation were
314 shown in the Supplement information and their time series were shown in Fig. S7. On
315 polluted days in winter, the daytime $P_{\text{OH-HONO}}$ was always significantly higher than the
316 $P_{\text{OH-O}_3}$ in winter and the maximal $P_{\text{OH-HONO}}$ and $P_{\text{OH-O}_3}$ were $1.73\pm 0.86 \times 10^7$ molecules
317 cm⁻³ s⁻¹ (2.43 ± 1.21 ppb h⁻¹) and $1.03\pm 1.06 \times 10^7$ molecules cm⁻³ s⁻¹ (1.45 ± 1.49 ppb h⁻
318 ¹), respectively (Fig. 2A). Owing to the high HONO concentration accumulated
319 throughout the night, the maximal $P_{\text{OH-HONO}}$ in winter was as about 2-6 times of that
320 was observed in the wintertime of Colorado, USA (~ 0.59 ppb h⁻¹) (Kim et al., 2014),
321 New York, USA (~ 0.40 ppb h⁻¹) (Kanaya et al., 2007) and Nanjing, China (0.90 ± 0.27
322 ppb h⁻¹) (Liu et al., 2019b). In the period from April to June, the daily maxima of $P_{\text{OH-}}$
323 HONO and $P_{\text{OH-O}_3}$ were $2.48\pm 1.42 \times 10^7$ molecules cm⁻³ s⁻¹ (3.48 ± 1.99 ppb h⁻¹) and
324 $6.51\pm 4.17 \times 10^7$ molecules cm⁻³ s⁻¹ (9.15 ± 5.86 ppb h⁻¹), respectively. These results
325 mean that the photolysis of HONO should play an important role in the initiation of the
326 daytime HO_x and RO_x chemistry on polluted days in winter, while photolysis of O₃
327 becomes more important from April to June. This is consistent with the previous

328 findings that HONO photolysis dominates the primary OH source in winter of BTH
329 (Xing et al., 2019; Tan et al., 2018), Colorado and New York City (Ren et al., 2006; Kim
330 et al., 2014), while photolysis of O₃ and HCHO related reactions usually dominated
331 primary OH production in summer (Alicke et al., 2003).

332 Oxidation of trace gas pollutants, in particular VOCs, by OH is their main removal
333 pathway in the troposphere (Atkinson and Arey, 2003), subsequently, contribute to
334 secondary aerosol formation (Kroll and Seinfeld, 2008). A very recent work has found
335 that oxidation of VOCs from local traffic emission is still efficient even under pollution
336 conditions (Guo et al., 2020). We partially ascribe this to the high HONO concentration
337 in winter Beijing. To confirm this assumption, 12 episodes in winter were chosen (Fig.
338 1) to uncover the connection between aerosol formation and HONO photolysis. The 1st,
339 3rd and 5th episodes were clean days and the other 9 episodes were typical haze events
340 with duration above 2 days. The features of these episodes were summarized in Table
341 S2. Fig. 2C shows the CO-normalized daytime profiles of OA and HONO in the 7th and
342 12th episodes as two examples. In all selected cases, HONO exhibited quick reduction
343 due to the photolysis after sunrise, and simultaneously, OA concentration started to
344 increase. This is similar to the evolution of the concentration of pollutants in a typical
345 smog chamber experiment. We further show the formation of OA ($\Delta C_{OA}/C_{CO}$) as a
346 function of the consumed HONO ($-\Delta C_{HONO}/C_{CO}$) in Fig. 2D. Except for the 4th episode
347 that was highly affected by firework emission during the Spring Festival, $\Delta C_{OA}/C_{CO}$
348 showed a linear dependence on $-\Delta C_{HONO}/C_{CO}$ in winter, and the correlation coefficient
349 was 0.75. As the meteorological condition was stagnant during these cases as indicated

350 by the low wind speed ($< 1.0 \text{ m s}^{-1}$, Fig. S5D), it was reasonable to ascribe the increase
351 of OA concentration to local secondary formation initiated by OH radical and
352 photolysis of HONO should play an important role in initiation the HO_x and RO_x
353 chemistry. This kind of correlation could not be seen for the pollution events from April
354 to June because the primary OH production was no longer dominated by HONO
355 photolysis as indicated by Fig. 2D. It should be noted that oxidation of biogenic alkenes
356 by O_3 might also contribute to OA formation. However, anthropogenic VOCs instead
357 of biogenic VOCs dominated the wintertime VOCs in Beijing (Liu et al., 2017a).
358 Although vehicles can emit isoprene (Zou et al., 2019), the contribution of isoprene to
359 the observed increase of OA concentration should be unimportant due to the low
360 concentration of isoprene in winter (Zou et al., 2019). Therefore, it is reasonable to
361 conclude that the increase of OA concentration in daytime might be mainly resulted
362 from oxidation of VOCs by OH.

363 Similar to OA, $\Delta C_{\text{nitrate}}/C_{\text{CO}}$ in winter also showed good linear correlation with -
364 $\Delta C_{\text{HONO}}/C_{\text{CO}}$ ($R=0.67$, Fig. S5E), suggesting that the increase of particle-phase nitrate
365 in the daytime should also be promoted by OH radical from HONO photolysis.
366 Interestingly, $\Delta C_{\text{ammonium}}/\text{CO}$ also showed a good correlation with $-\Delta C_{\text{HONO}}/C_{\text{CO}}$
367 ($R=0.61$, Fig. S5E), although particle-phase ammonium should not be directly related
368 to oxidation of NH_3 by OH. We explained the increased ammonium as the result of
369 enhanced neutralization of HNO_3 by NH_3 (Wang et al., 2018; Wen et al., 2018; Sun et
370 al., 2018) because NH_4^+ was adequate to neutralize both sulfate and nitrate as shown in
371 Fig.S8. This was consistent with the recent work which observed the important role of

372 photochemical reactions in daytime nitrate formation, while hydrolysis of N_2O_5 mainly
373 contributed to nighttime nitrate (Tian et al., 2019). Although a recent work has found
374 that daytime hydrolysis of N_2O_5 on hygroscopic aerosols is also an important source of
375 daytime nitrate in winter Beijing (Wang et al., 2017a), the linearly correlation between
376 $\Delta C_{\text{nitrate}}/C_{\text{CO}}$ and $\Delta C_{\text{HONO}}/C_{\text{CO}}$ at least implies that the promotion effect of HONO on
377 nitrate formation could not be excluded. On the other hand, the correlation between
378 $\Delta C_{\text{sulfate}}/C_{\text{CO}}$ and $-\Delta C_{\text{HONO}}/C_{\text{CO}}$ was much weaker ($R=0.26$), suggesting a weak
379 connection between particle-phase sulfate and gas-phase H_2SO_4 . This was also
380 consistent with the previous understanding that heterogeneous reactions of SO_2 were
381 the **dominant** pathway for sulfate formation (Zheng et al., 2015a;He et al., 2018;Zhang
382 et al., 2020). Overall, this work well supported the recent modeling results that HONO
383 could obviously promote the aerosol production in winter (Zhang et al., 2019a;Zhang
384 et al., 2019c;Xing et al., 2019;An et al., 2013) from the point of view of observation.

385 **3.3 HONO budget in polluted events.** To understand the possible sources of HONO
386 in polluted events in winter, the HONO budget was calculated for the events when the
387 $PM_{2.5}$ concentration was larger than $50 \mu\text{g m}^{-3}$ and the RH was less than 90 % according
388 to the method described in Section 2.2.

389 **Vehicle emission.** The E_{vehicle} was calculated **according to Eq. (2)** using the relative
390 emission rate of HONO to NO_x and the emission inventory of NO_x from vehicles. Firstly,
391 the ratio of HONO/ NO_x was calculated according to the method reported by Xu et al.
392 (Xu et al., 2015) and Li et al. (Li et al., 2018) from the fresh nighttime plumes which
393 were strictly satisfy the following criteria: 1) $NO_x > 45$ ppb (highest 25% of NO_x data);

394 2) $\Delta\text{NO}/\Delta\text{NO}_x > 0.8$, with good correlation between NO and NO_x ($R > 0.9$, $P < 0.05$);
395 3) Good correlation between HONO and NO_x ($R^2 > 0.65$, $P < 0.05$); and 4) Dataset from
396 5:00 am to 8:00 am. The mean emission ratio of HONO to NO_x was $1.8 \pm 0.5\%$ based
397 on 5 fresh vehicle exhaust plumes during our observation (Table S3). This value is
398 higher than that in Hongkong ($1.2 \pm 0.4\%$) (Xu et al., 2015), Beijing (1.3%) (Zhang et
399 al., 2019d) and Jinan ($0.53 \pm 0.20\%$) (Li et al., 2018) using the same method, while is
400 comparable with the result measured in tunnel experiments (2.1%) carried out in
401 Beijing (Yang et al., 2014). Secondly, low HONO concentration should be accompanied
402 with high NO_x and high ratio of $\Delta\text{NO}/\Delta\text{NO}_x$ if direct emission from vehicles was the
403 major source of HONO and the source from secondary formation was negligible in the
404 urban atmosphere. Therefore, we further estimated the HONO/ NO_x ratio using a low
405 limit correlation method (Li et al., 2012). In the 2D space of HONO versus NO_x (Fig.
406 S8), the lowest margin with $\Delta\text{NO}/\Delta\text{NO}_x$ larger than 0.8 were chosen for linear
407 correlation. The ratio of $\Delta\text{HONO}/\Delta\text{NO}_x$ is $1.17 \pm 0.05\%$. This value is lower than that
408 estimated through empirical method discussed above, while is very close to that
409 measured in Hongkong ($1.2 \pm 0.4\%$) (Xu et al., 2015) and ($1.23 \pm 0.35\%$) (Liang et al.,
410 2017), Guangzhou (1.0%) (Li et al., 2012) and Beijing (1.3% and 1.41%) (Zhang et al.,
411 2019d; Meng et al., 2019). Finally, several studies have measured the direct emission of
412 HONO from vehicle exhaust. The HONO/ NO_x was 0.18% from gasoline cars through
413 chassis dynamometer tests in China (Liu et al., 2017d), while it was 0-0.95% for
414 gasoline vehicles and 0.16-1.0% for diesel vehicles measured under real-world driving
415 test cycles in Japan (Trinh et al., 2017). Thus, three levels of vehicle emission factor

416 were considered. $1.17\pm 0.05\%$ was taken as the middle value which was very close to
417 the mean emission ratio (1.21) for all of these reported values in China (Li et al.,
418 2018; Xu et al., 2015; Yang et al., 2014; Liu et al., 2017d; Gall et al., 2016; Meng et al.,
419 2019), while 0.18% (Liu et al., 2017d) and 1.8 % were the lower limit and the upper
420 limit, respectively.

421 The E_{vehicle} was calculated using the hourly NO_x emission inventory from vehicles
422 in Beijing (Yang et al., 2019) after converted to emission flux of HONO ($F_{\text{HONO}}=F_{\text{NO}_x}\times$
423 HONO/NO_x) and the PBL height as described in Section 2.2. Thus, the calculated
424 emission rate reflected the diurnal variation of both the emission inventory and the PBL
425 height. The calculated hourly middle value of E_{vehicle} using the HONO/NO_x of 1.17%
426 was from 0.085 ± 0.038 to 0.34 ± 0.15 ppbv h^{-1} , which was slightly higher than the
427 daytime emission rate of HONO in Xi'an (Huang et al., 2017b). This is reasonable
428 when the vehicle population in Beijing is taken into consideration. The lower limit of
429 E_{vehicle} was $0.013\pm 0.006-0.053\pm 0.023$ ppbv h^{-1} , which was close to the estimated
430 emission rate of HONO in Jinan (Li et al., 2018). The upper limit was in the range of
431 $0.13\pm 0.06-0.53\pm 0.23$ ppbv h^{-1} .

432 **Soil emission.** The emission flux of HONO from soil depends on the water content, the
433 nitrogen nutrient content and the temperature of soil (Oswald et al., 2013). Oswald et
434 al. (2013) measured the emission flux of HONO from 17 soil samples, including
435 eucalyptus forest, tropical rain forest, coniferous forest, pasture, woody savannah,
436 grassland, stone desert, maize field, wheat field, jujube field an cotton field etc. Tropical
437 rain forest, coniferous forest and grassland are the typical plants in downtown Beijing

438 (Huang et al., 2017a). At the same time, their emission fluxes of HONO are comparable
 439 (Oswald et al., 2013). Thus, we used the emission flux from grassland to calculate the
 440 emission rate of HONO from soil in Beijing because the temperature and water holding
 441 content dependent emission flux of HONO was available for grassland soil. Three
 442 levels of water content including 25-35%, 35-45% and 45-55% were considered. The
 443 temperature dependence of F_{HONO} was calculated using the mean value of the F_{HONO}
 444 with different water content, while the low limit and upper limit of F_{HONO} were
 445 calculated using the emission flux from 45-55% of water content and 25-35% of water
 446 content, respectively. The lower limit, the middle value and the upper limit of the E_{soil}
 447 are $0.0032 \pm 0.0027 - 0.013 \pm 0.014$, $0.0046 \pm 0.0039 - 0.020 \pm 0.20$ and $0.0057 \pm 0.0047 -$
 448 0.025 ± 0.024 ppbv h⁻¹, respectively, calculated according to Eq. (2).

449 **Homogeneous reaction between NO and OH.** Direct measurement of OH
 450 concentration was unavailable in this work, while several methods were used to
 451 estimate the ambient OH concentration. In winter in Beijing, it has been found that the
 452 OH concentration is linearly correlated with J_{O1D} , that's, $c_{\text{OH}} = J_{\text{O1D}} \times 2 \times 10^{11}$ molecules
 453 cm⁻³ (Tan et al., 2019). However, Tan et al. (2018) reported a larger conversion factor
 454 (4.33×10^{11} molecules cm⁻³). Li et al. (2018) estimated the OH radical concentration
 455 considering both photolysis rate and NO₂ concentration, namely,

$$456 \quad c_{\text{OH}} = \frac{4.1 \times 10^9 \times (J_{\text{O1D}})^{0.83} \times (J_{\text{NO}_2})^{0.19} \times (140c_{\text{NO}_2} + 1)}{0.41c_{\text{NO}_2}^2 + 1.7c_{\text{NO}_2} + 1} \quad (15)$$

457 Overall, the estimated OH concentrations according to Eq. (15) were comparable with
 458 that estimated by Tan et al. (2019) (Fig. S10C). The method for the photolysis rates
 459 calculation were shown in the SI and the time series of the photolysis rates were shown

460 in Fig. S7. On polluted days, high concentration of NO₂ resulted into lower OH
 461 concentrations estimated using the Eq. (15). Therefore, the corresponding $P_{\text{NO-OH}}$ was
 462 taken as the low limit for homogeneous reaction between NO and HONO because
 463 polluted events were discussed in this work, while $P_{\text{NO-OH}}$ calculated using the OH
 464 concentration ($J_{\text{O1D}} \times 4.33 \times 10^{11}$ molecules cm⁻³) (Tan et al., 2018) was taken as the upper
 465 limit and $P_{\text{NO-OH}}$ calculated using the OH concentration ($J_{\text{O1D}} \times 2 \times 10^{11}$ molecules cm⁻³)
 466 (Tan et al., 2019) was the middle value. In the night, OH concentration usually varied
 467 from 1.0×10^5 molecules cm⁻³ (Li et al., 2012; Tan et al., 2018) in winter to 5×10^5
 468 molecules cm⁻³ in summer (Tan et al., 2017). The nighttime OH concentration was
 469 estimated linearly correlated with the product of nighttime O₃ concentration and alkenes
 470 concentration, namely,

$$471 \quad c_{\text{OH,night}} = 1 \times 10^5 + 4 \times 10^5 \times \frac{(c_{\text{O}_3} \times c_{\text{alkenes}})_{\text{night}} - (c_{\text{O}_3} \times c_{\text{alkenes}})_{\text{night,min}}}{(c_{\text{O}_3} \times c_{\text{alkenes}})_{\text{night,max}} - (c_{\text{O}_3} \times c_{\text{alkenes}})_{\text{night,min}}} \quad (16)$$

472 The time series of OH concentration calculated using different methods was shown in
 473 Fig. S11. Thus, the lower limit, the middle value and the upper limit of $P_{\text{NO-OH}}$ were
 474 0.007 ± 0.019 - 0.43 ± 0.26 , 0.026 ± 0.053 - 0.99 ± 0.79 and 0.028 ± 0.053 - 2.14 ± 1.71 ppbv h⁻¹,
 475 respectively, calculated according to Eqs. (3) and (4). The calculated middle value of
 476 $P_{\text{NO-OH}}$ (with mean daytime value of 0.49 ± 0.35 ppb h⁻¹) was comparable with these
 477 estimated values by Li et al. (2018) (0.4 ppb h⁻¹) and Huang et al. (2017b) (0.28 ppb h⁻¹).
 478 It should be noted that measured NO concentration was used to calculate the $P_{\text{NO-OH}}$.
 479 Besides vehicle emission, power plant and industries also contribute NO emission. 40 %
 480 of NO_x was from vehicle emission according to the emission inventory of NO_x in
 481 Beijing (He et al., 2002).

482 It should be noted that OH concentration was estimated based on J_{O1D} (Tan et al.,
483 2019; Tan et al., 2018) or J_{O1D} and J_{NO_2} (Li et al., 2018). As discussed in Section 3.2,
484 HONO was an important primary OH source in the daytime. Unfortunately, it could not
485 be parameterized for calculating OH concentration because the measured or modelled
486 OH concentration was unavailable in this work. This might underestimate the early
487 daytime OH concentration, subsequently, the contribution of homogeneous reaction of
488 NO with OH to HONO source. This need to be further investigated in the future.

489 **Photolysis of nitrate.** A recent work reported the photolysis rate of nitrate (J_{nitrate}) in
490 ambient $\text{PM}_{2.5}$ at a solar zenith angle of 0° (Bao et al., 2018). The J_{nitrate} varied from
491 1.22×10^{-5} to $4.84 \times 10^{-4} \text{ s}^{-1}$ with the mean value of $8.24 \times 10^{-5} \text{ s}^{-1}$. These values were
492 further normalized according to the zenith angle and UV light at our observation station
493 to calculate the low limit, the upper limit and the middle J_{nitrate} . The time series of the
494 measured nitrate concentration and the middle value of J_{nitrate} were shown in Fig. 1 and
495 Fig. S7, respectively. Therefore, the corresponding daytime lower limit, the middle
496 value and the upper limit of HONO from photolysis of nitrate were 0.0011 ± 0.0021 -
497 0.096 ± 0.092 , 0.0072 ± 0.0021 - 0.66 ± 0.092 and 0.042 ± 0.082 - $3.86 \pm 0.008 \text{ ppbv h}^{-1}$,
498 respectively, calculated in the light of Eqs. (3) and (8).

499 **Heterogeneous reactions of NO_2 on aerosol and ground surface.** The production of
500 HONO from heterogeneous reactions of NO_2 on aerosol surface was calculated
501 according to Eqs. (3) and (5). The aerosol surface concentration was measured with a
502 SMPS. The uptake coefficient (γ) of NO_2 on different particles varied from 5×10^{-9} to
503 9.6×10^{-6} (Ndour et al., 2009; Underwood et al., 2001; Underwood et al., 1999), while it

504 was recommended to be 1.2×10^{-8} (Crowley et al., 2010), which was used to calculate
505 the P_{aerosol} in the base case. It has been found that the γ highly depends on the relative
506 humidity (RH). The low limit bound of P_{aerosol} was calculated based on the RH
507 dependent uptake coefficient of NO_2 on kaolinite ($\gamma_{\text{NO}_2} = 4.47 \times 10^{39} / (1.75 \times 10^{46} + 1.93$
508 $\times 10^{45} \text{RH})$), while the upper limit of P_{aerosol} was calculated according to the RH
509 dependent γ on hematite ($\gamma_{\text{NO}_2} = 4.46 \times 10^{39} / (6.73 \times 10^{44} + 3.48 \times 10^{44} \text{RH})$) (Liu et al.,
510 2015). Heterogeneous reaction of NO_2 on black carbon (BC) was also considered in the
511 night. The surface area concentration of BC was calculated according to its specific
512 area ($87 \text{ m}^2 \text{ g}^{-1}$) (Su et al., 2018) and the measured mass concentration. The γ_{NO_2} on BC
513 is 1.17×10^{-5} , with a HONO yield of 0.8 (Han et al., 2013). The light enhanced uptake γ
514 of NO_2 (1.9×10^{-6}) on mineral dust was further parameterized (Ndour et al., 2008) after
515 normalized to the solar radiation intensity in Beijing.

516 The contribution of heterogeneous reaction of NO_2 on ground surface was
517 calculated similar to that on mineral dust. The same kinetics for heterogeneous reaction
518 of NO_2 on aerosol surface were used to calculate the nighttime contribution of ground
519 surface. A recent work observed a significant enhancement of NO_2 and HONO
520 formation by UV light on the real urban grime (Liu et al., 2019a). Thus, RH dependent
521 kinetic data measured on urban grime ($\gamma_{\text{NO}_2} = 7.4 \times 10^{-7} + 5.5 \times 10^{-8} \text{RH}$) was used to
522 calculate the daytime upper limit for heterogeneous uptake of NO_2 on the ground
523 surface. The A_s of aerosols varied from 1×10^{-4} to $4.8 \times 10^{-3} \text{ m}^{-1}$ with a mean value of
524 $1.4 \pm 0.5 \times 10^{-3} \text{ m}^{-1}$ during pollution events. This value is comparable with that used in
525 modeling studies (Zhang et al., 2016; Aumont et al., 2003). The A_s of ground surface

526 which was calculated according to Eq. (6) and (7) varied from 1.5×10^{-3} to $3.85 \times 10^{-2} \text{ m}^{-1}$
527 1 with a mean value of $1.3 \pm 0.9 \times 10^{-2} \text{ m}^{-1}$ during pollution events. The surface roughness
528 was 3.85 calculated according to Eq. (7). The Y_{HONO} was set to 0.5 because of the
529 hydrolysis reaction of NO_2 (Liu et al., 2015), while it was 0.8 for light enhanced
530 reaction (Liu et al., 2019a; Ndour et al., 2008) and on BC (Han et al., 2013).

531 The lower limit, the middle value and the upper limit of P_{aerosol} were 0.038 ± 0.030 -
532 0.087 ± 0.072 , 0.038 ± 0.030 - 0.088 ± 0.072 and 0.041 ± 0.032 - 0.092 ± 0.073 ppbv h^{-1} ,
533 respectively. The corresponding values were 0.00027 ± 0.00017 - 0.0020 ± 0.0012 ,
534 0.0014 ± 0.00095 - 0.0089 ± 0.006 and 0.0025 ± 0.0023 - 0.060 ± 0.032 ppbv h^{-1} for P_{ground} .
535 Although the A_s of ground surface was higher than that of aerosol, the larger γ_{NO_2}
536 (1.17×10^{-5}) on soot particles than that on other aerosols and ground surface led to a
537 larger production rate of HONO in this work. The P_{aerosol} calculated in this work was
538 on the same orders as soil emission, while it was lower than the P_{aerosol} estimated by
539 Huang et al. (Huang et al., 2017b) because different calculation methods have been
540 used. In their work, the production rate of HONO was estimated based on the
541 conversion rate (Huang et al., 2017b), whilst it was calculated based on the measured
542 aerosol surface area concentration and uptake coefficient of NO_2 on different particles
543 in this work.

544 It should be pointed out that HONO production from heterogeneous reaction of
545 NO_2 on both aerosol and ground surface greatly depend on the $\gamma_{\text{NO}_2, \text{BET}}$ and A_s . The A_s
546 of aerosols was comparable with the modeling input. However, the small nighttime $\gamma_{\text{NO}_2, \text{BET}}$
547 (10^{-8} - 10^{-7}) on dust were used in this work rather than the $\gamma_{\text{NO}_2, \text{BET}}$ (1×10^{-6}) used in

548 modelling studies (Zhang et al., 2016; Aumont et al., 2003; Gall et al., 2016). This leads
549 to a lower production rate of HONO from heterogeneous reaction of NO₂ on aerosols.
550 As for heterogeneous reaction of NO₂ on ground surface, besides the small $\gamma_{\text{NO}_2, \text{BET}}$
551 used in this work, the A_s of ground surface (0.0015 to 0.0385 m⁻¹) calculated using the
552 surface roughness and PBL height was also significantly lower than the fixed value of
553 0.3 m⁻¹ in modeling studies that might overestimate the contribution of HONO
554 production from heterogeneous reaction of NO₂ on ground surface. It should be noted
555 that the initial uptake coefficient (γ_{ini}) was parameterized in this work. This will
556 overestimate the contribution of heterogeneous reaction of NO₂ to HONO source
557 because the steady-state uptake coefficient is usually one order of magnitude lower than
558 γ_{ini} (Han et al., 2013; Liu et al., 2015). These results mean that heterogeneous reaction
559 might not be a major HONO source. This is consistent with a recent work that found
560 heterogeneous reaction being unimportant when compared with traffic emission during
561 haze events in winter in Beijing (Zhang et al., 2019d).

562 **Sinks of HONO.** The loss rates of HONO by photolysis ($L_{\text{photolysis}}$), homogeneous
563 reaction with OH radicals ($L_{\text{HONO-OH}}$) and dry deposition were calculated according to
564 Eqs. (9)-(11). The daytime J_{HONO} varied from 1.71×10^{-5} to 1.13×10^{-3} s⁻¹ on polluted
565 days in winter, while it was in the range of 5.89×10^{-5} to 1.53×10^{-3} s⁻¹ from April to June.
566 These values are comparable to modelling results (3.9×10^{-5} - 1.8×10^{-3} s⁻¹) (Gall et al.,
567 2016). The daytime $L_{\text{photolysis}}$ were in the range of 0.03-5.23 ppb h⁻¹ and 0.25-7.10 ppb
568 h⁻¹ in winter and the rest months, respectively. It was the major sink of HONO in the
569 daytime. The $L_{\text{HONO-OH}}$ varied from 0.0049 to 0.069 ppbv h⁻¹ in winter using the $k_{\text{HONO-OH}}$.

570 OH of $6 \times 10^{-12} \text{ cm}^3 \text{ molecule}^{-1} \text{ s}^{-1}$ (Atkinson et al., 2004) and the middle value of OH
571 concentrations. It was from 0.0050 to 0.085 ppbv h^{-1} from April to June. The $L_{\text{deposition}}$
572 was in the range of 0.004-0.056 ppbv h^{-1} in winter and 0.004-0.030 ppbv h^{-1} from April
573 to June, calculated according to Eq. (11).

574 As pointed in Section 2.2, vertical transport by advection is an important nocturnal
575 sink of HONO (Gall et al., 2016). In this work, the vertical distribution of HONO
576 concentration is unavailable. Recently, Meng et al. (2019) measured the vertical
577 distribution of HONO in Beijing in December, 2016. The concentration of HONO
578 showed nearly flat profiles from ground level to 240 m in pollution events after sunset,
579 while negative profiles of HONO were observed in pollution events during night (Meng
580 et al., 2019). The nighttime concentration gradient was $0.0047 \pm 0.0025 \text{ ppb m}^{-1}$ derived
581 from the nighttime dataset (Meng et al., 2019). In the daytime, we assume a zero
582 concentration gradient. On the other hand, the eddy diffusivity of heat in urban
583 environment was measured in New Delhi, Indian (Yadav et al., 2003). Using their
584 dataset with the wind speed lower than 2.0 m s^{-1} , we derived the relationship between
585 the K_h and the wind speed (WS) ($K_h = 0.9389 \times \text{WS} - 0.3374 \text{ m}^2 \text{ s}^{-1}$). The nighttime T_{vertical}
586 changed from 0.15 to 0.37 ppbv h^{-1} in winter, while it was from 0.12 to 0.68 ppbv h^{-1}
587 according to Eq. (12) from April to June. Because the wind speed was usually lower
588 than 1.0 m s^{-1} in pollution events (Fig. S6), horizontal transport should have little
589 influence on the daytime sources or sinks of HONO because of the short lifetime of
590 HONO (Spataro and Ianniello, 2014). In the night, 79 % of the wind speed was lower
591 than 1.0 m s^{-1} in winter, thus the air masses from suburban areas should have influence

592 on the sources and sinks of HONO in Beijing. If the HONO concentration at
593 background was zero, the vertical and horizontal transport rate of HONO varied from
594 0.17 to 0.61 ppbv h⁻¹ which is calculated in the light of Eq. (13) on haze days in winter
595 and from 0.15 to 0.74 ppbv h⁻¹ in pollution events from April to June. These values
596 were higher than that calculated according to Eq. (12). Because the background HONO
597 concentration was unavailable, we only considered the nighttime transport calculated
598 according to Eq. (12) in the following section.

599 **Comparison among different HONO sources.** Fig. 3 summarizes the diurnal patterns
600 of each sources with different parameterizations during the pollution events from
601 February to March. The black dots and lines mean the middle values, while the shadow
602 indicates the corresponding lower bound and upper bound. In the nighttime, vehicle
603 and soil emission, and homogeneous reaction between NO and OH were the important
604 sources of HONO. In the daytime, however, photolysis of nitrate and homogeneous
605 reaction between NO and OH dominated the sources of HONO. Heterogeneous
606 reactions of NO₂ on aerosol surface and ground surfaces were not the major HONO
607 source during night unlike the modelled results (Zhang et al., 2016; Aumont et al., 2003).

608 Fig. 4A-F shows the HONO budget estimated using the middle values among these
609 parameters during the polluted events. The mean production rate of HONO varied in
610 the range of 0.25 - 1.81 ppbv h⁻¹ from these identified sources, while the corresponding
611 loss rate was from 0.21 to 2.34 ppbv h⁻¹ during the polluted events in winter. The main
612 loss of HONO was the photolysis during the daytime (1.74± 0.44 ppbv h⁻¹), whereas it
613 was vertical transport in the nighttime (0.28±0.08 ppbv h⁻¹). Direct emission from

614 vehicles exhaust was the largest nighttime source of HONO (0.23 ± 0.06 ppbv h⁻¹),
615 followed by heterogeneous reactions of NO₂ on the ground surface (0.07 ± 0.01 ppbv h⁻¹),
616 homogeneous reaction between NO and OH (0.04 ± 0.01 ppbv h⁻¹), emission from
617 soil (0.014 ± 0.005 ppbv h⁻¹), and heterogeneous reactions of NO₂ on aerosol surface
618 (0.006 ± 0.002 ppbv h⁻¹). $P_{\text{NO-OH}}$ and P_{nitrate} dominated the daytime HONO production,
619 with daytime mean values of 0.49 ± 0.35 ppbv h⁻¹ and 0.34 ± 0.23 ppbv h⁻¹, respectively.
620 As shown in Fig. 4, these six sources still underestimated the daytime sources of HONO.
621 The P_{unknown} was 0.20 ± 0.24 ppbv h⁻¹ in February and March, while it was 0.50 ± 0.24
622 ppbv h⁻¹ from April to June.

623 The E_{vehicle} contributed $57.0\pm10.0\%$ and $51.5\pm20.1\%$ to the nighttime HONO
624 sources from February to March and the rest months, respectively, even when the
625 P_{unknown} was taken into consideration. The relative contribution of daytime E_{vehicle}
626 decreased to $15.2\pm15.4\%$ in winter and $9.7\pm7.8\%$ from April to June. Thus, the daily
627 mean fraction of the E_{vehicle} was $39.6\pm24.3\%$ and $34.0\pm24.3\%$ from February to March
628 and from April to June, respectively. This means that the E_{vehicle} dominates the nighttime
629 HONO source during the polluted events in Beijing, which is consistent with the
630 previous result that vehicle emission was the major nighttime or haze day HONO source
631 (51.1% - 52%) in Beijing (Zhang et al., 2019c; Meng et al., 2019). As pointed out in
632 Section 3.3, E_{vehicle} was calculated based on the NO_x inventory from vehicle sector. On
633 the other hand, NO is prone to be quickly converted to NO₂ and NO_z (including HONO,
634 HNO₃, N₂O₅, PAN and organonitrate etc) by O₃, HO₂, RO₂ and OH in the atmosphere.
635 It is reasonable to assume that local traffic emission dominates the ambient NO source

636 in the urban environment. Thus, homogeneous reaction between NO and OH in the
637 atmosphere could also be related to vehicle exhaust. As shown in Fig.3, although the
638 diurnal curve of $P_{\text{NO-OH}}$ coincided well with that of OH concentration (Fig. S10), which
639 means the $P_{\text{NO-OH}}$ should be mainly determined by OH concentration, the $P_{\text{NO-OH}}$ should
640 still reflect the indirect contribution of traffic related emission to HONO source because
641 the ambient NO concentration was used to calculate the $P_{\text{NO-OH}}$. Traffic-related HONO
642 sources ($E_{\text{vehicles}} + P_{\text{NO-OH}}$) might contribute $57.8 \pm 15.8\%$ and $48.6 \pm 15.9\%$ to the daily
643 HONO source in winter and the rest months, respectively. Even if 40 % of NO_x was
644 from vehicle exhaust in Beijing (He et al., 2002), traffic-related source ($E_{\text{vehicles}} +$
645 $0.4P_{\text{NO-OH}}$) might still contribute $46.9 \pm 20.5\%$ in winter and $39.9 \pm 20.5\%$ from April to
646 June to the corresponding daily HONO source. The contribution of traffic-related
647 source was still an important daytime source of HONO ($43.9 \pm 10.6\%$ for $E_{\text{vehicles}} + P_{\text{NO-OH}}$
648 OH, and $26.7 \pm 12.4\%$ for $E_{\text{vehicles}} + 0.4P_{\text{NO-OH}}$) on polluted days in winter.

649 As shown in Fig. 3, uncertainties existed when calculating each HONO source. To
650 further understand the role of traffic emission, we also estimated the lower limit of the
651 traffic-related contribution as follows: 1) the lower limit of E_{vehicle} was obtained by
652 using the lowest reported emission ratio of HONO/ NO_x from vehicles (0.18%) (Liu et
653 al., 2017d) rather than 1.17%, which was the empirical value calculated based on the
654 field measurement in Fig. S7; 2) the lower limit for homogeneous reaction between NO
655 and OH radical was calculated according to the method by Li et al. (2018); 3) the upper
656 limit of the emission rate from soil was estimated using the emission flux of HONO
657 with low water content (Oswald et al., 2013); 4) the upper limit of HONO production

658 rate from heterogeneous reaction of NO₂ on the aerosol was calculated using the large
659 RH-dependent uptake coefficient of NO₂ on hematite (Liu et al., 2015) rather the value
660 recommended by Crowley et al. (Crowley et al., 2010); 5) the upper limit for
661 heterogeneous reaction on ground surface was calculated using the RH-dependent
662 kinetic data measured on urban grime (Liu et al., 2019a). As shown in Fig. 5, traffic-
663 related source ($E_{\text{vehicles}} + P_{\text{NO-OH}}$) contributed 25.7 ± 15.8 % to the **daily HONO sources**
664 **in winter** if all NO was assumed to be dominated by local traffic emission, while it was
665 14.5 ± 15.8 % when 40 % of NO was considered as local traffic emission (He et al.,
666 2002). Under this circumstance, the daytime P_{unknown} of HONO in winter increased to
667 0.83 ± 0.36 ppbv h⁻¹, which was corresponding to 58.1 ± 8.6 % of the HONO source. This
668 means these assumptions might underestimate the contribution of the HONO sources.
669 In addition, P_{ground} , P_{aerosol} and P_{nitrate} could be also partially related to traffic emission
670 of NO_x (Lee et al., 2016; Tan et al., 2017). These results mean that the contribution of
671 traffic-related emission might be larger than our estimation in this work. Therefore, our
672 work at least suggests that traffic related emission should be a very important HONO
673 source in winter Beijing although more work is required based on comprehensive
674 modelling studies.

675 **4. Conclusions and atmospheric implications.**

676 In this work, the promotion effect of HONO on aerosol mass formation in polluted
677 events was observed based on the good correlation between the growth of OA and
678 nitrate mass concentration and the consumed HONO from early morning to noon during
679 the polluted days in winter. This promotion effect could be related to OH production

680 from photolysis of HONO on aerosol formation followed by oxidation process of the
681 corresponding precursors. Our observation supports well the recent modelling studies
682 that HONO may significantly promote secondary aerosol mass formation (Zhang et al.,
683 2019a;Zhang et al., 2019c;Xing et al., 2019;An et al., 2013). Based on **budget analysis**
684 calculations, traffic-related sources (direction emission and conversion of NO from
685 vehicle emission) was found to be an important contributor to HONO source during
686 polluted days in winter in Beijing. This means that HONO from the traffic-related
687 sources can have an important role in aerosol mass formation in the atmosphere.

688 Vehicle population in China is increasing very quickly (Liu et al., 2017b;Wang et
689 al., 2011). Thus, the negative influences of the vehicle emission on air quality will
690 increase especially in populous metropolitan areas (Yang et al., 2019;Guo et al., 2020),
691 such as Beijing and Shanghai, if targeted pollution control technologies are not applied.
692 It has been estimated that the vehicles emission accounted for over 40% of total urban
693 NO_x emissions in Beijing (He et al., 2002). In the atmosphere, NO_x involves very
694 complicated reaction network, from which finally leads to aerosol mass formation and
695 production of ozone in VOC limited environment. At the same time, reactions of NO_x
696 also leads to some reactive NO_z species (Seinfeld and Pandis, 2006). In particular,
697 HONO is an important precursor of OH, which governs the conversion of primary
698 pollutants to secondary pollutants in the atmosphere. Besides **indirect production** of
699 HONO from NO, the vehicles also directly emits HONO as discussed in this work.
700 Even if the low limit of emission factor was used to calculating the HONO source from
701 the vehicles, the traffic-related emission can still be an important source of HONO in

702 winter Beijing. Therefore, this work implies that mitigation of HONO and NO_x
703 emission from vehicles might be an effective way to reduce secondary aerosol mass
704 formation and can have a positive effect on severe haze events in wintertime Beijing.

705 It should be pointed out that we only considered O₃ and HONO when discussing
706 the sources of OH. Other sources such as HO₂ (and RO₂) with NO, ozonolysis of
707 alkenes and photolysis of OVOCs might also contribute to OH radicals in the
708 atmosphere (Tan et al., 2018). In the future it will be vital to comprehensively analyze
709 OH sources and to quantify the role of HONO in secondary aerosol mass formation
710 although photolysis of HONO is the major OH source in winter. On the other hand, as
711 discussed in Section 3.3, uncertainties about the HONO budget might originate from
712 the emission factors, OH concentration, and reaction kinetics and so on. **The source of**
713 **HONO from vehicles was calculated based on the emission inventories, which should**
714 **have a significant bias (Squires et al., 2020). For example, the emission flux of NO_x**
715 **calculated using the emission inventory from Yang et al. (2019) is as 2.4±0.5 times as**
716 **the reported emission flux reported by Squires et al. (2020).** To take the next step, it is
717 required to measure the emission factors from vehicle exhaust under real road
718 conditions in the future. When calculating the OH concentration, the factor between
719 OH concentration and $J_{\text{O}1\text{D}}$ might vary over locations and seasons due to different
720 NO_x/VOCs ratio (Holland et al., 2003). Direct measurements of OH concentration
721 would be helpful for decreasing the uncertainty of both OH sources and HONO budget
722 analysis. Finally, it is necessary to quantify the contribution of traffic-related source of
723 HONO on secondary aerosol formation based on modelling studies in the future.

724

725 *Data availability.* The experimental data are available upon request to the
726 corresponding authors.

727

728 *Supplement.* The supplement related to this article is available online at:

729

730 **Author information**

731 *Author contributions.* YL, WW and MK designed the experiments. YL wrote the paper
732 and performed HONO budget analysis. YZ, CL, WW, YC, MG and XW carried out
733 HONO measurement. ZF, FZ, JC, WD and KD did aerosol composition measurements.
734 BC and JK did particle size measurements. YW, BH and YW analyzed meteorological
735 data analysis. CY, FB, JK, TP, HH, MG and MK revised the manuscript.

736

737 **Acknowledgements:**

738 This research was financially supported by the National Natural Science Foundation of
739 China (41877306), the Ministry of Science and Technology of the People's Republic of
740 China (2019YFC0214701), Academy of Finland via Center of Excellence in
741 Atmospheric Sciences (272041, 316114, and 315203) and European Research Council
742 vShandong University via ATM-GTP 266 (742206), the Strategic Priority Research
743 Program of Chinese Academy of Sciences and Beijing University of Chemical
744 Technology.

745

746 **References:**

- 747 Aliche, B., Geyer, A., Hofzumahaus, A., Holland, F., Konrad, S., Patz, H. W., Schafer, J., Stutz, J., Volz-
748 Thomas, A., and Platt, U.: OH formation by HONO photolysis during the BERLIOZ experiment, *Journal of*
749 *Geophysical Research-Atmospheres*, 108, 17, 10.1029/2001jd000579, 2003.
- 750 An, J., Li, Y., Chen, Y., Li, J., Qu, Y., and Tang, Y.: Enhancements of major aerosol components due to
751 additional HONO sources in the North China Plain and implications for visibility and haze, *Adv. Atmos.*
752 *Sci.*, 30, 57-66, 10.1007/s00376-012-2016-9, 2013.
- 753 An, Z., Huang, R.-J., Zhang, R., Tie, X., Li, G., Cao, J., Zhou, W., Shi, Z., Han, Y., Gu, Z., and Ji, Y.: Severe
754 haze in northern China: A synergy of anthropogenic emissions and atmospheric processes, *Proc. Natl.*
755 *Acad. Sci. USA*, 116, 8657-8666, 10.1073/pnas.1900125116, 2019.
- 756 Atkinson, R., and Arey, J.: Atmospheric Degradation of Volatile Organic Compounds, *Chem. Rev.*, 103,
757 4605-4638, doi: 10.1021/cr0206420, 2003.
- 758 Atkinson, R., Baulch, D. L., Cox, R. A., Crowley, J. N., Hampson, R. F., Hynes, R. G., Jenkin, M. E., Rossi, M.
759 J., and Troe, J.: Evaluated kinetic and photochemical data for atmospheric chemistry: Volume I - gas
760 phase reactions of Ox, HOx, NOx and SOx species, *Atmos. Chem. Phys.*, 4, 1461-1738, 10.5194/acp-4-
761 1461-2004, 2004.
- 762 Aumont, B., Chervier, F., and Laval, S.: Contribution of HONO sources to the NOx/HOx/O3 chemistry in
763 the polluted boundary layer, *Atmos. Environ.*, 37, 487-498, [https://doi.org/10.1016/S1352-](https://doi.org/10.1016/S1352-2310(02)00920-2)
764 [2310\(02\)00920-2](https://doi.org/10.1016/S1352-2310(02)00920-2), 2003.
- 765 Bao, F., Li, M., Zhang, Y., Chen, C., and Zhao, J.: Photochemical Aging of Beijing Urban PM2.5: HONO
766 Production, *Environ. Sci. Technol.*, 52, 6309-6316, 10.1021/acs.est.8b00538, 2018.
- 767 Bianchi, F., Kurtén, T., Riva, M., Mohr, C., Rissanen, M. P., Roldin, P., Berndt, T., Crounse, J. D., Wennberg,
768 P. O., Mentel, T. F., Wildt, J., Junninen, H., Jokinen, T., Kulmala, M., Worsnop, D. R., Thornton, J. A.,
769 Donahue, N., Kjaergaard, H. G., and Ehn, M.: Highly Oxygenated Organic Molecules (HOM) from Gas-
770 Phase Autoxidation Involving Peroxy Radicals: A Key Contributor to Atmospheric Aerosol, *Chemical*
771 *Reviews*, 119, 3472-3509, 10.1021/acs.chemrev.8b00395, 2019.
- 772 Cheng, F., Wang, C., Wang, J., Tang, F., and Xi, X.: Trend analysis of building height and total floor space
773 in Beijing, China using ICESat/GLAS data, *International Journal of Remote Sensing*, 32, 8823-8835, 2011.
- 774 Cheng, Y., Zheng, G., Wei, C., Mu, Q., Zheng, B., Wang, Z., Gao, M., Zhang, Q., He, K., Carmichael, G.,
775 Poschl, U., and Su, H.: Reactive nitrogen chemistry in aerosol water as a source of sulfate during haze
776 events in China, *Sci. Adv.*, 2, 10.1126/sciadv.1601530, 2016.
- 777 Cho, M.-H., Niles, A., uili Huang, Inglese, J., Austin, C. P., Riss, T., and Xia, M.: A bioluminescent
778 cytotoxicity assay for assessment of membrane integrity using a proteolytic biomarker, *Toxicol. In Vitro.*,
779 22, 1099-1106, 2008.
- 780 Crowley, J. N., Ammann, M., Cox, R. A., Hynes, R. G., Jenkin, M. E., Mellouki, A., Rossi, M. J., Troe, J., and
781 Wallington, T. J.: Evaluated kinetic and photochemical data for atmospheric chemistry: Volume V –
782 heterogeneous reactions on solid substrates, *Atmos. Chem. Phys.*, 10, 9059-9223, doi: 10.5194/acp-10-
783 9059-2010, 2010.
- 784 Cui, L., Li, R., Zhang, Y., Meng, Y., Fu, H., and Chen, J.: An observational study of nitrous acid (HONO) in
785 Shanghai, China: The aerosol impact on HONO formation during the haze episodes, *Sci. Total Environ.*,
786 630, 1057-1070, 10.1016/j.scitotenv.2018.02.063, 2018.
- 787 Czader, B. H., Choi, Y., Li, X., Alvarez, S., and Lefer, B.: Impact of updated traffic emissions on HONO
788 mixing ratios simulated for urban site in Houston, Texas, *Atmos. Chem. Phys.*, 15, 1253-1263,

789 10.5194/acp-15-1253-2015, 2015.

790 Dillon, M. B., Lamanna, M. S., Schade, G. W., Goldstein, A. H., and Cohen, R. C.: Chemical evolution of
791 the Sacramento urban plume: Transport and oxidation, *J. Geophys. Res.- Atmos.*, 107, ACH 3-1-ACH 3-
792 15, 10.1029/2001jd000969, 2002.

793 Fu, G. Q., Xu, W. Y., Yang, R. F., Li, J. B., and Zhao, C. S.: The distribution and trends of fog and haze in the
794 North China Plain over the past 30 years, *Atmos. Chem. Phys.*, 14, 11949-11958, 10.5194/acp-14-11949-
795 2014, 2014.

796 Gall, E. T., Griffin, R. J., Steiner, A. L., Dibb, J., Scheuer, E., Gong, L., Rutter, A. P., Cevik, B. K., Kim, S., Lefer,
797 B., and Flynn, J.: Evaluation of nitrous acid sources and sinks in urban outflow, *Atmos. Environ.*, 127,
798 272-282, <https://doi.org/10.1016/j.atmosenv.2015.12.044>, 2016.

799 Gao, W., Tan, G., Hong, Y., Li, M., Nian, H., Guo, C., Huang, Z., Fu, Z., Dong, J., Xu, X., Cheng, P., and Zhou,
800 Z.: Development of portable single photon ionization time-of-flight mass spectrometer combined with
801 membrane inlet, *International Journal of Mass Spectrometry*, 334, 8-12,
802 <https://doi.org/10.1016/j.ijms.2012.09.003>, 2013.

803 Guo, S., Hu, M., Zamora, M. L., Peng, J., Shang, D., Zheng, J., Du, Z., Wu, Z., Shao, M., Zeng, L., Molina,
804 M. J., and Zhang, R.: Elucidating severe urban haze formation in China, *Proc. Natl. Acad. Sci. USA*, 111,
805 17373-17378, 10.1073/pnas.1419604111, 2014.

806 Guo, S., Hu, M., Peng, J., Wu, Z., Zamora, M. L., Shang, D., Du, Z., Zheng, J., Fang, X., Tang, R., Wu, Y.,
807 Zeng, L., Shuai, S., Zhang, W., Wang, Y., Ji, Y., Li, Y., Zhang, A. L., Wang, W., Zhang, F., Zhao, J., Gong, X.,
808 Wang, C., Molina, M. J., and Zhang, R.: Remarkable nucleation and growth of ultrafine particles from
809 vehicular exhaust, *Proc. Natl. Acad. Sci. USA*, 117 3427-3432, 10.1073/pnas.1916366117, 2020.

810 Hallquist, M., Wenger, J. C., Baltensperger, U., Rudich, Y., Simpson, D., Claeys, M., Dommen, J., Donahue,
811 N. M., George, C., Goldstein, A. H., Hamilton, J. F., Herrmann, H., Hoffmann, T., Iinuma, Y., Jang, M.,
812 Jenkin, M. E., Jimenez, J. L., Kiendler-Scharr, A., Maenhaut, W., McFiggans, G., Mentel, T. F., Monod, A.,
813 Prévôt, A. S. H., Seinfeld, J. H., Surratt, J. D., Szmigielski, R., and Wildt, J.: The formation, properties and
814 impact of secondary organic aerosol: current and emerging issues, *Atmos. Chem. Phys.*, 9, 5155-5236,
815 10.5194/acp-9-5155-2009, 2009.

816 Han, C., Liu, Y., and He, H.: Role of Organic Carbon in Heterogeneous Reaction of NO₂ with Soot, *Environ.*
817 *Sci Technol.*, 47, 3174-3181, 10.1021/es304468n, 2013.

818 Han, X., Zhang, M. G., Skorokhod, A., and Kou, X. X.: Modeling dry deposition of reactive nitrogen in
819 China with RAMS-CMAQ, *Atmos. Environ.*, 166, 47-61, 10.1016/j.atmosenv.2017.07.015, 2017.

820 He, H., Wang, Y., Ma, Q., Ma, J., Chu, B., Ji, D., Tang, G., Liu, C., Zhang, H., and Hao, J.: Mineral dust and
821 NO_x promote the conversion of SO₂ to sulfate in heavy pollution days, *Sci. Rep.*, 4, 10.1038/srep04172,
822 2014.

823 He, K., Huo, H., and Zhang, Q.: Urban air pollution in China: current status, characteristics, and progress,
824 *Annual Review of Energy Environment* 27, 397-431, 2002.

825 He, P. Z., Alexander, B., Geng, L., Chi, X. Y., Fan, S. D., Zhan, H. C., Kang, H., Zheng, G. J., Cheng, Y. F., Su,
826 H., Liu, C., and Xie, Z. Q.: Isotopic constraints on heterogeneous sulfate production in Beijing haze, *Atmos.*
827 *Chem. Phys.*, 18, 5515-5528, 10.5194/acp-18-5515-2018, 2018.

828 Hendrick, F., Muller, J. F., Clemer, K., Wang, P., De Maziere, M., Fayt, C., Gielen, C., Hermans, C., Ma, J.
829 Z., Pinardi, G., Stavrou, T., Vlemmix, T., and Van Roozendaal, M.: Four years of ground-based MAX-
830 DOAS observations of HONO and NO₂ in the Beijing area, *Atmos. Chem. Phys.*, 14, 765-781,
831 10.5194/acp-14-765-2014, 2014.

832 Holland, F., Hofzumahaus, A., Schafer, R., Kraus, A., and Patz, H. W.: Measurements of OH and HO₂

833 radical concentrations and photolysis frequencies during BERLIOZ, *Journal of Geophysical Research-*
834 *Atmospheres*, 108, 22, 10.1029/2001jd001393, 2003.

835 Hou, S., Tong, S., Ge, M., and An, J.: Comparison of atmospheric nitrous acid during severe haze and
836 clean periods in Beijing, China, *Atmos. Environ.*, 124, 199-206,
837 <https://doi.org/10.1016/j.atmosenv.2015.06.023>, 2016.

838 Hu, M., Zhou, F., Shao, K., Zhang, Y., Tang, X., and Slanina, J.: Diurnal variations of aerosol chemical
839 compositions and related gaseous pollutants in Beijing and Guangzhou, *Journal of Environmental*
840 *Science and Health, Part A*, 37, 479-488, 10.1081/ESE-120003229, 2002.

841 Huang, H., Chen, Y., Clinton, N., Wang, J., Wang, X., Liu, C., Gong, P., Yang, J., Bai, Y., Zheng, Y., and Zhu,
842 Z.: Mapping major land cover dynamics in Beijing using all Landsat images in Google Earth Engine,
843 *Remote Sensing of Environment*, 202, 166-176, <https://doi.org/10.1016/j.rse.2017.02.021>, 2017a.

844 Huang, L., Zhao, Y., Li, H., and Chen, Z.: Kinetics of Heterogeneous Reaction of Sulfur Dioxide on
845 Authentic Mineral Dust: Effects of Relative Humidity and Hydrogen Peroxide, *Environ. Sci. Technol.*, 49,
846 10797-10805, 10.1021/acs.est.5b03930, 2015.

847 Huang, R.-J., Zhang, Y., Bozzetti, C., Ho, K.-F., Cao, J.-J., Han, Y., Daellenbach, K. R., Slowik, J. G., Platt, S.
848 M., Canonaco, F., Zotter, P., Wolf, R., Pieber, S. M., Brun, E. A., Crippa, M., Ciarelli, G., Piazzalunga, A.,
849 Schwikowski, M., Abbaszade, G., Schnelle-Kreis, J., Zimmermann, R., An, Z., Szidat, S., Baltensperger, U.,
850 Haddad, I. E., and Prevot, A. S. H.: High secondary aerosol contribution to particulate pollution during
851 haze events in China, *Nature*, 514(7521), 218-222, 10.1038/nature13774, 2014.

852 Huang, R.-J., Yang, L., Cao, J., Wang, Q., Tie, X., Ho, K.-F., Shen, Z., Zhang, R., Li, G., Zhu, C., Zhang, N.,
853 Dai, W., Zhou, J., Liu, S., Chen, Y., Chen, J., and O'Dowd, C. D.: Concentration and sources of atmospheric
854 nitrous acid (HONO) at an urban site in Western China, *Sci. Total Environ.*, 593, 165-172,
855 10.1016/j.scitotenv.2017.02.166, 2017b.

856 Kanaya, Y., Cao, R., Akimoto, H., Fukuda, M., Komazaki, Y., Yokouchi, Y., Koike, M., Tanimoto, H., Takegawa,
857 N., and Kondo, a. Y.: Urban photochemistry in central Tokyo: 1. Observed and modeled OH and HO₂
858 radical concentrations during the winter and summer of 2004, *J. Geophys. Res.- Atmos.*, 112,
859 10.1029/2007JD008670, 2007.

860 Kim, S., VandenBoer, T. C., Young, C. J., Riedel, T. P., Thornton, J. A., Swarthout, B., Sive, B., Lerner, B.,
861 Gilman, J. B., Warneke, C., Roberts, J. M., Guenther, A., Wagner, N. L., Dubé, W. P., Williams, E., and
862 Brown, S. S.: The primary and recycling sources of OH during the NACHTT-2011 campaign: HONO as an
863 important OH primary source in the wintertime, *J. Geophys. Res.- Atmos.*, 119, 6886-6896,
864 doi:10.1002/2013JD019784, 2014.

865 Kroll, J. H., and Seinfeld, J. H.: Chemistry of secondary organic aerosol: Formation and evolution of low-
866 volatility organics in the atmosphere, *Atmos. Environ.*, 42, 3593-3624, 2008.

867 Kulmala, M.: Build a global Earth observatory, *Nature*, 553, 21-23, 10.1038/d41586-017-08967-y, 2018.

868 Lang, J., Zhang, Y., Zhou, Y., Cheng, S., Chen, D., Guo, X., Chen, S., Li, X., Xing, X., and Wang, H.: Trends of
869 PM_{2.5} and Chemical Composition in Beijing, 2000-2015, *Aerosol Air Qual. Res.*, 17, 412-425,
870 10.4209/aaqr.2016.07.0307, 2017.

871 Lee, J. D., Whalley, L. K., Heard, D. E., Stone, D., Dunmore, R. E., Hamilton, J. F., Young, D. E., Allan, J. D.,
872 Laufs, S., and Kleffmann, J.: Detailed budget analysis of HONO in central London reveals a missing
873 daytime source, *Atmos. Chem. Phys.*, 16, 2747-2764, 10.5194/acp-16-2747-2016, 2016.

874 Lelieveld, J., Evans, J. S., Fnais, M., Giannadaki, D., and Pozzer, A.: The contribution of outdoor air
875 pollution sources to premature mortality on a global scale, *Nature*, 525, 367-371, 10.1038/nature15371,
876 2015.

877 Li, D., Xue, L., Wen, L., Wang, X., Chen, T., Mellouki, A., Chen, J., and Wang, W.: Characteristics and
878 sources of nitrous acid in an urban atmosphere of northern China: Results from 1-yr continuous
879 observations, *Atmos. Environ.*, 182, 296-306, <https://doi.org/10.1016/j.atmosenv.2018.03.033>, 2018.

880 Li, X., Brauers, T., H"aseler, R., Bohn, B., Fuchs, H., Hofzumahaus, A., Holland, F., Lou, S., Lu, K. D., Rohrer,
881 F., Hu, M., Zeng, L. M., Zhang, Y. H., Garland, R. M., Su, H., Nowak, A., Wiedensohler, A., Takegawa, N.,
882 Shao, M., and Wahner, A.: Exploring the atmospheric chemistry of nitrous acid (HONO) at a rural site in
883 Southern China, *Atmos. Chem. Phys.*, 12, 1497-1513, 2012.

884 Li, Z. Q., Guo, J. P., Ding, A. J., Liao, H., Liu, J. J., Sun, Y. L., Wang, T. J., Xue, H. W., Zhang, H. S., and Zhu,
885 B.: Aerosol and boundary-layer interactions and impact on air quality, *Natl. Sci. Rev.*, 4, 810-833,
886 [10.1093/nsr/nwx117](https://doi.org/10.1093/nsr/nwx117), 2017.

887 Liang, Y., Zha, Q., Wang, W., Cui, L., Lui, K. H., Ho, K. F., Wang, Z., Lee, S.-c., and Wang, T.: Revisiting
888 nitrous acid (HONO) emission from on-road vehicles: A tunnel study with a mixed fleet, *J. Air Waste
889 Manage. Assoc.*, 67, 797-805, [10.1080/10962247.2017.1293573](https://doi.org/10.1080/10962247.2017.1293573), 2017.

890 Liggio, J., Li, S.-M., Hayden, K., Taha, Y. M., Stroud, C., Darlington, A., Drollette, B. D., Gordon, M., Lee, P.,
891 Liu, P., Leithead, A., Moussa, S. G., Wang, D., O'Brien, J., Mittermeier, R. L., Brook, J. R., Lu, G., Staebler,
892 R. M., Han, Y., Tokarek, T. W., Osthoff, H. D., Makar, P. A., Zhang, J., L. Plata, D., and Gentner, D. R.: Oil
893 sands operations as a large source of secondary organic aerosols, *Nature*, 534, 91-94,
894 [10.1038/nature17646](https://doi.org/10.1038/nature17646)
895 [http://www.nature.com/nature/journal/vaop/ncurrent/abs/nature17646.html#supplementary-](http://www.nature.com/nature/journal/vaop/ncurrent/abs/nature17646.html#supplementary-information)
896 [information](http://www.nature.com/nature/journal/vaop/ncurrent/abs/nature17646.html#supplementary-information), 2016.

897 Liu, C., Ma, Z., Mu, Y., Liu, J., Zhang, C., Zhang, Y., Liu, P., and Zhang, H.: The levels, variation
898 characteristics, and sources of atmospheric non-methane hydrocarbon compounds during wintertime
899 in Beijing, China, *Atmos. Chem. Phys.*, 17, 10633-10649, [10.5194/acp-17-10633-2017](https://doi.org/10.5194/acp-17-10633-2017), 2017a.

900 Liu, F., Beirle, S., Zhang, Q., van der A, R. J., Zheng, B., Tong, D., and He, K.: NO_x emission trends over
901 Chinese cities estimated from OMI observations during 2005 to 2015, *Atmos. Chem. Phys.*, 17, 9261-
902 9275, [10.5194/acp-17-9261-2017](https://doi.org/10.5194/acp-17-9261-2017), 2017b.

903 Liu, J., Li, S., Mekic, M., Jiang, H., Zhou, W., Loisel, G., Song, W., Wang, X., and Gligorovski, S.:
904 Photoenhanced Uptake of NO₂ and HONO Formation on Real Urban Grime, *Environmental Science &
905 Technology Letters*, 6, 413-417, [10.1021/acs.estlett.9b00308](https://doi.org/10.1021/acs.estlett.9b00308), 2019a.

906 Liu, T., Gong, S., He, J., Yu, M., Wang, Q., Li, H., Liu, W., Zhang, J., Li, L., Wang, X., Li, S., Lu, Y., Du, H.,
907 Wang, Y., Zhou, C., Liu, H., and Zhao, Q.: Attributions of meteorological and emission factors to the 2015
908 winter severe haze pollution episodes in China's Jing-Jin-Ji area, *Atmos. Chem. Phys.*, 17, 2971-2980,
909 [10.5194/acp-17-2971-2017](https://doi.org/10.5194/acp-17-2971-2017), 2017c.

910 Liu, Y., Han, C., Ma, J., Bao, X., and He, H.: Influence of relative humidity on heterogeneous kinetics of
911 NO₂ on kaolin and hematite, *Phys. Chem. Chem. Phys.*, 17, 19424-19431, doi: [10.1039/C5CP02223A](https://doi.org/10.1039/C5CP02223A),
912 2015.

913 Liu, Y., Lu, K., Ma, Y., Yang, X., Zhang, W., Wu, Y., Peng, J., Shuai, S., Hu, M., and Zhang, Y.: Direct emission
914 of nitrous acid (HONO) from gasoline cars in China determined by vehicle chassis dynamometer
915 experiments, *Atmos. Environ.*, 169, 89-96, [10.1016/j.atmosenv.2017.07.019](https://doi.org/10.1016/j.atmosenv.2017.07.019), 2017d.

916 Liu, Y., Nie, W., Xu, Z., Wang, T., Wang, R., Li, Y., Wang, L., Chi, X., and Ding, A.: Contributions of different
917 sources to nitrous acid (HONO) at the SORPES station in eastern China: results from one-year continuous
918 observation, *Atmos. Chem. Phys. Discuss.*, 2019, 1-47, [10.5194/acp-2019-219](https://doi.org/10.5194/acp-2019-219), 2019b.

919 Liu, Y. H., Lu, K. D., Li, X., Dong, H. B., Tan, Z. F., Wang, H. C., Zou, Q., Wu, Y. S., Zeng, L. M., Hu, M., Min,
920 K. E., Kecorius, S., Wiedensohler, A., and Zhang, Y. H.: A Comprehensive Model Test of the HONO Sources

921 Constrained to Field Measurements at Rural North China Plain, *Environ. Sci. Technol.*, 53, 3517-3525,
922 10.1021/acs.est.8b06367, 2019c.

923 Meng, F., Qin, M., Tang, K., Duan, J., Fang, W., Liang, S., Ye, K., Xie, P., Sun, Y., Xie, C., Ye, C., Fu, P., Liu, J.,
924 and Liu, W.: High resolution vertical distribution and sources of HONO and NO₂ in the nocturnal
925 boundary layer in urban Beijing, China, *Atmos. Chem. Phys. Discuss.*, 2019, 1-34, 10.5194/acp-2019-613,
926 2019.

927 Meusel, H., Tamm, A., Kuhn, U., Wu, D., Leifke, A. L., Fiedler, S., Ruckteschler, N., Yordanova, P., Lang-
928 Yona, N., Poehlker, M., Lelieveld, J., Hoffmann, T., Poeschl, U., Su, H., Weber, B., and Cheng, Y.: Emission
929 of nitrous acid from soil and biological soil crusts represents an important source of HONO in the remote
930 atmosphere in Cyprus, *Atmos. Chem. Phys.*, 18, 799-813, 10.5194/acp-18-799-2018, 2018.

931 Michoud, V., Colomb, A., Borbon, A., Miet, K., Beekmann, M., Camredon, M., Aumont, B., Perrier, S.,
932 Zapf, P., Siour, G., Ait-Helal, W., Afif, C., Kukui, A., Furger, M., Dupont, J. C., Haefelin, M., and Doussin, J.
933 F.: Study of the unknown HONO daytime source at a European suburban site during the MEGAPOLI
934 summer and winter field campaigns, *Atmos. Chem. Phys.*, 14, 2805-2822, 10.5194/acp-14-2805-2014,
935 2014.

936 Ndour, M., D'Anna, B., George, C., Ka, O., Balkanski, Y., K., J., S., and K., A., M.: Photoenhanced uptake
937 of NO₂ on mineral dust: Laboratory experiments and model simulations, *Geophys. Res. Lett.*, 35, L05812.
938 doi:05810.01029/02007GL032006, 2008.

939 Ndour, M., Nicolas, M., D'Anna, B., Ka, O., and George, C.: Photoreactivity of NO₂ on mineral dusts
940 originating from different locations of the Sahara desert, *Phys. Chem. Chem. Phys.*, 11, 1312-1319, 2009.

941 Oswald, R., Behrendt, T., Ermel, M., Wu, D., Su, H., Cheng, Y., Breuninger, C., Moravek, A., Mougin, E.,
942 Delon, C., Loubet, B., Pommerening-Röser, A., Sörgel, M., Pöschl, U., Hoffmann, T., Andreae, M. O.,
943 Meixner, F. X., and Trebs, I.: HONO Emissions from Soil Bacteria as a Major Source of Atmospheric
944 Reactive Nitrogen, *Science*, 341, 1233-1235, 10.1126/science.1242266, 2013.

945 Oswald, R., Ermel, M., Hens, K., Novelli, A., Ouwersloot, H. G., Paasonen, P., Petäjä, T., Sipilä, M., Keronen,
946 P., Bäck, J., Königstedt, R., Hosaynali Beygi, Z., Fischer, H., Bohn, B., Kubistin, D., Harder, H., Martinez, M.,
947 Williams, J., Hoffmann, T., Trebs, I., and Sörgel, M.: A comparison of HONO budgets for two
948 measurement heights at a field station within the boreal forest in Finland, *Atmos. Chem. Phys.*, 15, 799-
949 813, 10.5194/acp-15-799-2015, 2015.

950 Qin, M., Xie, P., Su, H., Gu, J., Peng, F., Li, S., Zeng, L., Liu, J., Liu, W., and Zhang, Y.: An observational study
951 of the HONO-NO₂ coupling at an urban site in Guangzhou City, South China, *Atmos. Environ.*, 43, 5731-
952 5742, 10.1016/j.atmosenv.2009.08.017, 2009.

953 Ren, X., Brune, W. H., Mao, J., Mitchell, M. J., Leshner, R. L., Simpas, J. B., Metcalf, A. R., Schwab, J. J., Cai,
954 C., Li, Y., Demerjian, K. L., Felton, H. D., Boynton, G., Adams, A., Perry, J., He, Y., Zhou, X., and Hou, J.:
955 Behavior of OH and HO₂ in the winter atmosphere in New York City, *Atmos. Environ.*, 40, 252-263,
956 <https://doi.org/10.1016/j.atmosenv.2005.11.073>, 2006.

957 Rohrer, F., Bohn, B., Brauers, T., Bruning, D., Johnen, F. J., Wahner, A., and Kleffmann, J.: Characterisation
958 of the photolytic HONO-source in the atmosphere simulation chamber SAPHIR, *Atmos. Chem. Phys.*, 5,
959 2189-2201, 10.5194/acp-5-2189-2005, 2005.

960 Sangwan, M., and Zhu, L.: Role of Methyl-2-nitrophenol Photolysis as a Potential Source of OH Radicals
961 in the Polluted Atmosphere: Implications from Laboratory Investigation, *J. Phys. Chem. A*, 122, 1861-
962 1872, 10.1021/acs.jpca.7b11235, 2018.

963 Seinfeld, J. H., and Pandis, S. N.: Atmospheric chemistry and physics: From air pollution to climate
964 change, Second ed., John Wiley and Sons, New Jersey, 2006.

965 Soergel, M., Regelin, E., Bozem, H., Diesch, J. M., Drewnick, F., Fischer, H., Harder, H., Held, A., Hosaynali-
966 Beygi, Z., Martinez, M., and Zetzsch, C.: Quantification of the unknown HONO daytime source and its
967 relation to NO₂, *Atmos. Chem. Phys.*, **11**, 10433-10447, 10.5194/acp-11-10433-2011, 2011.

968 Spataro, F., Ianniello, A., Esposito, G., Allegrini, I., Zhu, T., and Hu, M.: Occurrence of atmospheric nitrous
969 acid in the urban area of Beijing (China), *Sci. Total Environ.*, **447**, 210-224,
970 <https://doi.org/10.1016/j.scitotenv.2012.12.065>, 2013.

971 Spataro, F., and Ianniello, A.: Sources of atmospheric nitrous acid: State of the science, current research
972 needs, and future prospects, *J. Air Waste Manage. Assoc.*, **64**, 1232-1250,
973 10.1080/10962247.2014.952846, 2014.

974 Squires, F. A., Nemitz, E., Langford, B., Wild, O., Drysdale, W. S., Acton, W. J. F., Fu, P., Grimmond, C. S.
975 B., Hamilton, J. F., Hewitt, C. N., Hollaway, M., Kotthaus, S., Lee, J., Metzger, S., Pingingtha-Durden, N.,
976 Shaw, M., Vaughan, A. R., Wang, X., Wu, R., Zhang, Q., and Zhang, Y.: Measurements of traffic dominated
977 pollutant emissions in a Chinese megacity, *Atmos. Chem. Phys. Discuss.*, **2020**, 1-33, 10.5194/acp-2019-
978 1105, 2020.

979 Stutz, J., Wong, K. W., and Tsai, C.: Field Observations of Daytime HONO Chemistry and Its Impact on
980 the OH Radical Budget, in: *Disposal of Dangerous Chemicals in Urban Areas and Mega Cities*, Dordrecht,
981 2013, 1-14.

982 Su, H., Cheng, Y. F., Cheng, P., Zhang, Y. H., Dong, S., Zeng, L. M., Wang, X., Slanina, J., Shao, M., and
983 Wiedensohler, A.: Observation of nighttime nitrous acid (HONO) formation at a non-urban site during
984 PRIDE-PRD2004 in China, *Atmos. Environ.*, **42**, 6219-6232, 10.1016/j.atmosenv.2008.04.006, 2008a.

985 Su, H., Cheng, Y. F., Shao, M., Gao, D. F., Yu, Z. Y., Zeng, L. M., Slanina, J., Zhang, Y. H., and Wiedensohler,
986 A.: Nitrous acid (HONO) and its daytime sources at a rural site during the 2004 PRIDE-PRD experiment
987 in China, *Journal of Geophysical Research-Atmospheres*, **113**, 10.1029/2007jd009060, 2008b.

988 Su, P. H., Kuo, D. T. F., Shih, Y. H., and Chen, C. Y.: Sorption of organic compounds to two diesel soot black
989 carbons in water evaluated by liquid chromatography and polyparameter linear solvation energy
990 relationship, *Water Res.*, **144**, 709-718, 10.1016/j.watres.2018.07.064, 2018.

991 Sun, P., Nie, W., Chi, X., Xie, Y., Huang, X., Xu, Z., Qi, X., Xu, Z., Wang, L., Wang, T., Zhang, Q., and Ding,
992 A.: Two years of online measurement of fine particulate nitrate in the western Yangtze River Delta:
993 influences of thermodynamics and N₂O₅ hydrolysis, *Atmos. Chem. Phys.*, **18**, 17177-17190,
994 10.5194/acp-18-17177-2018, 2018.

995 Sun, Y. L., Wang, Z. F., Fu, P. Q., Yang, T., Jiang, Q., Dong, H. B., Li, J., and Jia, J. J.: Aerosol composition,
996 sources and processes during wintertime in Beijing, China, *Atmos. Chem. Phys.*, **13**, 4577-4592,
997 10.5194/acp-13-4577-2013, 2013.

998 Sun, Y. L., Wang, Z. F., Du, W., Zhang, Q., Wang, Q. Q., Fu, P. Q., Pan, X. L., Li, J., Jayne, J., and Worsnop,
999 D. R.: Long-term real-time measurements of aerosol particle composition in Beijing, China: seasonal
1000 variations, meteorological effects, and source analysis, *Atmos. Chem. Phys.*, **15**, 10149-10165,
1001 10.5194/acp-15-10149-2015, 2015.

1002 Tan, Z., Fuchs, H., Lu, K., Hofzumahaus, A., Bohn, B., Broch, S., Dong, H., Gomm, S., Häsel, R., He, L.,
1003 Holland, F., Li, X., Liu, Y., Lu, S., Rohrer, F., Shao, M., Wang, B., Wang, M., Wu, Y., Zeng, L., Zhang, Y.,
1004 Wahner, A., and Zhang, Y.: Radical chemistry at a rural site (Wangdu) in the North China Plain:
1005 observation and model calculations of OH, HO₂ and RO₂ radicals, *Atmos. Chem. Phys.*, **17**, 663-690,
1006 10.5194/acp-17-663-2017, 2017.

1007 Tan, Z., Rohrer, F., Lu, K., Ma, X., Bohn, B., Broch, S., Dong, H., Fuchs, H., Gkatzelis, G. I., Hofzumahaus,
1008 A., Holland, F., Li, X., Liu, Y., Liu, Y., Novelli, A., Shao, M., Wang, H., Wu, Y., Zeng, L., Hu, M., Kiendler-

1009 Scharr, A., Wahner, A., and Zhang, Y.: Wintertime photochemistry in Beijing: observations of ROx radical
1010 concentrations in the North China Plain during the BEST-ONE campaign, *Atmos. Chem. Phys.*, **18**, 12391-
1011 12411, 10.5194/acp-18-12391-2018, 2018.

1012 Tan, Z. F., Lu, K. D., Jiang, M. Q., Su, R., Wang, H. L., Lou, S. R., Fu, Q. Y., Zhai, C. Z., Tan, Q. W., Yue, D. L.,
1013 Chen, D. H., Wang, Z. S., Xie, S. D., Zeng, L. M., and Zhang, Y. H.: Daytime atmospheric oxidation capacity
1014 in four Chinese megacities during the photochemically polluted season: a case study based on box
1015 model simulation, *Atmos. Chem. Phys.*, **19**, 3493-3513, 10.5194/acp-19-3493-2019, 2019.

1016 Tang, Y., An, J., Wang, F., Li, Y., Qu, Y., Chen, Y., and Lin, J.: Impacts of an unknown daytime HONO source
1017 on the mixing ratio and budget of HONO, and hydroxyl, hydroperoxyl, and organic peroxy radicals, in
1018 the coastal regions of China, *Atmos. Chem. Phys.*, **15**, 9381-9398, 10.5194/acp-15-9381-2015, 2015.

1019 Tian, M., Liu, Y., Yang, F. M., Zhang, L. M., Peng, C., Chen, Y., Shi, G. M., Wang, H. B., Luo, B., Jiang, C. T.,
1020 Li, B., Takeda, N., and Koizumi, K.: Increasing importance of nitrate formation for heavy aerosol pollution
1021 in two megacities in Sichuan Basin, southwest China, *Environ. Pollut.*, **250**, 898-905,
1022 10.1016/j.envpol.2019.04.098, 2019.

1023 Tong, S., Hou, S., Zhang, Y., Chu, B., Liu, Y., He, H., Zhao, P., and Ge, M.: Exploring the nitrous acid (HONO)
1024 formation mechanism in winter Beijing: direct emissions and heterogeneous production in urban and
1025 suburban areas, *Faraday Discuss.*, **189**, 213-230, 10.1039/c5fd00163c, 2016.

1026 Trinh, H. T., Imanishi, K., Morikawa, T., Hagino, H., and Takenaka, N.: Gaseous nitrous acid (HONO) and
1027 nitrogen oxides (NOx) emission from gasoline and diesel vehicles under real-world driving test cycles, *J.*
1028 *Air Waste Manage. Assoc.*, **67**, 412-420, 10.1080/10962247.2016.1240726, 2017.

1029 Underwood, G. M., Miller, T. M., and Grassian, V. H.: Transmission FT-IR and Knudsen Cell Study of the
1030 Heterogeneous Reactivity of Gaseous Nitrogen Dioxide on Mineral Oxide Particles, *J. Phys. Chem. A*, **103**
1031 6184-6190, 1999.

1032 Underwood, G. M., Song, C. H., Phadnis, M., Carmichael, G. R., and Grassian, V. H.: Heterogeneous
1033 reactions of NO₂ and HNO₃ on oxides and mineral dust: A combined laboratory and modeling study, *J.*
1034 *Geophys. Res.-Atmos.*, **106**, 18055-18066, 10.1029/2000jd900552, 2001.

1035 Volkamer, R., Sheehy, P., Molina, L. T., and Molina, M. J.: Oxidative capacity of the Mexico City
1036 atmosphere – Part 1: A radical source perspective, *Atmos. Chem. Phys.*, **10**, 6969-6991, 10.5194/acp-
1037 10-6969-2010, 2010.

1038 Vu, T. V., Shi, Z., Cheng, J., Zhang, Q., He, K., Wang, S., and Harrison, R. M.: Assessing the impact of Clean
1039 Air Action Plan on Air Quality Trends in Beijing Megacity using a machine learning technique, *Atmos.*
1040 *Chem. Phys. Discuss.*, 2019, 1-18, 10.5194/acp-2019-173, 2019.

1041 Wang, G., Zhang, R., Gomez, M. E., Yang, L., Zamora, M. L., Hu, M., Lin, Y., Peng, J., Guoc, S., Meng, J., Li,
1042 J., Cheng, C., Hu, T., Ren, Y., Wang, Y., Gao, J., Cao, J., An, Z., Zhou, W., Li, G., Wang, J., Tian, P., Marrero-
1043 Ortiz, W., Secret, J., Du, Z., Zheng, J., Shang, D., Zeng, L., Shao, M., Wang, W., Huang, Y., Wang, Y., Zhu,
1044 Y., Li, Y., Hu, J., Pan, B., Cai, L., Cheng, Y., Ji, Y., Zhang, F., Rosenfeld, D., Liss, P. S., Duce, R. A., Kolb, C. E.,
1045 and Molina, M. J.: Persistent sulfate formation from London Fog to Chinese haze, *Proc. Natl. Acad. Sci.*
1046 *USA*, **113**, 13630-13635, 2016.

1047 Wang, H., Lu, K., Chen, X., Zhu, Q., Chen, Q., Guo, S., Jiang, M., Li, X., Shang, D., Tan, Z., Wu, Y., Wu, Z.,
1048 Zou, Q., Zheng, Y., Zeng, L., Zhu, T., Hu, M., and Zhang, Y.: High N₂O₅ Concentrations Observed in Urban
1049 Beijing: Implications of a Large Nitrate Formation Pathway, *Environmental Science & Technology Letters*,
1050 **4**, 416-420, 10.1021/acs.estlett.7b00341, 2017a.

1051 Wang, H. C., Lu, K. D., Chen, X. R., Zhu, Q. D., Wu, Z. J., Wu, Y. S., and Sun, K.: Fast particulate nitrate
1052 formation via N₂O₅ uptake aloft in winter in Beijing, *Atmos. Chem. Phys.*, **18**, 10483-10495,

1053 10.5194/acp-18-10483-2018, 2018.

1054 Wang, J., Zhang, X., Guo, J., Wang, Z., and Zhang, M.: Observation of nitrous acid (HONO) in Beijing,
1055 China: Seasonal variation, nocturnal formation and daytime budget, *Sci. Total Environ.*, 587, 350-359,
1056 10.1016/j.scitotenv.2017.02.159, 2017b.

1057 Wang, S., Zhou, R., Zhao, H., Wang, Z., Chen, L., and Zhou, B.: Long-term observation of atmospheric
1058 nitrous acid (HONO) and its implication to local NO₂ levels in Shanghai, China, *Atmos. Environ.*, 77, 718-
1059 724, 10.1016/j.atmosenv.2013.05.071, 2013.

1060 Wang, S., Nan, J., Shi, C., Fu, Q., Gao, S., Wang, D., Cui, H., Saiz-Lopez, A., and Zhou, B.: Atmospheric
1061 ammonia and its impacts on regional air quality over the megacity of Shanghai, China, *Sci. Rep.*, 5,
1062 15842-15842, 10.1038/srep15842, 2015.

1063 Wang, Y. L., Song, W., Yang, W., Sun, X. C., Tong, Y. D., Wang, X. M., Liu, C. Q., Bai, Z. P., and Liu, X. Y.:
1064 Influences of Atmospheric Pollution on the Contributions of Major Oxidation Pathways to PM_{2.5} Nitrate
1065 Formation in Beijing, *Journal of Geophysical Research-Atmospheres*, 124, 4174-4185,
1066 10.1029/2019jd030284, 2019.

1067 Wang, Y. S., Teter, J., and Sperling, D.: China's soaring vehicle population: Even greater than forecasted?,
1068 *Energy Policy*, 39, 3296-3306, 10.1016/j.enpol.2011.03.020, 2011.

1069 Wang, Z., Wang, W., Tham, Y. J., Li, Q., Wang, H., Wen, L., Wang, X., and Wang, T.: Fast heterogeneous
1070 N₂O₅ uptake and ClNO₂ production in power plant and industrial plumes observed in the nocturnal
1071 residual layer over the North China Plain, *Atmos. Chem. Phys.*, 17, 12361-12378, 10.5194/acp-17-
1072 12361-2017, 2017c.

1073 Wen, L., Xue, L., Wang, X., Xu, C., Chen, T., Yang, L., Wang, T., Zhang, Q., and Wang, W.: Summertime
1074 fine particulate nitrate pollution in the North China Plain: increasing trends, formation mechanisms and
1075 implications for control policy, *Atmos. Chem. Phys.*, 18, 11261-11275, 10.5194/acp-18-11261-2018,
1076 2018.

1077 Xing, L., Wu, J., Elser, M., Tong, S., Liu, S., Li, X., Liu, L., Cao, J., Zhou, J., El-Haddad, I., Huang, R., Ge, M.,
1078 Tie, X., Prévôt, A. S. H., and Li, G.: Wintertime secondary organic aerosol formation in Beijing–Tianjin–
1079 Hebei (BTH): contributions of HONO sources and heterogeneous reactions, *Atmos. Chem. Phys.*, 19,
1080 2343-2359, 10.5194/acp-19-2343-2019, 2019.

1081 Xu, Z., Wang, T., Wu, J., Xue, L., Chan, J., Zha, Q., Zhou, S., Louie, P. K. K., and Luk, C. W. Y.: Nitrous acid
1082 (HONO) in a polluted subtropical atmosphere: Seasonal variability, direct vehicle emissions and
1083 heterogeneous production at ground surface, *Atmos. Environ.*, 106, 100-109,
1084 10.1016/j.atmosenv.2015.01.061, 2015.

1085 Yadav, A. K., Raman, S., and Niyogi, D. D. S.: A note on the estimation of eddy diffusivity and dissipation
1086 length in low winds over a tropical urban terrain, *Pure and Applied Geophysics*, 160, 395-404,
1087 10.1007/s00024-003-8785-4, 2003.

1088 Yang, D., Zhang, S., Niu, T., Wang, Y., Xu, H., Zhang, K. M., and Wu, Y.: High-resolution mapping of vehicle
1089 emissions of atmospheric pollutants based on large-scale, real-world traffic datasets, *Atmos. Chem.*
1090 *Phys.*, 2019, 8831–8843, 10.5194/acp-2019-32, 2019.

1091 Yang, Q., Su, H., Li, X., Cheng, Y., Lu, K., Cheng, P., Gu, J., Guo, S., Hu, M., Zeng, L., Zhu, T., and Zhang, Y.:
1092 Daytime HONO formation in the suburban area of the megacity Beijing, China, *Science China-Chemistry*,
1093 57, 1032-1042, 10.1007/s11426-013-5044-0, 2014.

1094 Zhang, F., Wang, Y., Peng, J., Chen, L., Sun, Y., Duan, L., Ge, X., Li, Y., Zhao, J., Liu, C., Zhang, X., Zhang, G.,
1095 Pan, Y., Wang, Y., Zhang, A. L., Ji, Y., Wang, G., Hu, M., Molina, M. J., and Zhang, R.: An unexpected
1096 catalyst dominates formation and radiative forcing of regional haze, *Proc. Natl. Acad. Sci. USA*, 117,

1097 10.1073/pnas.1919343117, 2020.

1098 Zhang, J., An, J., Qu, Y., Liu, X., and Chen, Y.: Impacts of potential HONO sources on the concentrations
1099 of oxidants and secondary organic aerosols in the Beijing-Tianjin-Hebei region of China, *Sci. Total*
1100 *Environ.*, 647, 836-852, <https://doi.org/10.1016/j.scitotenv.2018.08.030>, 2019a.

1101 Zhang, J., Chen, J., Xue, C., Chen, H., Zhang, Q., Liu, X., Mu, Y., Guo, Y., Wang, D., Chen, Y., Li, J., Qu, Y.,
1102 and An, J.: Impacts of six potential HONO sources on HOx budgets and SOA formation during a
1103 wintertime heavy haze period in the North China Plain, *Sci. Total Environ.*, 681, 110-123,
1104 <https://doi.org/10.1016/j.scitotenv.2019.05.100>, 2019b.

1105 Zhang, J. M., Yang, L. X., Chen, J. M., Mellouki, A., Jiang, P., Gao, Y., Li, Y. Y., Yang, Y. M., and Wang, W. X.:
1106 Influence of fireworks displays on the chemical characteristics of PM_{2.5} in rural and suburban areas in
1107 Central and East China, *Sci. Total Environ.*, 578, 476-484, [10.1016/j.scitotenv.2016.10.212](https://doi.org/10.1016/j.scitotenv.2016.10.212), 2017.

1108 Zhang, J. W., Chen, J. M., Xue, C. Y., Chen, H., Zhang, Q., Liu, X. G., Mu, Y. J., Guo, Y. T., Wang, D. Y., Chen,
1109 Y., Li, J. L., Qu, Y., and An, J. L.: Impacts of six potential HONO sources on HOx budgets and SOA formation
1110 during a wintertime heavy haze period in the North China Plain, *Sci. Total Environ.*, 681, 110-123,
1111 [10.1016/j.scitotenv.2019.05.100](https://doi.org/10.1016/j.scitotenv.2019.05.100), 2019c.

1112 Zhang, L., Wang, T., Zhang, Q., Zheng, J., Xu, Z., and Lv, M.: Potential sources of nitrous acid (HONO) and
1113 their impacts on ozone: A WRF-Chem study in a polluted subtropical region, *Journal of Geophysical*
1114 *Research-Atmospheres*, 121, 3645-3662, [10.1002/2015jd024468](https://doi.org/10.1002/2015jd024468), 2016.

1115 Zhang, W., Tong, S., Ge, M., An, J., Shi, Z., Hou, S., Xia, K., Qu, Y., Zhang, H., Chu, B., Sun, Y., and He, H.:
1116 Variations and sources of nitrous acid (HONO) during a severe pollution episode in Beijing in winter
1117 2016, *The Science of the total environment*, 648, 253-262, [10.1016/j.scitotenv.2018.08.133](https://doi.org/10.1016/j.scitotenv.2018.08.133), 2019d.

1118 Zhang, X. Y., Zhong, J. T., Wang, J. Z., Wang, Y. Q., and Liu, Y. J.: The interdecadal worsening of weather
1119 conditions affecting aerosol pollution in the Beijing area in relation to climate warming, *Atmos. Chem.*
1120 *Phys.*, 18, 5991-5999, [10.5194/acp-18-5991-2018](https://doi.org/10.5194/acp-18-5991-2018), 2018.

1121 Zheng, B., Zhang, Q., Zhang, Y., He, K. B., Wang, K., Zheng, G. J., Duan, F. K., Ma, Y. L., and Kimoto, T.:
1122 Heterogeneous chemistry: a mechanism missing in current models to explain secondary inorganic
1123 aerosol formation during the January 2013 haze episode in North China, *Atmos. Chem. Phys.*, 15, 2031-
1124 2049, [doi: 10.5194/acp-15-2031-2015](https://doi.org/10.5194/acp-15-2031-2015), 2015a.

1125 Zheng, G. J., Duan, F. K., Su, H., Ma, Y. L., Cheng, Y., Zheng, B., Zhang, Q., Huang, T., Kimoto, T., Chang, D.,
1126 Pöschl, U., Cheng, Y. F., and He, K. B.: Exploring the severe winter haze in Beijing: the impact of synoptic
1127 weather, regional transport and heterogeneous reactions, *Atmos. Chem. Phys.*, 15, 2969-2983,
1128 [10.5194/acp-15-2969-2015](https://doi.org/10.5194/acp-15-2969-2015), 2015b.

1129 Zhu, W. H., Xu, X. D., Zheng, J., Yan, P., Wang, Y. J., and Cai, W. Y.: The characteristics of abnormal
1130 wintertime pollution events in the Jing-Jin-Ji region and its relationships with meteorological factors, *Sci.*
1131 *Total Environ.*, 626, 887-898, [10.1016/j.scitotenv.2018.01.083](https://doi.org/10.1016/j.scitotenv.2018.01.083), 2018.

1132 Zou, Y., Deng, X. J., Deng, T., Yin, C. Q., and Li, F.: One-Year Characterization and Reactivity of Isoprene
1133 and Its Impact on Surface Ozone Formation at A Suburban Site in Guangzhou, China, *Atmosphere*, 10,
1134 [10.3390/atmos10040201](https://doi.org/10.3390/atmos10040201), 2019.

1135

1136

1137 **Figure captions**

1138 Fig. 1. An overviewed measurement of non-refractory-PM_{2.5} (NR-PM_{2.5}), HONO, NO_x,
1139 PM_{2.5} and meteorological parameters from Feb. 1 to July 1, 2018. (A) the mass
1140 concentration of different components of PM_{2.5}, (B) the mass fraction of individual
1141 component, (C) HONO and NO_x concentration, (D) temperature and RH, (E) wind
1142 speed and wind direction, (F) UVB and PBL height and (G) visibility and PM_{2.5}
1143 concentration during observation. We consider the period before Apr. 1 as winter.
1144 During the winter period, 12 cases are selected and numbered, including three clean
1145 cases (1, 3, and 5, marked in yellow) and the rest 9 pollution episodes (marked in blue).

1146 **Fig. 2.** Contribution of HONO to OH production and correlation between OA and
1147 HONO concentration. Diurnal production rates of OH from photolysis of HONO and
1148 O₃ on polluted days with PM_{2.5} concentration larger than 50 μg m⁻³ and RH less than
1149 90 % (A) from Feb 1 to Mar 31, (B) from Apr 1 to Jun 30; (C) Daytime variation of
1150 OA/CO and HONO/CO concentration for the 7th and 12th episodes and (D) correlation
1151 of the daytime OA/CO increased and consumed HONO/CO.

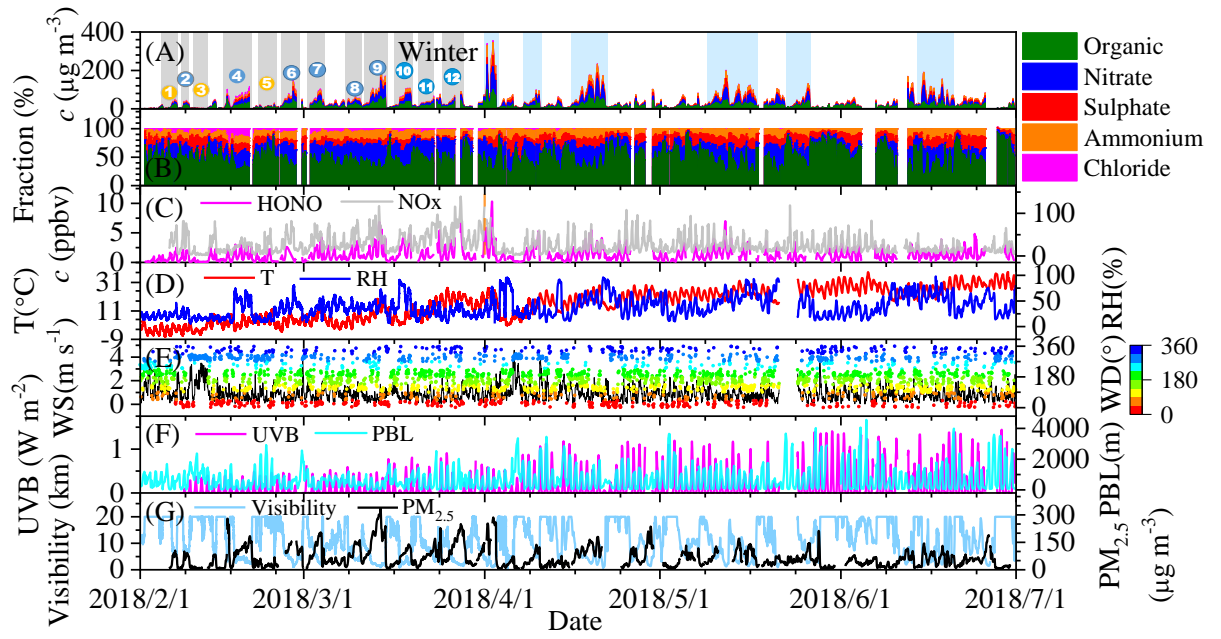
1152 **Fig. 3.** Diurnal pattern of HONO sources calculated with different parameterizations.
1153 The low bound, the middle value, and upper bound of (A) soil emission calculated
1154 based on 45-55%, 35-45% and 25-35% of water content, (B) vehicle emission with
1155 relative emission factor to NO_x of 0.18%, 1.17±0.05% and 1.8 %, (C) production from
1156 reaction between NO and OH, whose concentration estimated using Xu (Xu et al.,
1157 2015), (Tan et al., 2019)

1158 **Fig. 4.** The budget of HONO (A) and (B) Diurnal production rates of HONO, (C) and

1159 (D) loss rates of HONO, (E) and (F) relative contribution of each source on polluted
1160 days with $\text{PM}_{2.5}$ concentrations higher than $50 \mu\text{g m}^{-3}$ and RH less than 90 %. The left
1161 column shows the data from February 1 to March 31) and the right one shows the data
1162 from April 1 to June 30.

1163 **Fig. 5.** (A)-(B) Diurnal production rates and (C)-(D) diurnal loss rates of HONO; (E)-
1164 (F) relative contribution of HONO sources on polluted days with $\text{PM}_{2.5}$ concentrations
1165 higher than $50 \mu\text{g m}^{-3}$ and RH less than 90 %. The E_{vehicle} is calculated using the low
1166 limit of HONO/NO_x from vehicles (0.18%) (Liu et al., 2017d) and the $P_{\text{NO-OH}}$ is
1167 calculated using the low limit of OH concentration, while the upper limit of E_{soil} , P_{aerosol}
1168 and P_{ground} are used as described in the text.

1169 **Figures**

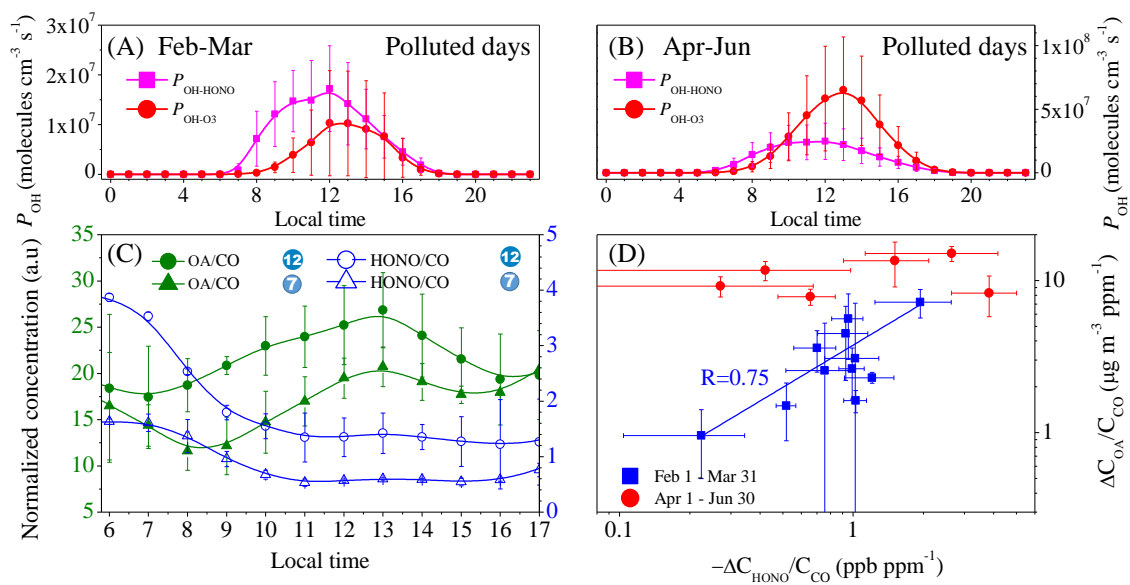


1170

1171

1172

Fig. 1.

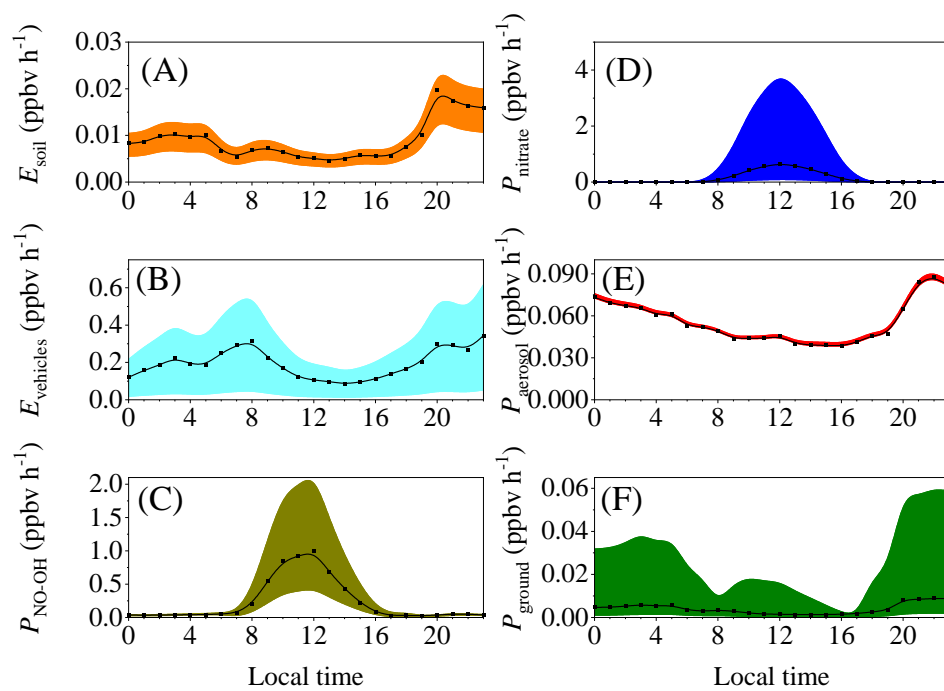


1173

1174

1175

Fig. 2.

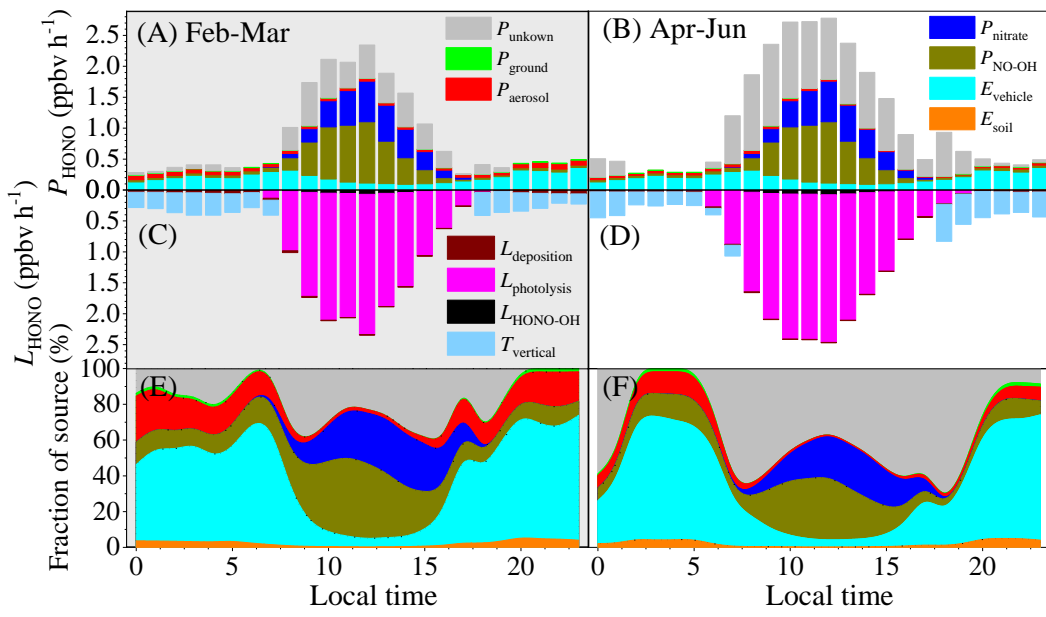


1176

1177

1178

Fig. 3

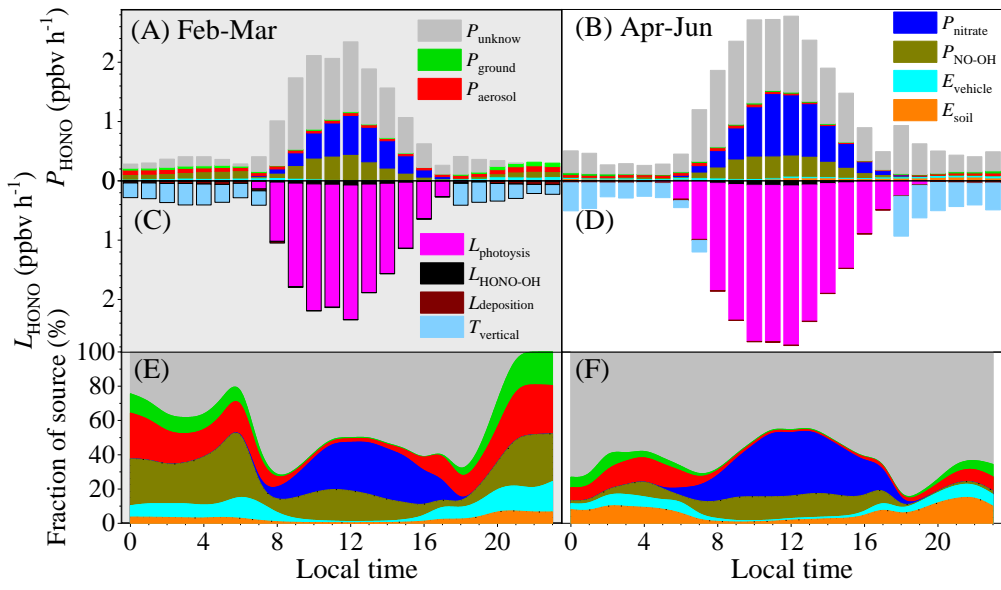


1179

1180

1181

Fig. 4.



1182

1183

Fig. 5.

1 **The promotion effect of nitrous acid on aerosol formation in**
2 **wintertime Beijing: possible contribution of traffic-related**
3 **emission**

4

5 Yongchun Liu^{1*}, Yusheng Zhang¹, Chaofan Lian^{2,6}, Chao Yan³, Zeming Feng¹, Feixue
6 Zheng¹, Xiaolong Fan¹, Yan Chen^{2,6}, Weigang Wang^{2,6*}, Biwu Chu^{3,4}, Yonghong Wang³,
7 Jing Cai³, Wei Du³, Kaspar R. Daellenbach³, Juha Kangasluoma^{1,3}, Federico Bianchi^{1,3},
8 Joni Kujansuu^{1,3}, Tuukka Petäjä³, Xuefei Wang⁶, Bo Hu⁵, Yuesi Wang⁵, Maofa Ge²,
9 Hong He⁴ and Markku Kulmala^{1,3*}

10

11 1. Aerosol and Haze Laboratory, Advanced Innovation Center for Soft Matter Science and
12 Engineering, Beijing University of Chemical Technology, Beijing, 100029, China

13 2. State Key Laboratory for Structural Chemistry of Unstable and Stable Species, Beijing
14 National Laboratory for Molecular Sciences, Institute of Chemistry, Chinese Academy of
15 Sciences, Beijing 100190, China

16 3. Institute for Atmospheric and Earth System Research/Physics, Faculty of Science, University
17 of Helsinki, P.O. Box 64, FI-00014, Finland

18 4. State Key Joint Laboratory of Environment Simulation and Pollution Control, Research
19 Center for Eco-Environmental Sciences, Chinese Academy of Sciences, Beijing, 100085, China

20 5. State Key Laboratory of Atmospheric Boundary Layer Physics and Atmospheric Chemistry,
21 Institute of Atmospheric Physics, Chinese Academy of Sciences, Beijing, 100029, China

22 6. University of Chinese Academy of Sciences, Beijing 100049, PR China

23

24

25 **Supplement information**

26 **Non-refractory PM_{2.5} (NR-PM_{2.5}) measurement.** Concentration of NR-PM_{2.5} was
27 measured with a ToF-ACSM (Aerodyne Co. Ltd., USA). The operation protocol and
28 the configuration of ToF-ACSM has been described well in previous work (Fröhlich et
29 al., 2013). Namely, PM_{2.5} particles from the inlet were focused by a PM_{2.5} aerodynamic
30 lens (Williams et al., 2013), and then vaporized by a standard vaporizer heated at 600
31 °C followed by electronic ionization (EI, 70 eV). The non-refractory components
32 including chloride, nitrate, sulfate, ammonia and organics were measured using a time-
33 of-flight mass spectrometer with unit mass resolution (UMR). The concentrations of
34 the above species were calculated based on the measured fragments signals, the signal
35 ions (SI), the fragment table, the measured ionization efficiency (IE) of nitrate and the
36 corresponding relative ionization efficiency (RIE) for sulfate, chloride, ammonia and
37 organics. IE calibration of nitrate was performed using 300 nm dry NH₄NO₃ every
38 month during this observation study.

39 **VOCs measurement.** VOCs were measured using a Single Photo Ionization Time-of-
40 flight Mass spectrometer (SPI-ToF-MS 3000R, Hexin Mass Spectrometry). 0.8 L min⁻¹
41 of filtered air was sucked from the whole sampling tube and heated to 80 °C in the
42 inlet. VOCs were selectively enriched continuously through a polydimethylsiloxane
43 (PDMS) membrane, and then ionized by VUV light (10.5 eV) with a deuterium lamp.
44 The concentration of VOCs was determined with the time-of-flight mass spectrometer
45 (ToF-MS) based upon external standard curves of PAMS and TO-15 standard gases
46 (Linde Electronics & Specialty Gases, USA). VOCs with m/z from 40 to 300 were

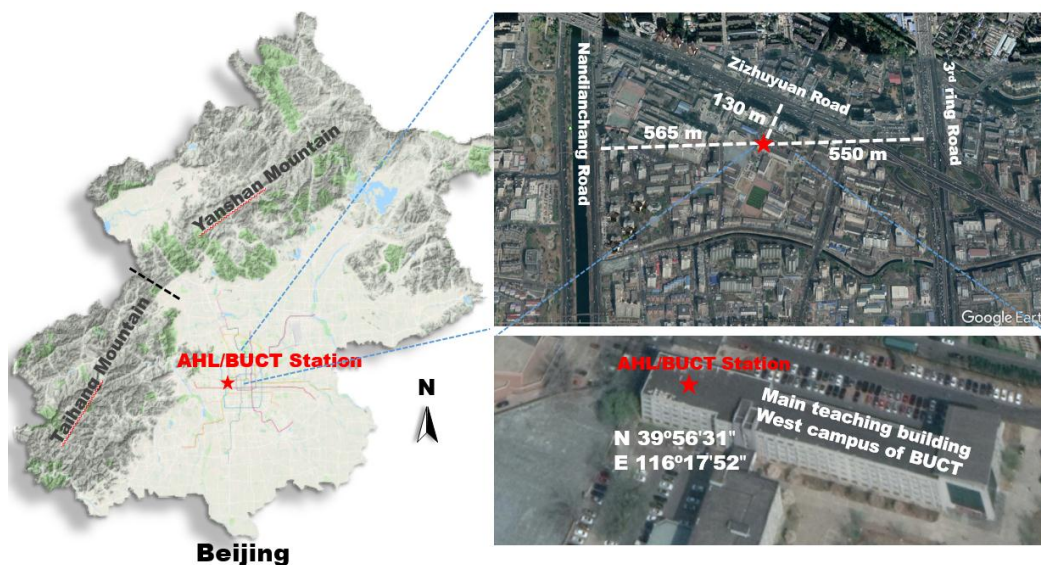
47 recorded with 3 min of time resolution, while hourly averaged concentration were
48 reported in this work. Calibration was performed every week.

49 **HONO measurement.** HONO in ambient air directly sampled from the window of the
50 laboratory was absorbed by a solution containing 0.06 mol L⁻¹ sulfnilamide in 1 mol L⁻¹
51 HCl, and then transformed into an azo dye by *N*-(1-naphthyl) ethylene-
52 diaminedihydrochloride (0.8 mmol L⁻¹). The azo dye was pumped into Teflon absorption
53 cells (Liquid Core Waveguide, LCW) and detected by a mini-spectrometer with a diode
54 array detector (Ocean Optics, SD2000). The HONO concentrations was obtained by
55 subtracting the calibrated signal of the second coil from the first coil using external
56 nitrile standard solutions. Zero point calibration was performed every day using
57 scrubbed zero air (Tong et al., 2016).

58 **Photolysis rate constants of HONO and O₃.** Photolysis rate constants of NO₂(J_{NO_2}),
59 HONO(J_{HONO}) and O₃(J_{O_3}) under clear sky conditions were calculated according to the
60 solar zenith angle and the location using a box model (FACSIMILE 4). NO₂ photolysis
61 sensor (J_{NO_2} , Metcon) was unavailable, while UVB is always available during our
62 observation study. However, it was available from Aug 17 to Sep 16, 2018. A
63 calibration function between the measured UVB light intensity and J_{NO_2} was
64 established to correct the influence the climatological O₃ column, aerosol optical depth
65 and cloud cover on surface UV light intensity from Aug 17 to Sep 16, 2008. As shown
66 in Figure S10, the model well predicted the J_{NO_2} . Then the J_{NO_2} during this campaign
67 study was predicted using the model. We further confirmed the calculated J_{NO_2} by
68 comprising the OH concentration estimated by the J_{OH} according to the equation

69 $(COH=J_{OH} \times 2 \times 10^{11} \text{ molecules cm}^{-3})$ (Tan et al., 2019) and the measured OH
70 concentration at Huairou, which is 60 km northeast from BUCT, from Jan 11 to Mar 10,
71 2016. As shown in Figure S10C, the estimated diurnal curve of OH is comparable with
72 that measured at Huairou. **Fig. S7 shows the calculated photolysis rates.**
73

74 **Supplementary figures**

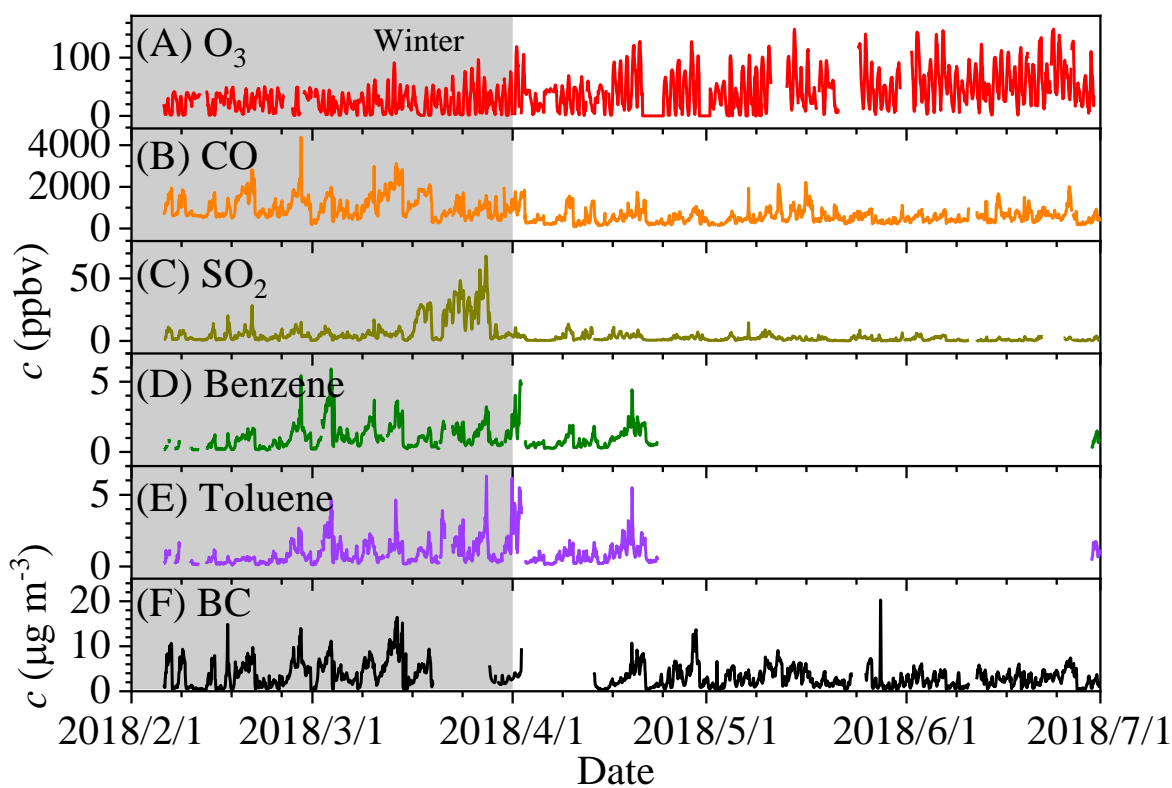


75

76 Figure S1. Location of AHL/BUCT observation station. The map was

77

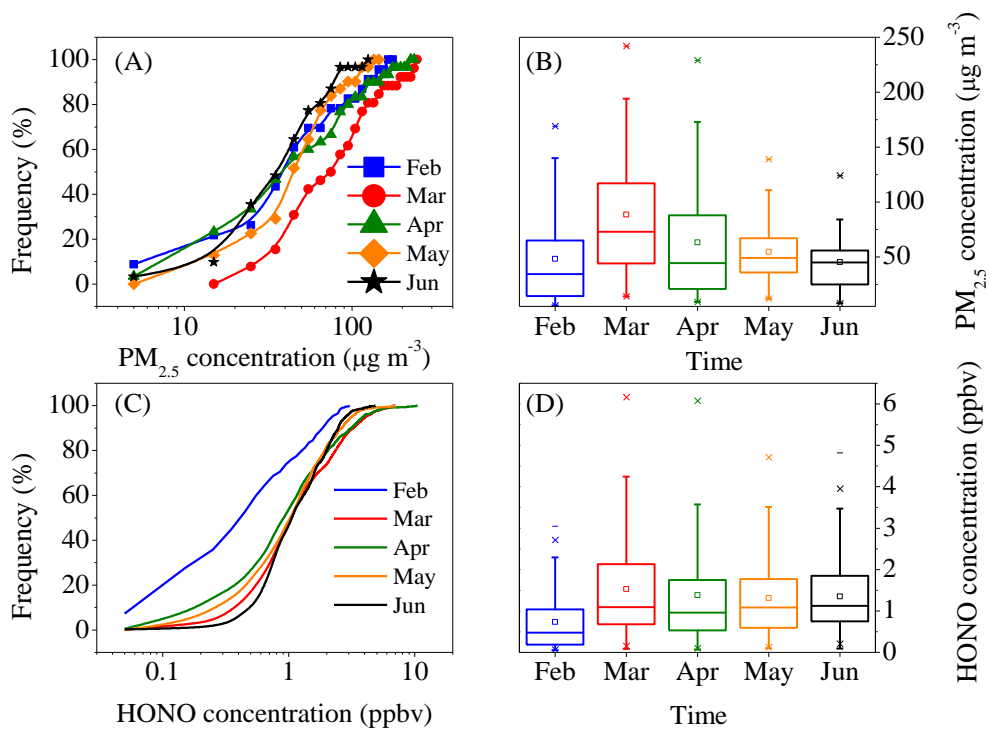
made from Wemap and Google Earth.



78

79 Figure S2. Hourly averaged (A)-(F) concentration of pollutants from Feb 1 to Jun 30,

80 2018.



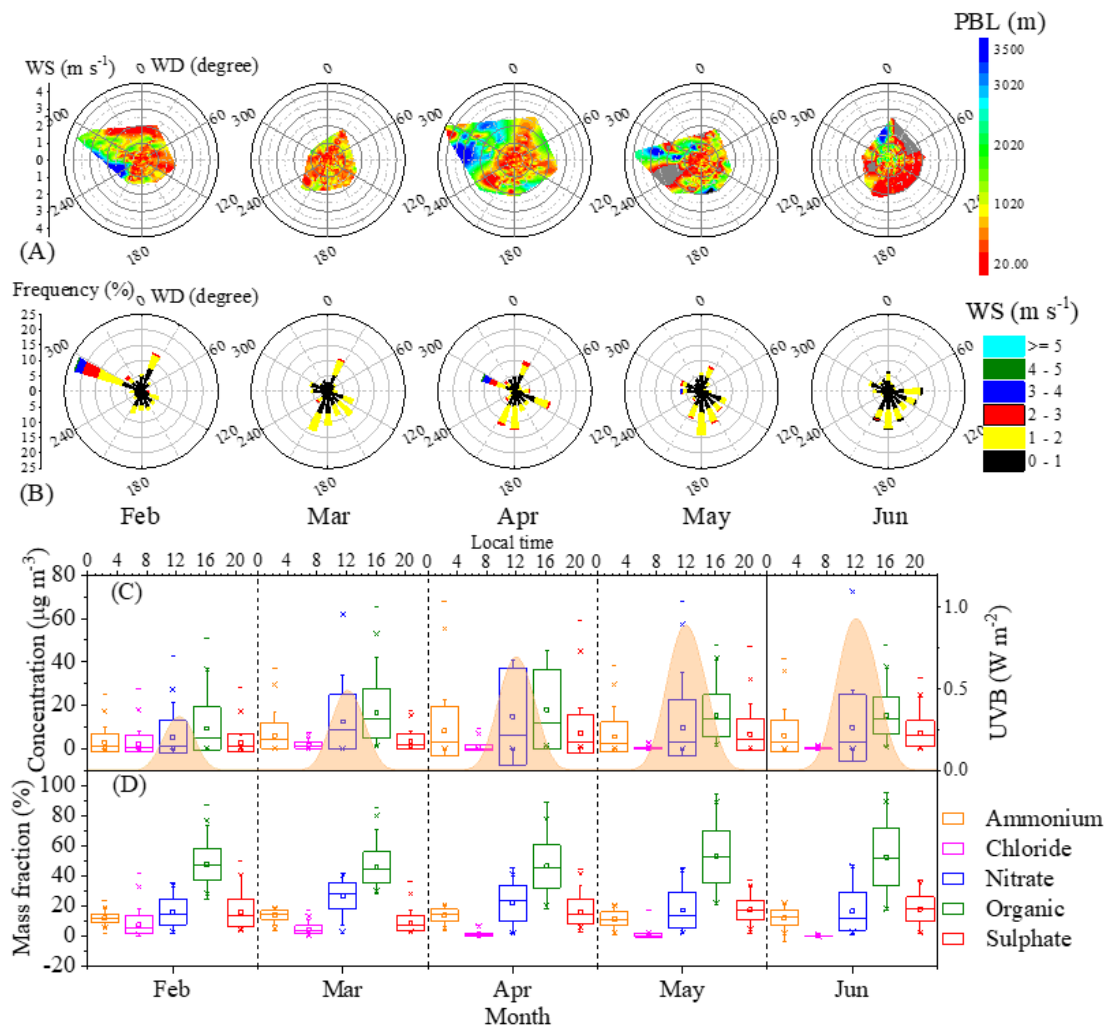
81

82

83 Figure S3. The monthly cumulative frequency of PM_{2.5} and HONO and the monthly

84 mean concentration of PM_{2.5} and HONO.

85



86

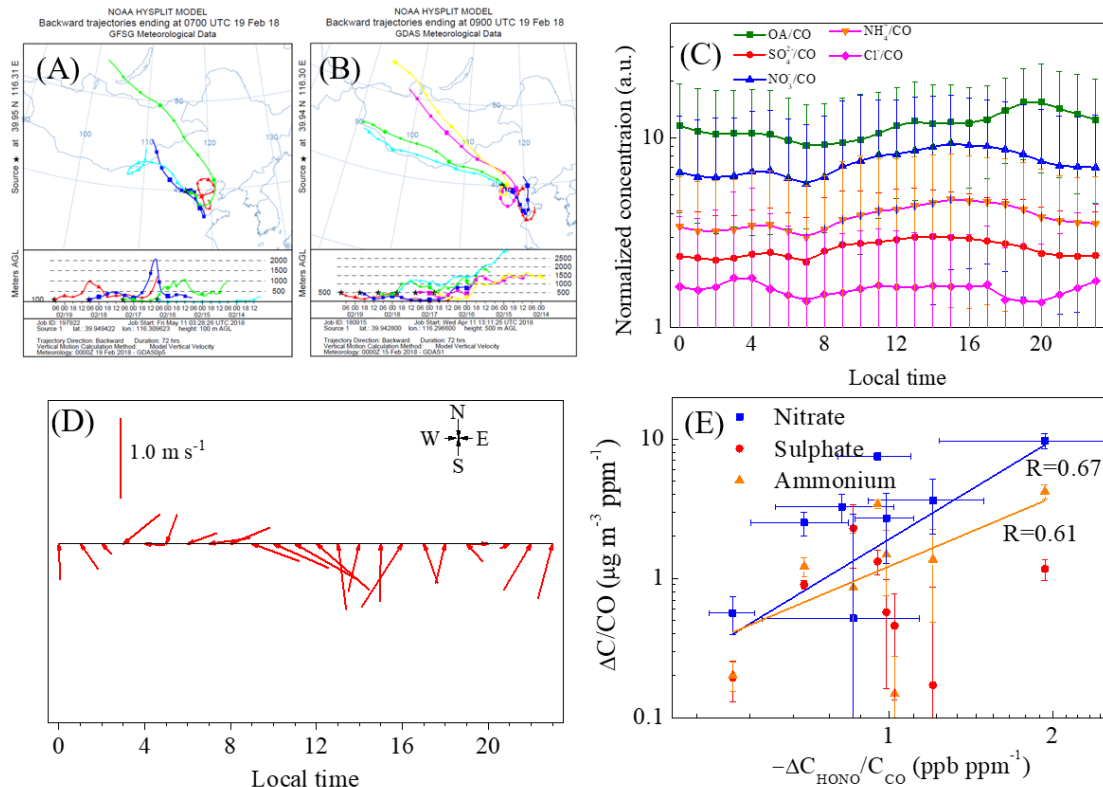
87 Figure S4. (A)-(B) monthly Windrose-PBL plots, and monthly averaged (C) UVB

88 intensity, mass concentration and (D) fraction of individual component in NR-PM_{2.5}

89 composition from Feb to Jun, 2018.

90

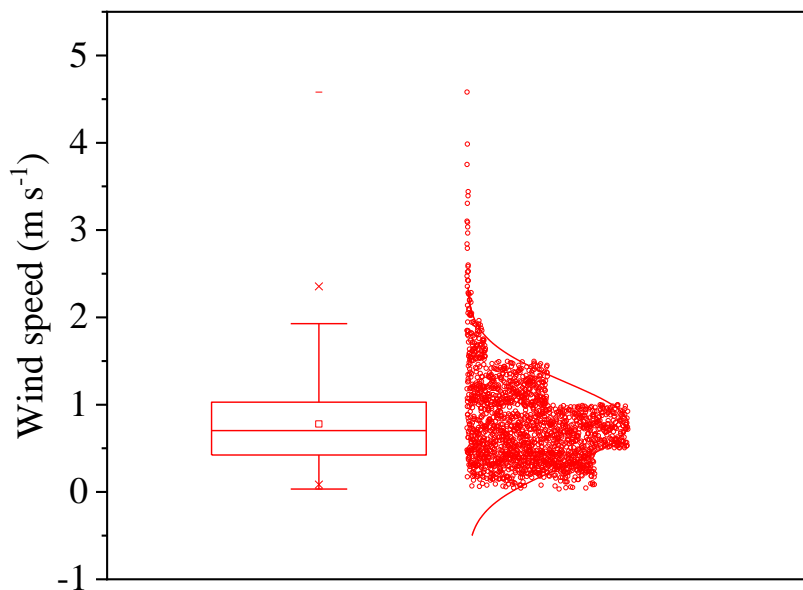
91



92

93 Figure S5. Transport of air mass during Chinese New Year based on back trajectory
 94 analysis (A) at 100 and (B) 500 m height; (C) Diurnal variation of NR-PM_{2.5} normalized
 95 to CO concentration from Feb 1 to March 31; (D) Hourly averaged wind speed variation
 96 in the 12th episode; (E) Correlation of the concentration increment of individual
 97 component and consumed HONO normalized to CO in the daytime.

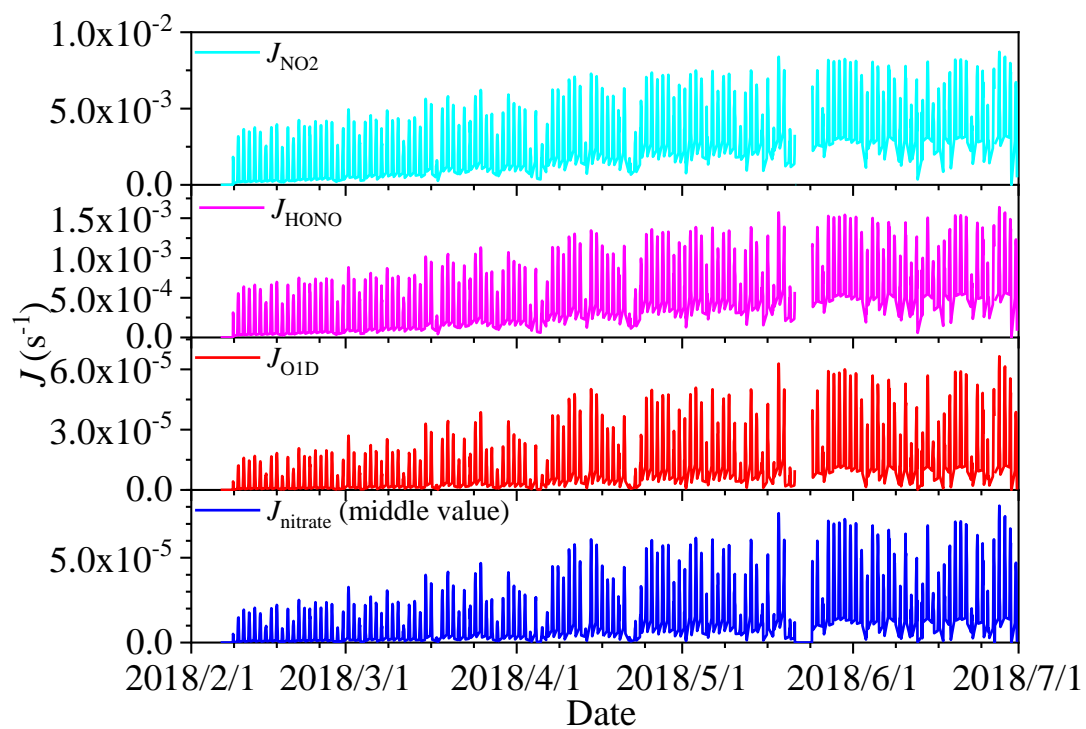
98



99

100 Figure S6. Distribution of wind speed when the $\text{PM}_{2.5}$ concentration was larger than 50

101 $\mu\text{g m}^{-3}$ and the RH was less than 90 %.



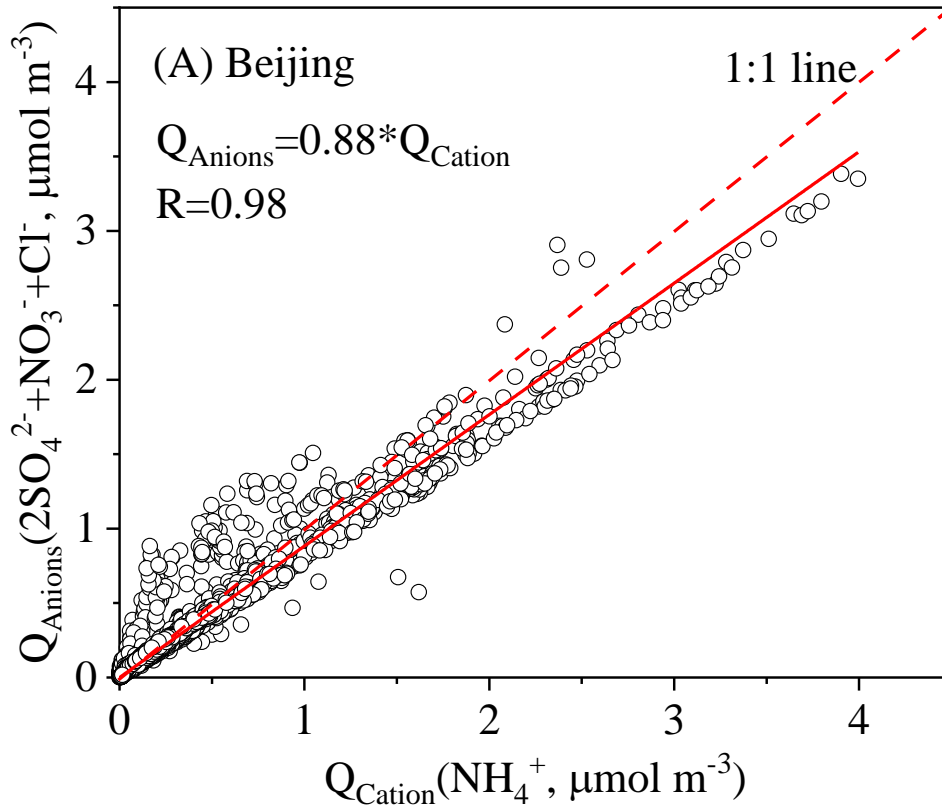
102

103 Fig. S7. The photolysis rate of NO_2 , HONO, O_3 (O1D) and nitrate (middle value)

104

from 8:00 am to 6:00 pm.

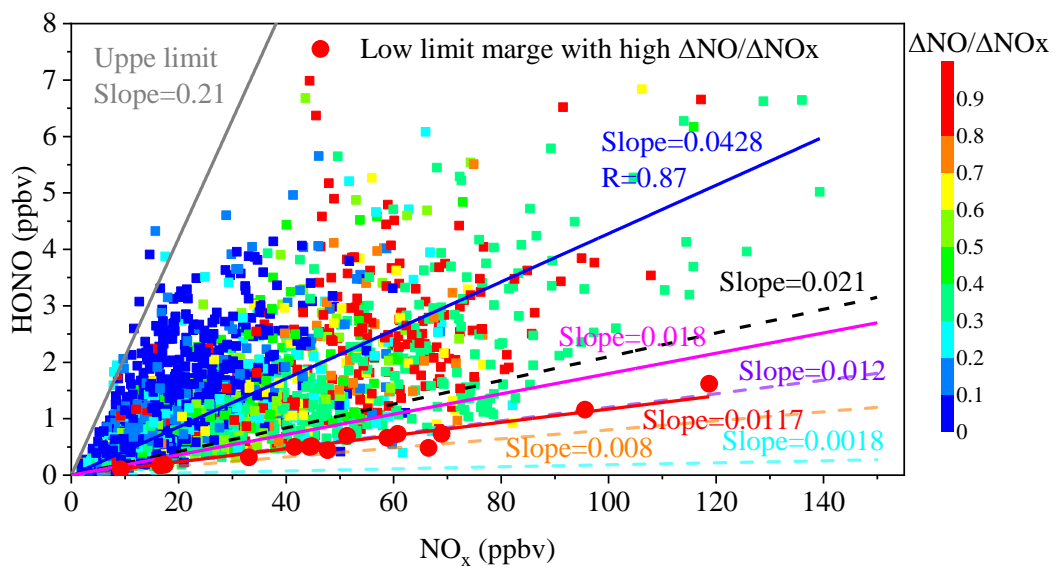
105



106

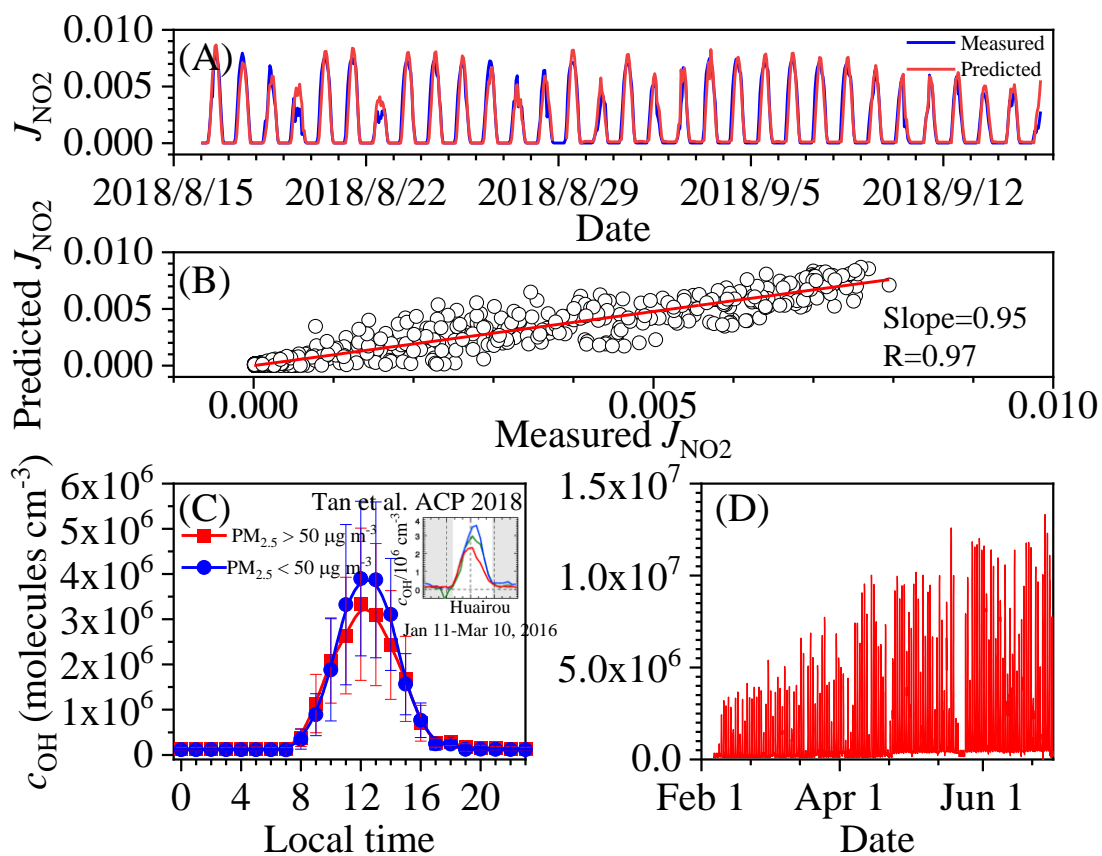
107 Figure S8. Correlation of the charge between inorganic anions and cations in non-
 108 refractory $\text{PM}_{2.5}$ in Beijing.

109



110

111 Figure S9. Correlation of measured HONO concentration with NO_x concentration.



112

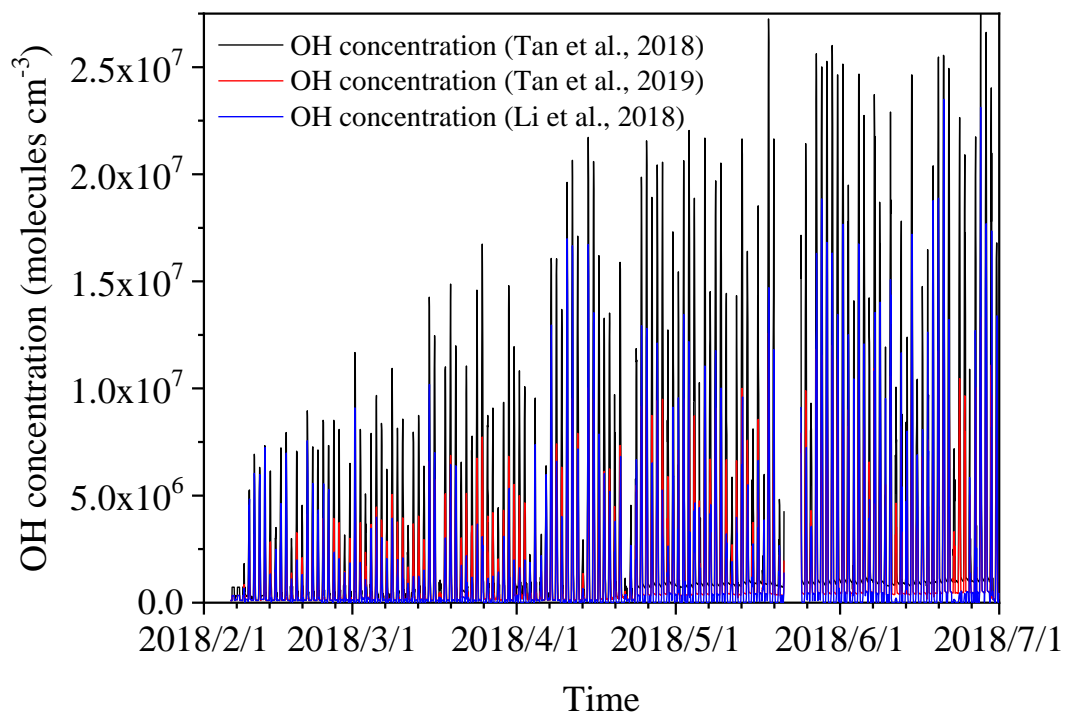
113 Figure S10. (A) Measured and predicted J_{NO_2} and (B) the correlation between measured

114 and predicted J_{NO_2} from Aug. 15 to Sep. 16; (C) calculated diurnal curve of OH

115 concentration based on $J_{\text{O}1\text{D}}$ compared with that measured at Huairou (60 km northeast

116 from BUCT) from Jan 11 to Mar 10, 2016; (D) OH concentrations estimated using

117 $c_{\text{OH}}=J_{\text{O}1\text{D}}\times 2\times 10^{11}$ (Tan et al., 2019).



118
119
120

Fig. S11. Estimated OH concentration using different methods.

Supplementary tables

Table S1. ANOVA statistics analysis for the monthly mean fraction of the individual component in NR-PM_{2.5} and HONO concentration.

Component	Fraction of NR-PM _{2.5} (%) or Concentration of gaseous pollutants (ppbv)				
	Feb	Mar	Apr	May	Jun
Ammonium	Feb (12.2±2.9)				
	Mar (14.2±2.8)	Significant			
	Apr (14.0±4.0)	Significant	Not significant		
	May (11.6±4.6)	Not significant	Significant	Significant	
	Jun (12.2±5.2)	Not significant	Significant	Significant	Not significant
Chloride	Feb (7.7±6.1)				
	Mar (4.4±2.6)	Significant			
	Apr (1.1±1.2)	Significant	Significant		
	May (0.7±1.1)	Significant	Significant	Not significant	
	Jun (0.3±0.2)	Significant	Significant	Significant	Not significant
Nitrate	Feb (16.2±8.5)				
	Mar (26.7±8.8)	Significant			
	Apr (22.0±11.7)	Significant	Significant		
	May (17.3±11.8)	Not significant	Significant	Significant	
	Jun (16.7±12.8)	Not significant	Significant	Significant	Not significant
Organic	Feb (47.9±10.7)				
	Mar (45.9±10.2)	Not significant			
	Apr (46.5±14.2)	Not significant	Significant		
	May (52.9±17.0)	Not significant	Significant	Significant	
	Jun (52.6±18.7)	Significant	Significant	Significant	Not significant

Sulfate	Feb (16.0±9.1)					
	Mar (8.8±5.4)	Significant				
	Apr (16.4±8.2)	Not significant	Significant			
	May (17.5±6.6)	Significant	Significant	Not significant		
	Jun (18.2±8.0)	Significant	Significant	Significant	Not significant	
BC	Feb (3.0±2.8)					
	Mar (4.6±3.1)	Significant				
	Apr (3.2±2.6)	Not significant	Significant			
	May (2.8±2.1)	Not significant	Significant	Not significant		
	Jun (2.6±1.5)	Significant	Significant	Significant	Not significant	
HONO	Feb (0.73±0.70)					
	Mar (1.53±1.25)	Significant				
	Apr (1.38±1.35)	Significant	Not significant			
	May (1.31±1.00)	Significant	Significant	Not significant		
	Jun (1.35±0.80)	Significant	Significant	Not significant	Not significant	
NO _x	Feb (20.4±17.3)					
	Mar (40.5±24.0)	Significant				
	Apr (22.8±18.6)	Not significant	Significant			
	May (25.0±15.9)	Significant	Significant	Not significant		
	Jun (19.0±12.1)	Not significant	Significant	Significant	Significant	Significant
SO ₂	Feb (3.8±3.3)					
	Mar (12.1±13.0)	Significant				
	Apr (2.8±2.4)	Significant	Significant			
	May (1.8±1.7)	Significant	Significant	Not significant		
	Jun (1.3±1.2)	Significant	Significant	Significant	Not significant	
CO	Feb (959.6±554.6)					

	Mar (1075.0±571.8)	Significant			
	Apr (546.6±378.1)	Significant	Significant		
	May (554.1±336.9)	Significant	Significant	Not significant	
	Jun (583.4±286.2)	Significant	Significant	Not significant	Not significant
O ₃	Feb (22.6±14.6)				
	Mar (23.8±19.2)	Not significant			
	Apr (43.5±29.0)	Significant	Significant		
	May (42.5±28.3)	Significant	Significant	Not significant	
	Jun (57.2±30.7)	Significant	Significant	Significant	Significant

Note: “Significant” or “Not significant” denotes that the difference of the monthly mean fractions or concentrations is significant or not significant at the 0.05 level.

Tab. S2. Mean concentrations of HONO and PM_{2.5} in selected episodes

Episode No.	Duration	HONO (ppb)	Average PM _{2.5} concentration	NR-PM _{2.5} Concentration (%)									
				Chloride		Nitrate		Organic		Sulphate		Ammonium	
				(%)	($\mu\text{g m}^{-3}$)	(%)	($\mu\text{g m}^{-3}$)	(%)	($\mu\text{g m}^{-3}$)	(%)	($\mu\text{g m}^{-3}$)	(%)	($\mu\text{g m}^{-3}$)
1	Feb 2-5	0.38±0.28	9.3±4.5	4.0±2.3	0.26±0.39	12.3±5.6	0.80±1.17	51.1±10.0	2.68±3.00	20.6±9.2	0.69±0.24	12.0±3.2	0.54±0.49
2	Feb 8-9	0.90±0.72	44.5±3.5	6.3±2.9	1.59±1.46	15.8±7.9	4.20±3.87	49.9±4.8	9.63±7.64	17.3±8.8	2.31±1.42	10.8±1.0	2.14±1.69
3	Feb 10-12	0.31±0.40	9.0±0.8	5.2±3.5	0.18±0.22	6.8±3.9	0.30±0.44	48.6±10.6	1.75±1.72	28.1±11.5	0.74±0.38	11.2±2.5	0.35±0.23
4	Feb 16-19	1.38±0.86	101.5±26.8	15.5±4.2	9.04±4.94	25.0±4.1	13.15±7.73	32.2±3.8	18.21±8.25	14.4±3.7	7.82±4.39	12.9±1.5	6.85±3.78
5	Feb 21-24	0.64±0.58	24.3±7.0	5.5±4.1	0.60±0.51	14.9±6.3	1.80±1.38	56.3±10.0	5.83±2.94	11.8±5.0	1.17±0.67	11.6±2.8	1.24±0.77
6	Feb 25-28	0.87±0.64	108.8±42.9	5.2±1.4	2.94±1.97	27.1±3.9	15.3±8.77	42.5±6.8	22.83±9.68	10.4±3.8	6.44±5.78	14.7±1.8	8.34±5.30
7	Mar 2-3	1.41±0.84	120.0±47.0	8.3±2.2	4.23±1.72	26.5±4.8	15.29±9.44	44.4±6.2	23.40±10.49	7.2±1.9	4.36±3.37	13.5±1.9	7.74±4.76
8	Mar 8-10	1.36±0.89	88.7±34.2	4.8±1.8	1.87±1.09	28.3±5.2	11.00±6.20	43.0±7.0	15.65±7.15	9.0±2.8	3.10±1.42	14.9±2.0	5.58±2.92
9	Mar 11-14	2.27±1.68	170.3±75.4	3.5±0.9	2.48±1.32	34.8±4.3	28.32±19.09	36.8±5.0	27.90±15.78	8.1±1.8	6.60±4.72	16.8±1.5	13.57±8.99
10	Mar 16-19	1.88±1.38	66.0±25.7	3.8±1.7	1.99±1.18	30.2±6.3	17.40±12.45	35.9±2.8	20.87±10.52	13.5±5.1	7.00±4.92	16.5±1.0	9.17±5.86
11	Mar 21-23	1.41±0.72	83.7±22.1	5.3±2.8	2.54±2.30	31.5±3.8	12.23±5.22	45.1±6.7	18.02±5.46	4.4±1.0	1.67±0.92	13.7±1.6	5.38±2.08
12	Mar 25-27	2.22±1.34	129.5±51.9	2.0±0.7	0.94±0.64	35.3±3.6	16.32±9.90	41.5±5.4	20.46±10.18	5.7±1.2	2.56±1.68	15.6±1.6	7.11±4.37

1 Table S3. The summary of the HONO/NO_x ratio from vehicles in this study and the
 2 reported emission ratio of HONO/NO_x from vehicles in China.

No.	Time	$\Delta\text{NO}/\Delta\text{NO}_x$	$R_{\Delta\text{NO}/\Delta\text{NO}_x}$	$\Delta\text{HONO}/\Delta\text{NO}_x$	$R_{\Delta\text{HONO}/\Delta\text{NO}_x}$
1	2018/2/6 5:00-8:00	1.00	0.99	1.3%	0.92
2	2018/2/8 5:00-8:00	0.94	0.99	1.8%	0.96
3	2018/3/3 5:00-8:00	0.98	0.99	2.4%	0.96
4	2018/3/13 5:00-8:00	1.00	0.99	1.4%	0.86
5	2018/4/15 5:00-7:00	0.82	0.97	2.3%	0.99
Mean		0.95±0.08	-	1.8±0.5%	-
Time	Place	Methods	$\Delta\text{HONO}/\Delta\text{NO}_x$		Reference
			Range	Mean	
2015/9/1-2016/8/31	Ji'nan, Shandong	Empirical analysis of field data	0.19%-0.87%	0.53±0.20%	(Li et al., 2018)
2011/8/3-2012/5/31	Hongkong	Empirical analysis of field data	0.5%-1.6%	1.2±0.4%	(Xu et al., 2015)
2015/3/11-2015/3/21	Hongkong	Tunnel experiment	-	1.24±0.35%	(Liang et al., 2017)
2014	Beijing	Tunnel experiment	-	2.1%	(Yang et al., 2014)
2017	Beijing	Chassis dynamometer test	0.03%-0.42%	0.18%	(Liu et al., 2017)
2016/12/16-2016/12/24	Beijing	Empirical analysis of field data	-	1.3%	(Zhang et al., 2018)
2016/12/7-2016/12/13	Beijing	Low limit correlation of field data	-	1.41%	(Meng et al., 2019)
2018/2/1-2018/6/30	Beijing	Low limit correlation of field data	-	1.17%	This study
2018/2/1-2018/6/30	Beijing	Empirical analysis of field data	1.3-2.4%	1.8±0.5%	This study

3

4 **References:**

- 5 Fröhlich, R., Cubison, M. J., Slowik, J. G., Bukowiecki, N., Prévôt, A. S. H., Baltensperger, U., Schneider,
 6 J., Kimmel, J. R., Gonin, M., Rohner, U., Worsnop, D. R., and Jayne, J. T.: The ToF-ACSM: a portable
 7 aerosol chemical speciation monitor with TOFMS detection, *Atmos. Meas. Tech.*, 6, 3225-3241,
 8 10.5194/amt-6-3225-2013, 2013.
- 9 Li, D., Xue, L., Wen, L., Wang, X., Chen, T., Mellouki, A., Chen, J., and Wang, W.: Characteristics and
 10 sources of nitrous acid in an urban atmosphere of northern China: Results from 1-yr continuous
 11 observations, *Atmos. Environ.*, 182, 296-306, <https://doi.org/10.1016/j.atmosenv.2018.03.033>, 2018.
- 12 Liang, Y., Zha, Q., Wang, W., Cui, L., Lui, K. H., Ho, K. F., Wang, Z., Lee, S.-c., and Wang, T.: Revisiting

13 nitrous acid (HONO) emission from on-road vehicles: A tunnel study with a mixed fleet, *J. Air Waste*
14 *Manage. Assoc.*, 67, 797-805, 10.1080/10962247.2017.1293573, 2017.

15 Liu, Y., Lu, K., Ma, Y., Yang, X., Zhang, W., Wu, Y., Peng, J., Shuai, S., Hu, M., and Zhang, Y.: Direct
16 emission of nitrous acid (HONO) from gasoline cars in China determined by vehicle chassis
17 dynamometer experiments, *Atmos. Environ.*, 169, 89-96, 10.1016/j.atmosenv.2017.07.019, 2017.

18 Meng, F., Qin, M., Tang, K., Duan, J., Fang, W., Liang, S., Ye, K., Xie, P., Sun, Y., Xie, C., Ye, C., Fu,
19 P., Liu, J., and Liu, W.: High resolution vertical distribution and sources of HONO and NO₂ in the
20 nocturnal boundary layer in urban Beijing, China, *Atmos. Chem. Phys. Discuss.*, 2019, 1-34,
21 10.5194/acp-2019-613, 2019.

22 Tan, Z. F., Lu, K. D., Jiang, M. Q., Su, R., Wang, H. L., Lou, S. R., Fu, Q. Y., Zhai, C. Z., Tan, Q. W.,
23 Yue, D. L., Chen, D. H., Wang, Z. S., Xie, S. D., Zeng, L. M., and Zhang, Y. H.: Daytime atmospheric
24 oxidation capacity in four Chinese megacities during the photochemically polluted season: a case study
25 based on box model simulation, *Atmos. Chem. Phys.*, 19, 3493-3513, 10.5194/acp-19-3493-2019, 2019.

26 Tong, S., Hou, S., Zhang, Y., Chu, B., Liu, Y., He, H., Zhao, P., and Ge, M.: Exploring the nitrous acid
27 (HONO) formation mechanism in winter Beijing: direct emissions and heterogeneous production in
28 urban and suburban areas, *Faraday Discuss.*, 189, 213-230, 10.1039/c5fd00163c, 2016.

29 Williams, L. R., Gonzalez, L. A., Peck, J., Trimborn, D., McInnis, J., Farrar, M. R., Moore, K. D., Jayne,
30 J. T., Robinson, W. A., Lewis, D. K., Onasch, T. B., Canagaratna, M. R., Trimborn, A., Timko, M. T.,
31 Magoon, G., Deng, R., Tang, D., de la Rosa Blanco, E., Prevot, A. S. H., and Worsnop, D. R.:
32 Characterization of an aerodynamic lens for transmitting particles greater than 1 micrometer in diameter
33 into the Aerodyne aerosol mass spectrometer, *Atmos. Meas. Tech.*, 6, 3271-3280, 10.5194/amt-6-3271-
34 2013, 2013.

35 Xu, Z., Wang, T., Wu, J., Xue, L., Chan, J., Zha, Q., Zhou, S., Louie, P. K. K., and Luk, C. W. Y.: Nitrous
36 acid (HONO) in a polluted subtropical atmosphere: Seasonal variability, direct vehicle emissions and
37 heterogeneous production at ground surface, *Atmos. Environ.*, 106, 100-109,
38 10.1016/j.atmosenv.2015.01.061, 2015.

39 Yang, Q., Su, H., Li, X., Cheng, Y., Lu, K., Cheng, P., Gu, J., Guo, S., Hu, M., Zeng, L., Zhu, T., and
40 Zhang, Y.: Daytime HONO formation in the suburban area of the megacity Beijing, China, *Science*
41 *China-Chemistry*, 57, 1032-1042, 10.1007/s11426-013-5044-0, 2014.

42 Zhang, W., Tong, S., Ge, M., An, J., Shi, Z., Hou, S., Xia, K., Qu, Y., Zhang, H., Chu, B., Sun, Y., and
43 He, H.: Variations and sources of nitrous acid (HONO) during a severe pollution episode in Beijing in
44 winter 2016, *The Science of the total environment*, 648, 253-262, 10.1016/j.scitotenv.2018.08.133, 2018.

45